Received: 3 November 2020 | Revised: 9 January 2021 | Accepted: 24 January 2021

DOI: 10.1002/wcms.1519

ADVANCED REVIEW

WIREs COMPUTATIONAL MOLECULAR SCIENCE WILEY

Dielectric continuum methods for quantum chemistry

John M. Herbert

Department of Chemistry and Biochemistry, The Ohio State University, Columbus, Ohio, USA

Correspondence
John M. Herbert, Department of Chemistry and Biochemistry, The Ohio State University, Columbus, OH 43210, USA.
Email: herbert@chemistry.ohio-state.edu

Funding information
National Science Foundation, Grant/Award Numbers: CHE-1665322, CHE-1955282

Edited by: Sunoj Raghavan, Associate Editor

Abstract

This review describes the theory and implementation of implicit solvation models based on continuum electrostatics. Within quantum chemistry this formalism is sometimes synonymous with the polarizable continuum model, a particular boundary-element approach to the problem defined by the Poisson or Poisson–Boltzmann equation, but that moniker belies the diversity of available methods. This work reviews the current state-of-the art, with emphasis on theory and methods rather than applications. The basics of continuum electrostatics are described, including the nonequilibrium polarization response upon excitation or ionization of the solute. Nonelectrostatic interactions, which must be included in the model in order to obtain accurate solvation energies, are also described. Numerical techniques for implementing the equations are discussed, including linear-scaling algorithms that can be used in classical or mixed quantum/classical biomolecular electrostatics calculations. Anisotropic models that can describe interfacial solvation are briefly described.

This article is categorized under:

Electronic Structure Theory > Ab Initio Electronic Structure Methods
Molecular and Statistical Mechanics > Free Energy Methods

KEYWORDS

electrostatics, implicit solvation, Poisson–Boltzmann, polarizable continuum

1 | OVERVIEW

The use of dielectric continuum models in quantum chemistry dates to the mid-1970s,[1–6] to when the field itself was still in its infancy. In their simplest form, these models describe the solvent in terms of a single parameter ε_s, the (static) dielectric constant. This is a dimensionless quantity equal to the electric permittivity relative to vacuum and ranging (for simple liquids) from $\varepsilon_s \approx 2$ for nonpolar solvents such as benzene and hexane, up to $\varepsilon_s = 78$ for water and $\varepsilon_s = 110$ for formamide. This constant describes the solvent's ability to screen charge, and the Coulomb interaction between charges Q_1 and Q_2 separated by a distance r is modified from $V(r) = Q_1Q_2/4\pi\varepsilon_0 r$ in the gas phase to $V(r) = Q_1Q_2/4\pi\varepsilon_0\varepsilon_s r$ within the dielectric medium. The continuum description of a solvent represents the ultimate in coarse-graining, reducing it to a single parameter, with obvious advantages for quantum chemistry where cost rises steeply with system size. Within a continuum description, there is no need for sampling over solvent degrees of freedom (e.g., reorganization in response to an electron transfer event that modifies the solute's charge distribution), because this averaging is implicitly encoded into the value of ε_s. While advantageous from the standpoint of cost, limitations of the continuum description are equally apparent: "specific" solvation effects such as hydrogen bonding are not captured, and dielectric continuum theory alone does not describe nonelectrostatic interactions including dispersion and Pauli repulsion. Absent the latter, there is nothing to imbue the molecules with finite size, necessitating *ad hoc* introduction of a "solute cavity" to define the interface between the atomistic solute and the continuum solvent, as depicted in Figure 1.

Some of the aforementioned limitations can be overcome, in principle, by admission of a small number of explicit solvent molecules into the atomistic part of the calculation, in what is often called a "semicontinuum" or a "cluster-continuum" approach.[8] As such, the continuum description serves as a flexible starting point for the description of solvation effects in quantum chemistry. The development of continuum models for quantum chemistry was pioneered by Tomasi and coworkers in Pisa,[9–16] originally as an outgrowth of efforts to use the electrostatic potential to understand chemical reactivity.[17–20] Tomasi and coworkers introduced the term *polarizable continuum model* (PCM), which will be formally introduced in Section 2.3 to refer to a particular class of continuum solvation models that replace the three-dimensional differential equations of continuum electrostatics with a two-dimensional boundary-element problem, defined on the surface of a cavity Γ (Figure 1) that represents the interface between atomistic solute and continuum solvent. Although PCMs are ubiquitous in quantum chemistry, they are not the only continuum solvation models that are used in the field, and not the only ones discussed herein. In any case, the combination of a quantum-mechanical (QM) description of the atomistic solute sets up a *self-consistent reaction-field* (SCRF) problem in which the solute's charge distribution both polarizes, and is polarized by, its environment. The two effects must be iterated to self-consistency.

The remainder of this review is organized as follows. Section 2 provides the elementary specification of the continuum electrostatics problem, starting from the Poisson and Poisson–Boltzmann equations. The mechanics of turning that formalism into a computationally tractable model are discussed in Section 3, with an emphasis on the smooth discretization approach developed by this author's group.[21–25] The focus here is on continuum solvation models in quantum chemistry but the formalism in Sections 2 and 3 is perfectly applicable to biomolecular implicit solvent calculations, in which a macromolecular solute is described using a classical force field.[23] Section 3 also introduces the various flavors of PCM that can be found in the literature and discusses how they can be understood in relation to one another. It should be noted that the solution of Poisson's equation or its PCM equivalent specifies only the *electrostatic* contribution to the solvation energy. Other contributions including cavitation, dispersion, Pauli repulsion, and hydrogen bonding must be included in order to predict free energies of solvation ($\Delta_{\text{solv}}\mathcal{G}$) that are in reasonable agreement with experiment. Section 4 introduces models for nonelectrostatic contributions and provides an overview of the accuracy that can be expected for $\Delta_{\text{solv}}\mathcal{G}^{\circ}$. Section 5 introduces several "nonequilibrium" formulations of continuum electrostatics that describe the continuum's response to a sudden change in the solute's charge density, as in photoexcitation or photoionization. This provides the machinery to compute solvent effects on vertical excitation energies, vertical ionization energies (VIEs), or fluorescence energies. Finally, Section 6 discusses modifications to the isotropic continuum model that are necessary in order to describe anisotropic solvation environments, such as the liquid/vapor interface or the solid-state/aqueous interface.

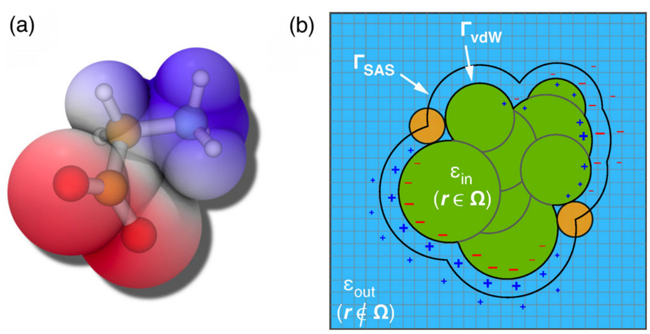

FIGURE 1 (a) Zwitterionic tautomer of glycine ($^{-}O_2CCH_2NH_3^{+}$) in a molecular van der Waals (vdW) cavity constructed from atom-centered spheres. Coloring reflects the sign and magnitude of the molecular electrostatic potential evaluated at the cavity surface, $\varphi^{\rho}(\mathbf{s})$ for $\mathbf{s}\in\Gamma$. (b) Schematic illustration of the same molecular cavity (in green) embedded in a dielectric medium (in blue), illustrating how the continuum polarizes in response to the solute's electrostatic potential. The orange probe sphere illustrates how the atomic radii that define the vdW surface might be augmented to afford a "solvent-accessible surface" (SAS). The region interior to the solute cavity is designated as Ω, and for a sharp dielectric interface one sets $\varepsilon(\mathbf{r}) \equiv \varepsilon_{\text{in}}$ for $\mathbf{r}\in\Omega$. If the solute is described using quantum chemistry then the natural choice is $\varepsilon_{\text{in}} = 1$. Outside of the cavity, the permittivity function $\varepsilon(\mathbf{r})$ takes the value ε_{out}, which is usually the static dielectric constant of the solvent, ε_{s}. Panel (b) is adapted from Ref. 7; copyright 2008 John Wiley & Sons

This review is focused on the theoretical framework and computational mechanics of continuum solvation models, not on applications. Some limited data are provided in order to describe the performance of the models, but the reader is directed to several general reviews for a more complete overview of continuum solvation methods in action.[8,13–15,26–28] Other, more specialized reviews describe the application of PCMs to specific types of spectroscopy.[29–35] In lieu of a great deal of data, the present work provides copious references to the primary literature. More so than other aspects of quantum chemistry, this author finds that solvation modeling is often treated by users more as engineering than science, in the sense that acronyms are quoted from software manuals and models are used seemingly without introspection. A primary goal of the present work is to elucidate the underlying physics of these models, which is not monolithic, emphasizing both similarities and differences between various approaches.

2 | CONTINUUM ELECTROSTATICS

This section reviews the basic electrostatic formalism that underlies continuum solvation theory. The physical model is defined by Poisson's equation in three-dimensional space (Section 2.1) but is not fully specified without a surface to demarcate the boundary of the atomistic region (Section 2.2). The PCM approach is introduced in Section 2.3 as a reformulation of the Poisson problem into a boundary-element or "apparent surface charge" (ASC) method. Common variants of the PCM approach are compared side-by-side in Section 2.4.

2.1 | Poisson's equation

The basic tenet of dielectric continuum theory is an assumption that the electric response of a given medium can be coarse-grained in the form of a dipole density $\mathbf{P}(\mathbf{r})$ that defines the macroscopic polarization. In the presence of a dielectric medium, the role of the electric field $\mathbf{E}(\mathbf{r})$ in vacuum is supplanted by the electric displacement field (or electric induction) $\mathbf{D}(\mathbf{r})$, which is defined as

$$\mathbf{D}(\mathbf{r}) = \mathbf{E}(\mathbf{r}) + 4\pi\mathbf{P}(\mathbf{r}) = \varepsilon(\mathbf{r})\mathbf{E}(\mathbf{r}) \ . \tag{2.1}$$

The electric permittivity $\varepsilon(\mathbf{r})$ is defined by the manner in which polarization $\mathbf{P}$ is induced by the external field $\mathbf{E}$, and Equation (2.1) amounts to the definition of a *linear* dielectric material, whose polarization is proportional to field strength. Nonlinear susceptibilities are harder to describe within a continuum formalism and have received less attention.[13] Whereas a fully general discussion of (linear) dielectric materials would allow for a permittivity that is a function of frequency also (or even a nonlocal function of space and/or time, in some formulations),[36–39] the ground-state SCRF problem does not require such generality. Unless otherwise specified, ε will mean the *static* (zero-frequency) dielectric constant, ε_s. (The continuum electrostatics community has stubbornly resisted the suggestion[40] that "dielectric constant" is obsolete nomenclature that should be replaced by "relative electric permittivity".) If the medium is anisotropic, then the scalar ε is replaced by a 3×3 tensor, which could be used to model a liquid crystal in which the electric susceptibility depends on the orientation of the applied field.[41,42] Such cases are not considered in this review, although a different form of anisotropic solvation is considered in Section 6. Herein, ε is a scalar.

That said, Equation (2.1) does express the permittivity as a scalar-valued *function*, $\varepsilon(\mathbf{r})$, rather than simply a dielectric *constant*. This allows for a situation such as that depicted in Figure 1b, wherein a "solute cavity" (two-dimensional surface Γ) defines an interface between the continuum solvent and an atomistic region. Within the cavity, Coulomb interactions between electrons and nuclei are included explicitly in the Hamiltonian and therefore $\varepsilon = 1$ in this region. Outside of the cavity, $\varepsilon(\mathbf{r}) \equiv \varepsilon_s$. Given a charge density $\rho(\mathbf{r})$ for the solute, including both nuclei and electrons, Maxwell's equation for the displacement field $\mathbf{D}(\mathbf{r})$ is

$$\hat{\nabla}\cdot\mathbf{D}(\mathbf{r}) = 4\pi\rho(\mathbf{r}), \tag{2.2}$$

which can be rewritten in the more familiar form of *Poisson's equation*,

$$\hat{\nabla}\cdot\left[\varepsilon(\mathbf{r})\hat{\nabla}\varphi(\mathbf{r})\right] = -4\pi\rho(\mathbf{r}), \tag{2.3}$$

upon recognizing that the electric field $\mathbf{E}(\mathbf{r}) = -\hat{\nabla}\varphi(\mathbf{r})$ stems from the gradient of the electrostatic potential, $\varphi(\mathbf{r})$. All of these equations are expressed in Gaussian electrostatic units, where $4\pi\varepsilon_0 = 1$.[43]

Poisson's equation is the mathematical starting point for continuum electrostatics. Given $\rho(\mathbf{r})$ from an electronic structure calculation, Equation (2.3) is solved for $\varphi(\mathbf{r})$ throughout space, including both the atomistic region and the surrounding dielectric medium. This potential can be separated into two parts,

$$\varphi(\mathbf{r}) = \varphi^{\rho}(\mathbf{r}) + \varphi_{\text{rxn}}(\mathbf{r}), \tag{2.4}$$

where the first term is the electrostatic potential generated by the solute's charge density:

$$\varphi^{\rho}(\mathbf{r}) = \int \frac{\rho(\mathbf{r}')}{\|\mathbf{r}-\mathbf{r}'\|} d\mathbf{r}'. \tag{2.5}$$

The quantity $\varphi_{\text{rxn}}(\mathbf{r})$ is a "reaction field" arising from the polarization of the continuum, which results in an additional charge density $\rho_{\text{pol}}(\mathbf{r})$. Having obtained $\rho(\mathbf{r})$ from Schrödinger's equation and then $\varphi(\mathbf{r})$ by solving Equation (2.3), the electrostatic solvation energy can be expressed variously as[22,44]

$$\mathcal{G}_{\text{elst}} = \frac{1}{2}\int \varphi_{\text{rxn}}(\mathbf{r})\ \rho(\mathbf{r})\ d\mathbf{r} = \frac{1}{2}\int \varphi^{\rho}(\mathbf{r})\ \rho_{\text{pol}}(\mathbf{r})\ d\mathbf{r}. \tag{2.6}$$

In this review, we refer to $\mathcal{G}_{\text{elst}}$ as the *electrostatic energy* because that is the terminology that is typically used in the textbook theory of dielectric materials,[43] but the same quantity is sometimes called the *polarization energy*, $\mathcal{G}_{\text{pol}}$.[22] It makes little sense to separate electrostatics from polarization in this context, although the reader may (if desired) substitute the phrase "electrostatics + polarization" wherever "electrostatics" is used herein. In any case, $\mathcal{G}_{\text{elst}}$ is a *free* energy insofar as the dielectric formalism implicitly accounts for averaging over solvent degrees of freedom. The factor of 1/2 in Equation (2.6) reflects the fact that the interaction energy is reduced, by precisely half its value, on account of the work required to polarize the environment.[9,22,45–47] (This is exemplified by the charging work in the Born ion model,[46] and is valid within linear-response (LR) theory. Alternative justifications for the factor of 1/2 can also be made.[9])

From the point of view of electronic structure theory, $\mathcal{G}_{\text{elst}}[\varepsilon,\rho]$ is a functional of both the permittivity $\varepsilon(\mathbf{r})$ and the solute's charge density, $\rho(\mathbf{r})$. The total (free) energy is

$$\mathcal{G}_0[\Psi] = \langle\Psi|\hat{\mathscr{H}}_{\text{vac}}|\Psi\rangle + \mathcal{G}_{\text{elst}}[\varepsilon,\rho]. \tag{2.7}$$

The first term represents the gas-phase energy functional $\mathcal{U}[\Psi] = \langle\Psi|\hat{\mathscr{H}}_{\text{vac}}|\Psi\rangle$ and would equal the electronic energy *in vacuo* if $|\Psi\rangle$ were the gas-phase wave function. Upon solution of the SCRF problem, however, the wave function is polarized by the medium so the numerical value of $\mathcal{U}$ is not equal to the gas-phase energy. The total energy functional $\mathcal{G}_0[\Psi]$ can also be expressed as

$$\mathcal{G}_0[\Psi] = \left\langle\Psi\middle|\hat{\mathscr{H}}_{\text{vac}} + \frac{1}{2}\hat{\mathscr{R}}_0\middle|\Psi\right\rangle, \tag{2.8}$$

in which $\hat{\mathscr{R}}_0$ is a reaction-field operator that generates the integral in Equation (2.6).[48] For electronic structure models based on density functional theory (DFT), the Schrödinger energy functional $\mathcal{U}[\Psi]$ is replaced by a functional $\mathcal{U}[\rho]$, but the continuum formalism is unchanged. Minimization of either $\mathcal{G}_0[\Psi]$, or $\mathcal{G}_0[\rho]$, in conjunction with Poisson's equation to obtain the electrostatic potential that defines $\hat{\mathscr{R}}_0$, defines the SCRF problem. If the electronic structure model satisfies a variational principle, as it does for self-consistent field (SCF) models, then the total energy defined by Equation (2.7) satisfies a variational principle as well.[22,49]

Equation (2.3) is sometimes called the "generalized" form of Poisson's equation, with the "ordinary" form being

$$\varepsilon \hat{\nabla}^2 \varphi(\mathbf{r}) = -4\pi\rho(\mathbf{r}). \tag{2.9}$$

The distinction is that the permittivity function $\varepsilon(\mathbf{r})$ in Equation (2.3) is replaced by a scalar in Equation (2.9). The ordinary form of Poisson's equation is often taken to define the continuum electrostatics problem, but this requires additional specification because $\varepsilon = 1$ in atomistic QM calculations. Some sort of molecular surface is needed to delineate the boundary with the continuum, as shown in Figure 1 where the cavity is defined by a union of atom-centered spheres. Given a cavity surface, Equation (2.9) is shorthand for Equation (2.3) with the permittivity function

$$\varepsilon(\mathbf{r}) = \begin{cases} \varepsilon_{\text{in}}, & \mathbf{r} \in \Omega \\ \varepsilon_{\text{out}}, & \mathbf{r} \notin \Omega \end{cases}. \tag{2.10}$$

Note that $\varphi(\mathbf{r})$ is continuous across the cavity surface but its derivative is not,[9] as becomes obvious when the first $\hat{\nabla}$ in Equation (2.3) acts upon the step function $\varepsilon(\mathbf{r})$ in Equation (2.10). For QM applications it makes sense to set $\varepsilon_{\text{in}} = 1$, and in fact any other choice represents an inconsistent treatment of the Coulomb interactions unless the Coulomb operators that define $\hat{\mathscr{H}}_{\text{vac}}$ are modified, which is seldom done. In classical biomolecular electrostatics calculations, however, larger values (typically $\varepsilon_{\text{in}} = 2-4$,[7,50,51] but sometimes $\varepsilon_{\text{in}} = 10-20$[51–55]) are frequently employed in an effort to approximate a "dielectric constant of protein". It should be noted, however, that the very notion that such a "constant" exists has been vociferously criticized.[50,56–59] If the surrounding environment does not have orientational freedom then it is unclear that any single dielectric constant is appropriate; heterogeneous systems of this sort formally require a spatially nonlocal permittivity function, $\varepsilon(\mathbf{r}, \mathbf{r}')$.[60]

This discussion illustrates the fact that Equation (2.3) is widely used in classical electrostatics calculations,[61–64] even if the focus of the present work is on the QM-SCRF problem. In the classical case, $\rho(\mathbf{r})$ is comprised of point charges (or higher-order multipoles[65,66]) that come from a force field, for example,

$$\rho(\mathbf{r}) = \sum_{A}^{\text{atoms}} Q_A \delta(\mathbf{r} - \mathbf{R}_A). \tag{2.11}$$

Moreover, for biomolecular applications the aqueous solvent of interest often contains some concentration of dissolved ions. The continuum analogue of that situation is described by the *Poisson–Boltzmann equation*,[7,67–70]

$$\hat{\nabla} \cdot \left[\varepsilon(\mathbf{r}) \hat{\nabla} \varphi(\mathbf{r}) \right] = -4\pi[\rho(\mathbf{r}) + \rho_{\text{ions}}(\mathbf{r})], \tag{2.12}$$

in which the right side of Equation (2.3) is augmented with a term that accounts for a thermal distribution of "mobile" ions.[7,68] Whereas the solute's charge density $\rho(\mathbf{r})$ reflects atomistic modeling, the density $\rho_{\text{ions}}(\mathbf{r})$ is described statistically.[68,71] For an electrolyte with dissolved ion concentrations $\{c_i\}$, for a collection of species $i = 1, 2, \ldots$ whose individual ionic charges are denoted $\{Q_i\}$, the statistical charge density for the mobile ions is[7,72]

$$\rho_{\text{ions}}(\mathbf{r}) = \sum_{i}^{\text{ions}} Q_i c_i \lambda_i(\mathbf{r}) \exp\left(\frac{-Q_i \varphi(\mathbf{r})}{k_{\text{B}} T} \right). \tag{2.13}$$

Here, the *ion accessibility function* $\lambda_i(\mathbf{r})$ represents some type of step function to exclude the mobile ions from the atomistic region. The combination of Equation (2.13) with Equation (2.12) is sometimes known as the *size-modified* version of the (nonlinear) Poisson–Boltzmann equation.[7,73] In the case of a 1:1 electrolyte with monovalent ions ($Q_1 = e = -Q_2$), Equation (2.13) reduces to

$$\rho_{\text{ions}}(\mathbf{r}) = -2c\lambda(\mathbf{r}) \sinh\left(\frac{e\varphi(\mathbf{r})}{k_{\text{B}} T} \right). \tag{2.14}$$

At physiological ionic strengths, the hyperbolic sine function can be linearized without significant error,[74,75] resulting in

$$\hat{\boldsymbol{\nabla}}\left[\varepsilon(\mathbf{r})\hat{\boldsymbol{\nabla}}\varphi(\mathbf{r})\right] = -4\pi\rho(\mathbf{r}) + \kappa^2\lambda(\mathbf{r})\varphi(\mathbf{r}) \tag{2.15}$$

where

$$\kappa = \left(\frac{8\pi e^2 c}{k_{\mathrm{B}}T}\right)^{1/2}. \tag{2.16}$$

Equation (2.15) is known as the *linearized* Poisson–Boltzmann equation.[7,70] (Historically, it is the linearized version that was solved by Debye and Hückel,[76–78] for a spherical cavity surface.) The dissolved ions screen electrostatic interactions over a length scale $\sim\kappa^{-1}$ known as the *Debye screening length*, such that the potential that appears in Debye–Hückel theory is the Yukawa potential $e^{-\kappa r}/(\varepsilon_s r)$.[7,68,77–79]

Within the biomolecular electrostatics community there has been significant discussion regarding the accuracy of the linearization approximation, with various studies noting that the nonlinear form affords better agreement with explicit solvent simulations when the ionic strength is high.[75,80] Deficiencies in the Poisson–Boltzmann model itself (even in its nonlinear form and especially for polyvalent ions) have also been pointed out.[81] These arise due to statistical correlations between ion positions that are neglected by the model in Equation (2.13). It is therefore worth noting that for the small solutes that characterize most quantum chemistry applications, the effect of the mobile ions on $\mathcal{G}_{\mathrm{elst}}$ is quite modest,[73,79] although there are effects on activity coefficients.[73,82] These effects are presumably magnified for a solute the size of a protein, but the intermediate size regime has hardly been explored.

Methods for solving the partial differential equations introduced in this section will be described below. Before that, however, there is one more aspect of the model problem itself that must be considered, namely, the definition a surface to define the boundary between atomistic solute and continuum solvent.

2.2 | Solute cavity

For the case of a sharp dielectric boundary [Equation (2.10)], the generalized Poisson equation has an analytic solution if the cavity surface is spherical and contains the entire charge density $\rho(\mathbf{r})$. For a solute consisting of a single point charge, Q, centered in a spherical cavity of radius $\bar{R}$ in a medium with dielectric constant ε, this solution affords the well-known Born model,[46,83]

$$\Delta\mathcal{G}_Q = -\frac{Q^2}{2\bar{R}}\left(\frac{\varepsilon-1}{\varepsilon}\right). \tag{2.17}$$

Here, $\Delta\mathcal{G}$ indicates the change in $\mathcal{G}_{\mathrm{elst}}$ from its gas-phase value of zero to the solution-phase value obtained from Equation (2.6). Replacing the point charge Q by a point dipole μ, the solvation energy is

$$\Delta\mathcal{G}_\mu = -\frac{(\varepsilon-1)\mu^2}{(2\varepsilon+1)\bar{R}^3}. \tag{2.18}$$

(This result is often attributed to Onsager,[84] although it was derived somewhat earlier by Bell,[85] and is a special case of multipolar formulas derived by Kirkwood,[86] which also predate Onsager's work.) The dipole solvation energy can alternatively be written $\Delta\mathcal{G}_\mu = -\frac{1}{2}(\boldsymbol{\mu}\cdot\mathbf{E}_{\mathrm{rxn}})$, where

$$\mathbf{E}_{\mathrm{rxn}} = \underbrace{\frac{1}{\bar{R}^3}\left(\frac{2(\varepsilon-1)}{2\varepsilon+1}\right)}_{g_1(\varepsilon,\bar{R})}\boldsymbol{\mu} = g_1(\varepsilon,\bar{R})\boldsymbol{\mu} \tag{2.19}$$

is the "reaction field" induced by $\boldsymbol{\mu}$.[45] For a polarizable dipole ($\boldsymbol{\mu} = \boldsymbol{\mu}_0 + \boldsymbol{\alpha}\cdot\mathbf{E}_{\mathrm{rxn}}$), the reaction field feeds back into the value of the dipole moment.[45,87] This was the model considered by Onsager,[84] and it constitutes the earliest example of a SCRF model. It has been used to formulate a microscopic theory for the bulk dielectric constant in polar liquids,[84,87–91] going beyond the Clausius–Mossotti equation,[92,93] although the results are not particularly quantitative.[89]

For modern purposes, a dipolar description of the solute constitutes a needless approximation. The aforementioned results for $\Delta\mathcal{G}_Q$ and $\Delta\mathcal{G}_\mu$ are special cases of a general formula derived by Kirkwood,[86] which describes an arbitrary multipole centered in a spherical cavity. (These formulas have since been considered in detail by many others.[65,94–100]) Recognizing that any charge distribution has an expansion in spherical multipoles $\Theta_{\ell m} = \langle\Psi|\hat{\Theta}_{\ell m}|\Psi\rangle$, the general result is[98,100]

$$\mathcal{G}_{\mathrm{elst}} = -\frac{1}{2}\sum_{\ell\geq 0}\sum_{m=-\ell}^{\ell}\left[\frac{(\ell+1)(\varepsilon-1)}{\ell+(\ell+1)\varepsilon}\right]\frac{\Theta_{\ell m}^2}{\bar{R}^{2\ell+1}}. \tag{2.20}$$

This is often expressed in terms of reaction-field factors

$$g_\ell(\varepsilon,\bar{R}) = \left[\frac{(\ell+1)(\varepsilon-1)}{\ell+(\ell+1)\varepsilon}\right]\frac{1}{\bar{R}^{2\ell+1}}, \tag{2.21}$$

with the $\ell = 1$ factor appearing in Equation (2.19). Kirkwood's original result is actually more general, in that it allows a value $\varepsilon_{\mathrm{in}} \neq 1$ inside the cavity,[86] whereas Equation (2.20) holds for $\varepsilon_{\mathrm{in}} = 1$ and $\varepsilon_{\mathrm{out}} = \varepsilon$. In the many decades since Kirkwood's original result, analytic formulas have also been derived for multipoles centered in ellipsoidal cavities,[95,101] for off-center point charges[102] and higher-order off-center multipoles,[99] for multipoles in a layered dielectric material,[103,104] and for interactions between multipoles contained in disjoint spheres with a dielectric medium in between.[105] The point-multipole model has also been generalized to include frequency dependence $\varepsilon(\omega)$, within the Debye relaxation model.[106]

Insofar as any charge distribution $\rho(\mathbf{r})$ can be expressed in terms of a single-center multipole expansion, if carried to sufficiently high order, these analytic results provide a general solution to the continuum problem for charge distributions of arbitrary complexity in spherical or ellipsoidal cavities, assuming that there is no penetration of $\rho(\mathbf{r})$ into the continuum region. (The latter effect, known as *volume polarization*,[107–113] is discussed below.) Use of Equation (2.20) has been called a "generalized Kirkwood" solvation model,[65] a Kirkwood–Onsager model,[114,115] or simply "SCRF" in older literature. The latter term is ambiguous because any model that iterates the solute–continuum electrostatic interaction to self-consistency can be described as an SCRF model, including all of the PCMs described in Section 2.3 as well as methods based directly on Poisson's equation.[28,44] The term "Kirkwood–Onsager model" similarly risks confusion with the Onsager model of a polarizable point dipole. It is therefore less ambiguous, and also more straightforward, to refer to Equation (2.20) as the *multipolar expansion method*.[100] Using multipolar formulas for $\hat{\mathscr{R}}_0$ in Equation (2.8), this method can be turned into a multipolar SCRF for quantum chemistry. Multipolar methods are reviewed elsewhere,[9,116] but have largely been rendered obsolete by the PCMs described in Section 2.3. In the absence of volume polarization, the latter afford an exact (albeit numerical) solution to the continuum electrostatics problem but unlike the multipolar expansion formulas, PCMs can used in conjunction with a molecule-shaped cavity.

Spherical boundary conditions make more sense if a large number of explicit solvent molecules are included as part of the atomistic solute region, and such approaches are known as *solvent boundary potential* methods.[117–119] These have been developed as replacements for periodic boundary conditions in both QM/MM simulations[120–126] and in QM-only calculations.[127–130] Spherical cavities make little sense for single molecules, however, and it is clear from the multipolar formulas that $\Delta\mathcal{G}$ will be quite sensitive to the cavity radius. Onsager's suggestion for the radius is $\bar{R} = (3V_{\mathrm{m}}/4\pi N_{\mathrm{A}})^{1/3}$,[84] where V_{m} is the molar volume of the solute and N_{A} is Avogadro's constant, but this proves to be impossible to reconcile with the macroscopic dielectric constant, using any value of $\bar{R}$ that resembles molecular size.[91,131,132] Stated differently, there is no reason to expect that a cavity radius that affords the experimental solvation energy should coincide with a realistic estimate of molecular size. Even for molecule-shaped cavities, results in Section 3.3 demonstrate that $\mathcal{G}_{\text{elst}}$ is quite sensitive to cavity construction.

Examples of some molecule-shaped cavity constructions are provided in Figure 2. A simple union of atom-centered spheres is often called a *van der Waals* (vdW) cavity surface. The atomic radii might simply be empirical parameters of the model,[133] or they could be estimates of atomic radii that are either calculated[134] or deduced from crystal structures.[135,136] In the case that the radii are intended to represent realistic measures of atomic size, the implicit solvent should not be allowed to approach all the way to the vdW radii of the solute atoms. This exclusion effect can be incorporated in several ways, most commonly by scaling the atomic vdW radii by a factor $\alpha_{\text{vdW}} > 1$. A scaling factor $\alpha_{\text{vdW}} = 1.2$ was used in early models,[137] and factors $\alpha_{\text{vdW}} \approx 1.1 - 1.2$ have since become standard choices, albeit with little theoretical justification to choose one value over another within a modest range. Alternatively, and with somewhat better justification, the atomic vdW radii can be augmented by a "probe radius" representing the assumed size of a solute molecule, which can be estimated from the liquid structure of the neat solvent. For example, the value $R_{\text{probe}} = 1.4$ Å is often used for water, representing half the distance to the first peak in the oxygen–oxygen radial distribution function.[138] However, values for water as small as $R_{\text{probe}} = 0.2$ Å have sometimes been used in an effort to match solvation energy benchmarks from simulations with explicit solvent.[139] The cavity surface generated using atomic radii $R_A = R_{\text{vdW},A} + R_{\text{probe}}$ is known as the *solvent-accessible surface* (SAS), which was first introduced in the context of protein crystallography, as a means to measure accessible surface area. The SAS is often used to define the ion accessibility function $\lambda(\mathbf{r})$ in Equation (2.15). Note that it does not make sense to augment a scaled vdW radius ($R_A = \alpha_{\text{vdW}} R_{\text{vdW},A}$) with a probe radius, as that would double-count the size of the exclusion layer.

Both the vdW surface and the SAS exhibit cusps where atomic spheres intersect. These cusps are eliminated in the *solvent-excluded surface* (SES) that is generated by the probe sphere as it rolls over the vdW surface; see Figure 2. (In principle, this procedure could be applied to eliminate cusps in the SAS as well, however those cusps are less problematic, numerically speaking.[25]) The center of the probe sphere traces out the SAS while its points of contact with the vdW surface, combined with concave arcs of the probe sphere that smooth over the cusps, constitute the SES. The SES is also known as the Connolly surface,[140] or sometimes simply the "molecular surface,"[141] as it is intended to approximate the true shape of the molecule. However, these names have sometimes been used interchangeably or ambiguously in the literature,[142] and in particular the term "Lee-Richards surface"[143] has been used to mean either the SAS or the SES.[25,139,142] (The nomenclature used here is standard in the quantum chemistry literature, however.[144]) The SES has an analytic construction,[25,140] although it has most often been constructed numerically, for visualization purposes.[145–148]

To a greater or lesser degree, each of these cavity definitions seems physically reasonable. Beyond that, there is little theoretical justification for any of them, and no guarantee that small changes in the atomic radii will not have a significant impact on computed observables.[113,149] It has been suggested that the "optimal" atomic radius for a given atom likely ought to vary as a function of its partial atomic charge,[150,151] and probably as a function of the solvent's dielectric constant as well.[94,132,152,153] In quantum chemistry, the latter effect is generally neglected whereas the former is handled

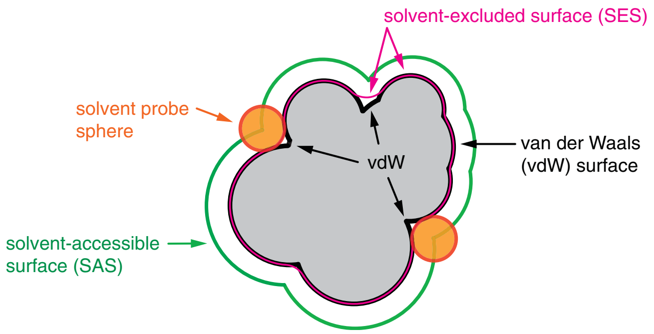

FIGURE 2 Various constructions of the solute cavity surface, using a set of atomic spheres (in gray) whose envelope defines the van der Waals (vdW) surface, shown in black. The solvent-accessible surface (SAS, in green) is defined either by augmenting the atomic radii by a probe radius ($R_A = R_{\text{vdW},A} + R_{\text{probe}}$) or equivalently as the center point of the probe sphere as it rolls over the vdW surface. (In the example that is shown, R_{probe} is smaller than any of the vdW radii.) The solvent-excluded surface (SES, in magenta) is traced out by arcs of the probe that connect points of contact between the probe and the vdW surface. The SES, which has sometimes been called simply the "molecular surface," eliminates cusps that appear in the vdW surface along seams of intersection between atom-centered spheres

empirically, if at all. A less empirical definition uses an isocontour of the molecule's own charge density $\rho(\mathbf{r})$ to define the cavity surface,[110,112,154–156] recognizing that $\rho(\mathbf{r})$ is ultimately responsible for molecular size and shape. The isodensity definition is technically challenging, however. It is discussed further in Section 3.3.

With the introduction of a molecule-shaped cavity, one must forego analytic solution of Poisson's equation. A variety of numerical algorithms have been introduced,[72] both for classical biomolecular applications[157–167] and for electronic structure calculations.[44,168–170] The Poisson and Poisson–Boltzmann equations are partial differential equations for $\varphi(\mathbf{r})$, whose solution requires discretization of three-dimensional space extending well into the continuum region. Slow asymptotic decay, $\varphi(r) \sim (\varepsilon r)^{-1}$, necessitates the use of multiresolution techniques for efficiency.[44,63,70,157,159,167] Worth mentioning also is the Langevin dipoles model,[171–173] which discretizes the continuum solvent using a three-dimensional grid of point dipoles, and is therefore a direct realization of the conceptual notion that $\mathbf{P}$ is a dipole density. As compared to these approaches, each of which requires discretization of three-dimensional space, a much more efficient two-dimensional formulation of the continuum electrostatics problem is often feasible. Transformation of the continuum electrostatics problem into an integral equation defined on the cavity surface Γ forms the mathematical basis underlying the class of methods known as PCMs,[13–15] which are described next.

2.3 | Polarizable continuum models

In quantum chemistry, PCMs are so ubiquitous as to be nearly synonymous with continuum solvation itself. This popularity stems from efficiency, which in turn derives from a transformation of the volumetric polarization theory embodied by the Poisson and Poisson–Boltzmann equations (Section 2.1) into a surface charge problem that can be solved far more efficiently, using numerical methods that are described in Section 3.2. This transformation, and basic working equations for PCMs, are introduced in this section.

Physically speaking, polarization of the continuum extends beyond the solute cavity surface, as indicated pictorially in Figure 1b. Transformation of the three-dimensional polarization problem into a two-dimensional problem defined on the cavity surface Γ thus relies on a characteristic feature of a sharp dielectric interface, namely, a discontinuity in the electric field and a concomitant buildup of charge at the interface. This occurs at any dielectric interface, including the one that defines the boundary between atomistic solute and continuum solvent. Let $\mathbf{s}\in\Gamma$ denote a point on the solute cavity surface, and let $\mathbf{n_s}$ be the outward-pointing unit vector normal to the cavity surface at the point $\mathbf{s}$. At a sharp interface in the electric permittivity, as in Equation (2.10), the surface-normal component of the electric field satisfies a "jump" boundary condition:[9,72,108]

$$\varepsilon_{\text{out}}(\mathbf{n_s}\cdot\hat{\boldsymbol{\nabla}})\varphi(\mathbf{s})\big|_{\mathbf{s}=\mathbf{s}^+} = \varepsilon_{\text{in}}(\mathbf{n_s}\cdot\hat{\boldsymbol{\nabla}})\varphi(\mathbf{s})\big|_{\mathbf{s}=\mathbf{s}^-}. \tag{2.22}$$

This ensures that the electric displacement $\mathbf{D}(\mathbf{r}) = \varepsilon(\mathbf{r})\,\mathbf{E}(\mathbf{r})$ is continuous across the interface.[43,45] The notation $\mathbf{s}^{\pm}$ indicates that these are one-sided derivatives, to be evaluated either immediately inside ($\mathbf{s}^-\in\Omega$) or outside ($\mathbf{s}^+\notin\Omega$) of the solute cavity, since φ is only semi-differentiable at the interface.

Polarization of the continuum manifests as a surface charge that accumulates at the boundary between the atomistic and continuum regions, in order to satisfy Equation (2.22), and whose magnitude is proportional to the normal electric field at the dielectric interface.[43] Let us call that charge $\sigma(\mathbf{s})$, where $\mathbf{s}\in\Gamma$, so as to distinguish it from a volume charge such as $\rho(\mathbf{r})$, where $\mathbf{r}\in\mathbb{R}^3$. Introducing the notation $\hat{\partial}_{\mathbf{s}} = \mathbf{n_s}\cdot\hat{\boldsymbol{\nabla}}$ to indicate the normal derivative, the surface charge at the dielectric boundary can be expressed in several equivalent ways,[14,108] two of which are

$$\sigma(\mathbf{s}) = \frac{1}{4\pi}\left(\frac{\varepsilon_{\text{out}}-\varepsilon_{\text{in}}}{\varepsilon_{\text{in}}}\right)\hat{\partial}_{\mathbf{s}}\varphi(\mathbf{s})\bigg|_{\mathbf{s}=\mathbf{s}^+} = \frac{1}{4\pi}\left(\frac{\varepsilon_{\text{out}}-\varepsilon_{\text{in}}}{\varepsilon_{\text{out}}}\right)\hat{\partial}_{\mathbf{s}}\varphi(\mathbf{s})\bigg|_{\mathbf{s}=\mathbf{s}^-}. \tag{2.23}$$

These differ depending on whether the normal electric field is evaluated immediately inside or outside of the cavity. In the usual quantum chemistry case where $\varepsilon_{\text{in}} = 1$ and $\varepsilon_{\text{out}} = \varepsilon_{\text{s}}$, the first form of this equation (in which the field is evaluated within the continuum region) is merely the definition of the polarization,

$$\mathbf{P} = \left(\frac{\varepsilon_{\mathrm{s}}-1}{4\pi}\right)\mathbf{E}, \tag{2.24}$$

as obtained from Equation (2.1). If the entirety of the solute charge $\rho(\mathbf{r})$ is confined within the cavity surface, then Equation (2.23) is simply a reflection of Gauss' law. For cavities that are realistic approximations to the size and shape of a molecular solute, however, the tails of a QM charge distribution penetrate into the continuum region.[107–113] This outlying or "escaped" charge is discussed in more detail below, but will be ignored for now.

It has been argued that the second form of Equation (2.23), in which the derivative is evaluated inside of the cavity, should be used in order to avoid "self-polarization" of the medium.[9] Then taking $\varepsilon_{\mathrm{in}} = 1$ and $\varepsilon_{\mathrm{out}} = \varepsilon_{\mathrm{s}}$ and recognizing that $\mathbf{E} = -\hat{\boldsymbol{\nabla}}\varphi$, one obtains a model

$$\sigma(\mathbf{s}) = -\frac{1}{4\pi}\left(\frac{\varepsilon_{\mathrm{s}}-1}{\varepsilon_{\mathrm{s}}}\right)\underbrace{[\mathbf{E}^{\rho}(\mathbf{s})+\mathbf{E}^{\sigma}(\mathbf{s})]\cdot\mathbf{n}_{\mathbf{s}}}_{E_{\perp}(\mathbf{s})} = \frac{1}{4\pi}\left(\frac{\varepsilon_{\mathrm{s}}-1}{\varepsilon_{\mathrm{s}}}\right)\left(\frac{\partial\varphi}{\partial\mathbf{n}_{\mathbf{s}}}\right)_{\mathbf{s}=\mathbf{s}^{-}} \tag{2.25}$$

that corresponds to the original PCM introduced by Tomasi and coworkers.[3–5,9] Here, the induced surface charge density $\sigma(\mathbf{s})$ is proportional to $E_{\perp}(\mathbf{s}) = \mathbf{E}(\mathbf{s}) \cdot \mathbf{n}_{\mathbf{s}}$, which is separated into two contributions in Equation (2.25), analogous to how $\varphi(\mathbf{r})$ is partitioned in Equation (2.4). One contribution to the electric field is $\mathbf{E}^{\rho} = -\hat{\boldsymbol{\nabla}}\varphi^{\rho}$, which comes directly from the solute, whereas the reaction-field contribution is $\mathbf{E}^{\sigma} = -\hat{\boldsymbol{\nabla}}\varphi^{\sigma}$ with

$$\varphi^{\sigma}(\mathbf{r}) = \int_{\mathbf{s}\in\Gamma} \frac{\sigma(\mathbf{s})}{\|\mathbf{s}-\mathbf{r}\|} d\mathbf{s}. \tag{2.26}$$

To compute $\varphi^{\sigma}(\mathbf{r})$, it is only necessary to discretize the cavity surface Γ rather than the whole of three-dimensional space. Historically, Equation (2.25) was the first example of an ASC formulation of the continuum electrostatics problem. In contemporary quantum chemistry, the term "ASC model" is essentially synonymous with PCM; multipolar expansions and other simplified treatments see very little use, because the model defined by Equation (2.25) makes it easy to use the exact charge density $\rho(\mathbf{r})$, in conjunction with a cavity of arbitrary shape. For a spherical cavity, Equation (2.25) is equivalent to the use of the Kirkwood multipolar expansion formulas if the latter are carried to arbitrary order.[174]

In early literature, the model defined by Equation (2.25) was often called "the" ASC-PCM,[9] whereas in contemporary literature it is usually called D-PCM.[13,15] The somewhat arbitrary decision to use the second form of Equation (2.23) can be avoided by noting that the discontinuity in $E_{\perp}$ at the cavity surface can be expressed as[108]

$$\hat{\partial}_{\mathbf{s}}\varphi^{\sigma}(\mathbf{s})|_{\mathbf{s}=\mathbf{s}^{-}} = 2\pi\sigma(\mathbf{s}) + \hat{\partial}_{\mathbf{s}}\varphi^{\sigma}(\mathbf{s}), \tag{2.27a}$$

$$\hat{\partial}_{\mathbf{s}}\varphi^{\sigma}(\mathbf{s})|_{\mathbf{s}=\mathbf{s}^{+}} = -2\pi\sigma(\mathbf{s}) + \hat{\partial}_{\mathbf{s}}\varphi^{\sigma}(\mathbf{s}). \tag{2.27b}$$

Adding these two equations and combining them with Equation (2.23) affords a different expression for the surface charge,[108,174,175] namely

$$\sigma(\mathbf{s}) = \left(\frac{f_{\varepsilon}}{2\pi}\right)\hat{\partial}_{\mathbf{s}}[\varphi^{\rho}(\mathbf{s}) + \varphi^{\sigma}(\mathbf{s})], \tag{2.28}$$

in which the normal derivative is evaluated *at* (rather than *near*) the point $\mathbf{s}\in\Gamma$. The permittivity-dependent prefactor in this expression is

$$f_{\varepsilon} = \frac{\varepsilon_{\mathrm{out}} - \varepsilon_{\mathrm{in}}}{\varepsilon_{\mathrm{out}} + \varepsilon_{\mathrm{in}}}. \tag{2.29}$$

For a QM solute the only sensible choice is $\varepsilon_{\text{in}} = 1$, and much of the literature assumes this *a priori*. (For an exception, see Ref. 176.) The more general notation in Equation (2.29) is retained for now, in order to accommodate different values of ε_{in} that are sometimes used in biomolecular electrostatics calculations.[7,50–55]

The model of Equation (2.28) can be recast in a convenient form by defining an operator $\hat{D}^{\dagger}$ that acts on surface functions according to[110–112]

$$\hat{D}^{\dagger}\sigma(\mathbf{s}) = \int_{\Gamma} d\mathbf{s}'\sigma(\mathbf{s}')\frac{\partial}{\partial \mathbf{n}_{\mathbf{s}}}\left(\frac{1}{\|\mathbf{s}-\mathbf{s}'\|}\right) = -E_{\perp}^{\sigma}(\mathbf{s}). \tag{2.30}$$

The first equality defines $\hat{D}^{\dagger}$ and the second follows upon realization that $\partial/\partial\mathbf{n}_{\mathbf{s}} = \mathbf{n}_{\mathbf{s}}\cdot\hat{\boldsymbol{\nabla}}$ can be pulled outside of the integral, leaving $(\mathbf{n}_{\mathbf{s}}\cdot\hat{\boldsymbol{\nabla}})\varphi^{\sigma}(\mathbf{s}) = -E_{\perp}^{\sigma}(\mathbf{s})$. The operator $\hat{D}^{\dagger}$ is often called $\hat{D}^{*}$ in the literature,[110–112,176,177] but the notation used here reflects the fact that $\hat{D}^{\dagger}$ is the adjoint of the double-layer operator $\hat{D}$ that is introduced below. Using $\hat{D}^{\dagger}$ to rewrite Equation (2.28) affords an alternative to Equation (2.25), namely

$$\left[\left(\frac{2\pi}{f_{\varepsilon}}\right)\hat{1} - \hat{D}^{\dagger}\right]\sigma(\mathbf{s}) = -E_{\perp}^{\rho}(\mathbf{s}). \tag{2.31}$$

This equation makes clear that the sole ingredient needed to determine the induced surface charge is

$$E_{\perp}^{\rho}(\mathbf{s}) = -\left(\mathbf{n}_{\mathbf{s}}\cdot\hat{\boldsymbol{\nabla}}\right)\varphi^{\rho}(\mathbf{s}) = -\left(\frac{\partial\varphi^{\rho}}{\partial\mathbf{n}_{\mathbf{s}}}\right), \tag{2.32}$$

which is the surface-normal electric field originating with the solute. Chipman refers to Equation (2.31) as the *surface polarization for electrostatics* (SPE) method,[111] but others have called it D-PCM,[177] or simply PCM,[178] though the latter is ambiguous and should be discouraged.

The D-PCM approach, which requires explicit calculation of the electric field at the cavity surface, has been largely superseded by alternative ASC-PCMs that determine $\sigma(\mathbf{s})$ using only the electrostatic potential and not its derivatives, as the latter may be more sensitive to discretization error. The modern approach is known as the *integral equation formalism* (IEF-) PCM,[177,179] and is based on a reformulation of the continuum electrostatics problem as a boundary-value problem.[180–182] This reformulation is exact provided that the escaped charge is zero (e.g., for a classical solute), and we continue to defer a discussion of the escaped charge problem. IEF-PCM is formulated in terms of integral operators $\hat{S}$ and $\hat{D}$ that, in the language of integral equations,[177] act on surface functions to generate the single- and double-layer potentials, respectively. These operators are defined by

$$\hat{S}\sigma(\mathbf{s}) = \int_{\Gamma} d\mathbf{s}'\frac{\sigma(\mathbf{s}')}{\|\mathbf{s}'-\mathbf{s}\|} = \varphi^{\sigma}(\mathbf{s}), \tag{2.33}$$

which generates the electrostatic potential associated with the surface charge distribution $\sigma(\mathbf{s})$, and

$$\hat{D}\sigma(\mathbf{s}) = \int_{\Gamma} d\mathbf{s}'\sigma(\mathbf{s}')\underbrace{\frac{\partial}{\partial\mathbf{n}_{\mathbf{s}'}}\left(\frac{1}{\|\mathbf{s}'-\mathbf{s}\|}\right)}_{D(\mathbf{s},\mathbf{s}')}, \tag{2.34}$$

which generates the double-layer potential. The operator $\hat{D}$ is the adjoint of $\hat{D}^{\dagger}$ in Equation (2.30),[13] as becomes clear upon reversing the indices of the kernel $D(\mathbf{s}, \mathbf{s}')$. Using $\hat{S}$ and $\hat{D}$, the continuum electrostatics problem can be recast as an integral equation on the surface of the cavity:[13]

$$\left[\left(\frac{2\pi}{f_{\varepsilon}}\right)\hat{1} - \hat{D}\right]\hat{S}\sigma(\mathbf{s}) = \left(-2\pi\hat{1} + \hat{D}\right)\varphi^{\rho}(\mathbf{s}). \tag{2.35}$$

Equation (2.35) is the basic working equation of IEF-PCM. In early papers, the working equation was formulated somewhat differently and required $E_{\perp}^{\rho}$ in addition to φ^{ρ}.[180–182] That form is sometimes called simply "IEF,"[111,177] to distinguish it from IEF-PCM, the latter of which requires φ^{ρ} but not its derivative and should therefore be more stable towards discretization. Equivalence of the two forms is demonstrated in Ref. 183. In fact, Equation (2.35) can be cast into a variety of equivalent forms,[110,111,177] by taking advantage of the fact that $\hat{S} = \hat{S}^{\dagger}$ and

$$\hat{D}\hat{S} = \hat{S}\hat{D}^{\dagger}. \tag{2.36}$$

However, except for spherical cavities (for which $\hat{D} = \hat{D}^{\dagger}$),[110] the operator identity in Equation (2.36) is typically not preserved upon discretization,[24,178] with the practical result that various forms of Equation (2.35) are *inequivalent* as finite-dimensional matrix equations.[23,24] This point is discussed further when these matrix equations are introduced in Section 3.1.

For now, we simply note that Equation (2.35) is an exact reformulation of the *classical* continuum electrostatics problem, meaning the problem that is defined by Poisson's equation with a sharp dielectric boundary and where the solute's charge density $\rho(\mathbf{r})$ is contained entirely within the cavity. For such cases, which includes any classical force-field description of the solute, the solution of Equation (2.35) for $\sigma(\mathbf{s})$ constitutes an exact solution to the electrostatics problem, and the electrostatic solvation energy is[22]

$$\mathcal{G}_{\text{elst}} = \frac{1}{2}\int_{\mathbb{R}^3} \varphi^{\sigma}(\mathbf{r})\ \rho(\mathbf{r})\ d\mathbf{r} = \frac{1}{2}\int_{\Gamma} \varphi^{\rho}(\mathbf{s})\ \sigma(\mathbf{s})\ d\mathbf{s}. \tag{2.37}$$

These integrals are analogous to the two forms of $\mathcal{G}_{\text{elst}}$ in Equation (2.6), but the second form in Equation (2.37) requires only surface integration. Use of this ASC formulation in lieu of discretizing three-dimensional space offers significant advantages over the traditional approach to biomolecular electrostatics, which require discretization far enough into the continuum such that $\varphi^{\rho}(\mathbf{r})$ has decayed to zero. Moreover, most contemporary biomolecular electrostatics calculations are based on finite-difference evaluation of the Laplacian $\hat{\nabla}^2\varphi(\mathbf{r})$ that appears in Poisson's equation,[184,185] but this leads to problems obtaining smooth forces for molecular dynamics.[186–188] In contrast, discretization of $\hat{D}\sigma(\mathbf{s})$ and $\hat{S}\sigma(\mathbf{s})$ can be accomplished in a manner that affords inherently smooth forces;[21–23] see Section 3.2. Especially for biomolecular applications, it is worth noting that IEF-PCM has been adapted to provide a solution to the linearized Poisson–Boltzmann problem,[79,180,181,189] including the "size-modified" version that accounts for the finite size of the mobile ions.[79] Large biomolecular solutes have been tackled in this way,[23,190–193] although this requires iterative solvers for the matrix equations that define the PCM. Linear-scaling implementations that can handle biomolecular solutes are discussed in Section 3.4.

For QM solutes there is always escaped charge for realistic cavity sizes, therefore IEF-PCM is not a fully equivalent substitute for Poisson's equation. The extent to which this is a problem is unclear from the original derivation of IEF-PCM provided by Cancès et al.,[177,180–182] which does not provide much physical insight, nor does it emphasize the assumption (inherent in the derivation) that there is no outlying charge. That issue was addressed directly by Chipman,[108–111] who assumes from the start that there is outlying charge and consequently the correct reaction-field potential is not $\varphi^{\sigma}(\mathbf{r})$ but rather

$$\varphi_{\text{rxn}}(\mathbf{r}) = \varphi^{\sigma}(\mathbf{r}) + \varphi^{\beta}(\mathbf{r}). \tag{2.38}$$

As above, $\varphi^{\sigma}(\mathbf{r})$ arises from the accumulation of charge $\sigma(\mathbf{s})$ at the dielectric interface, but in an exact formulation it must be accompanied by an additional potential $\varphi^{\beta}(\mathbf{r})$ due to "volume polarization," that is, polarization arising from the outlying charge. Introducing $\varphi^{\beta}(\mathbf{s})$ as an additional term contributing to the surface potential in Equation (2.28), and recognizing that $\hat{\partial}_{\mathbf{s}}\varphi^{\sigma}(\mathbf{s}) = \hat{D}^{\dagger}\sigma(\mathbf{s})$, an exact equation for $\sigma(\mathbf{s})$ that includes the effects of volume polarization is[110]

$$\begin{aligned}\left[\hat{1} - \left(\frac{f_{\varepsilon}}{2\pi}\right)\hat{D}^{\dagger}\right]\sigma(\mathbf{s}) &= \frac{f_{\varepsilon}}{2\pi}\left[\hat{\partial}_{\mathbf{s}}\varphi^{\rho}(\mathbf{s}) + \hat{\partial}_{\mathbf{s}}\varphi^{\beta}(\mathbf{s})\right] \\ &= -\frac{f_{\varepsilon}}{2\pi}\left[E_{\perp}^{\rho}(\mathbf{s}) + E_{\perp}^{\beta}(\mathbf{s})\right].\end{aligned} \tag{2.39}$$

The potential $\varphi^{\beta}(\mathbf{r})$ can be modeled as the electrostatic potential generated by a charge density

$$\beta(\mathbf{r}) = \begin{cases} 0 & \text{for } \mathbf{r}\in\Omega \\ \left(\varepsilon_{\text{out}}^{-1} - \varepsilon_{\text{in}}^{-1}\right)\rho(\mathbf{r}) & \text{for } \mathbf{r}\notin\Omega \end{cases}, \tag{2.40}$$

and this density satisfies a vacuum-like Poisson equation

$$\hat{\nabla}^2 \varphi^\beta(\mathbf{r}) = -4\pi\beta(\mathbf{r}). \tag{2.41}$$

Numerical solution of Equations (2.39) and (2.41) constitutes an exact solution to the continuum electrostatics problem,[107] even in the presence of outlying charge. Chipman refers to this approach as the *surface and volume polarization for electrostatics* (SVPE) method.[111] It is challenging in practice, because the volume charge density $\beta(\mathbf{r})$ is discontinuous at the cavity surface, but Equation (2.39) can be recast into a form that requires only the surface-normal electric field $E_\perp^\rho(\mathbf{s})$ along with the solution of the ASC-PCM that is introduced next.[112] This provides a practical means to access *exact* electrostatics, even in the presence of outlying charge, while staying within a two-dimensional surface integral (boundary-element) formalism.

A simplified (if approximate) treatment is possible that eliminates the normal electric field in Equation (2.39) and ultimately connects back to IEF-PCM. This model is obtained by introducing an additional surface charge $\alpha(\mathbf{s})$, distinct from $\sigma(\mathbf{s})$ and defined by the condition

$$\hat{S}\alpha(\mathbf{s}) = \varphi^\beta(\mathbf{s}). \tag{2.42}$$

This condition implies that the electrostatic potential $\varphi^\alpha = \hat{S}\alpha$ arising from $\alpha(\mathbf{s})$ must reproduce φ^β on the cavity surface, $\mathbf{s}\in\Gamma$.[107–110] This also ensures that $\varphi^\alpha(\mathbf{r}) = \varphi^\beta(\mathbf{r})$ for all interior points $\mathbf{r}\in\Omega$, and while the two potentials may differ *outside* of the cavity, those contributions are scaled by ε_s^{-1} and are therefore less important. (This is confirmed in numerical tests.[107,113]) Assuming that the true surface charge, augmented to reflect volume polarization, is $\tilde{\sigma}(\mathbf{s}) = \alpha(\mathbf{s}) + \sigma(\mathbf{s})$, the term $\hat{\partial}_\mathbf{s}\varphi^\beta(\mathbf{s})$ in Equation (2.39) can be manipulated into a form that is consistent with the ASC formalism.[110] The result is a model that Chipman calls *surface and simulation of volume polarization for electrostatics* [SS(V)PE],[110–112]

$$\underbrace{\hat{S}\left(\hat{1} - \frac{f_\varepsilon}{2\pi}\hat{D}^\dagger\right)}_{\hat{K}_\varepsilon}\tilde{\sigma}(\mathbf{s}) = \underbrace{f_\varepsilon\left(\frac{1}{2\pi}\hat{D} - \hat{1}\right)}_{\hat{Y}_\varepsilon}\varphi^\rho(\mathbf{s}). \tag{2.43}$$

Using the identity in Equation (2.36), this equation is easily rearranged to afford the IEF-PCM working equation in Equation (2.35); as such, SS(V)PE and IEF-PCM are equivalent at the level of integral operators.[110,111,183] (They differ in practice, as described in Section 3.1.) Importantly, what the derivation of SS(V)PE makes clear is that the surface charge determined by Equation (2.35) implicitly contains the (approximate) effects of volume polarization; this was not evident from the original derivation presented by Cancès and coworkers.[177,180–182] Chipman's derivation clarifies that both approaches constitute an exact treatment of continuum electrostatics in the limiting case that there is no escaped charge.

2.4 | Comparison of boundary-element methods

Section 2.3 introduced both exact and approximate reformulations of Poisson's equation within a surface integral or boundary-element formalism, so it is instructive to compare some of these methods side-by-side. Table 1 provides electrostatic solvation energies ($\mathcal{G}_{\text{elst}}$) for several small molecules and ions,[111] in both a nonpolar solvent (toluene, $\varepsilon_s = 2.4$) and in water ($\varepsilon_s = 78$). The SVPE method [Equation (2.39)] provides the exact result but the approximate SS(V)PE approach predicts $\mathcal{G}_{\text{elst}}$ to within 0.1 kcal/mol, smaller than typical discretization errors.[24] However, the SPE method of Equation (2.31), which is equivalent to the older D-PCM approach, exhibits noticeable differences, especially

TABLE 1 Electrostatic solvation energies in toluene ($\varepsilon_s = 2.4$) and in water ($\varepsilon_s = 78.3$), computed with various approaches.[a]

		$\mathcal{G}_{\text{elst}}$ (kcal/mol)					
					C-PCM[b]		
Solute	ε_s	**SVPE**	**SS(V)PE**	**SPE**	$\zeta = 0$	$\zeta = 1/2$	Q_{out} **(a.u.)**[c]
H_2O	2.4	−3.9	−3.9	−4.0	−4.8	−3.9	
CH_3CONH_2	2.4	−5.3	−5.0	−5.2	−5.9	−4.8	
NO^+	2.4	−52.2	−52.2	−55.3	−52.5	−43.4	
CN^-	2.4	−39.4	−39.4	−35.0	−39.4	−32.5	
H_2O	78.3	−8.6	−8.6	−8.7	−8.6	−8.6	−0.06
CH_3CONH_2	78.3	−10.9	−10.8	−11.1	−10.9	−10.8	−0.15
NO^+	78.3	−89.5	−89.5	−94.7	−89.5	−88.9	−0.07
CN–	78.3	−67.4	−67.3	−56.8	−67.3	−66.9	−0.17

Note: The SVPE method [Equation (2.39)] affords the exact result and SPE is the method in Equation (2.31).
[a]From Ref. 111. All calculations used an isodensity cavity with $\rho_0 = 0.001$ a.u.
[b]Using a renormalization factor $\tilde{f}_\varepsilon(\zeta)$; see Equation (2.46).
[c]From Ref. 113.

for ions. The amount of outlying charge (Q_{out}) is also quantified in Table 1. For future reference we note the obvious definition

$$Q_{\text{out}} = \int_{\mathbb{R}^3} \rho(\mathbf{r})\, d\mathbf{r} - Q_{\text{in}}, \tag{2.44a}$$

where

$$Q_{\text{in}} = \int_{\mathbf{r}\in\Omega} \rho(\mathbf{r})\, d\mathbf{r}. \tag{2.44b}$$

The charge density $\rho(\mathbf{r})$ includes both nuclei and electrons, so $Q_{\text{in}} + Q_{\text{out}} = 0$ for a neutral molecule. As typified by the examples in Table 1, the magnitude of the escaped charge is generally $|Q_{\text{out}}| \approx 0.1 - 0.2e$ for small solutes.[107,113]

By arbitrarily dropping the $\hat{D}$- and $\hat{D}^\dagger$-dependent terms in Equation (2.43), one obtains a model $\hat{S}\sigma = -f_\varepsilon \varphi^\rho$. Let us rewrite this as

$$\hat{S}\sigma(\mathbf{s}) = -\tilde{f}_\varepsilon(\zeta)\, \varphi^\rho(\mathbf{s}), \tag{2.45}$$

where the scaling factor

$$\tilde{f}_\varepsilon(\zeta) = \frac{\varepsilon_s - 1}{\varepsilon_s + \zeta} \tag{2.46}$$

is reminiscent of f_ε in Equation (2.29), with $\varepsilon_{\text{in}} = 1$ and $\varepsilon_{\text{out}} = \varepsilon_s$, but introduces a parameter ζ. The model defined by Equation (2.45) has a long history and a variety of names, one of which is the *conductor-like screening model* (COSMO), introduced by Klamt and coworkers.[194–197] The name hints at the original derivation: for a conductor ($\varepsilon_s = \infty$), the total electrostatic potential vanishes at the cavity surface and the ASC formulation of the Poisson problem is simply $\hat{S}\sigma = -\varphi^\rho$.[109] A scaling factor $\tilde{f}_\varepsilon(\zeta)$ is then introduced to account for the fact that ε_s is finite. With $\zeta = 0$, the model in Equation (2.45) has variously been called the *conductor-like PCM* (C-PCM),[198,199] or else "generalized COSMO" (GCOSMO).[200–203]

Note that the neglected double-layer operator embodies the electric field discontinuity at the cavity surface, and as a result the model defined by Equation (2.45) fails to satisfy the correct jump boundary condition.[79,177] Perhaps for this reason, Klamt and coworkers use a "dual cavity" implementation of this model,[194,196,204–206] in which Equation (2.45) is first solved using a SAS cavity and then the surface charge $\sigma(\mathbf{s})$ is projected inward, onto a smaller vdW cavity (i.e., omitting R_{probe} from the atomic radii). The smaller cavity is used to evaluate $\mathcal{G}_{\text{elst}}$. This strategy can be understood as an attempt to mimic the effects of the double-layer operator, $\hat{D}$, although it is discussed by Klamt and coworkers as a correction for outlying charge.[196] These authors claim that dual-cavity COSMO is less sensitive to outlying charge as compared to what they characterize as "dielectric boundary conditions" (meaning other PCMs),[196,204] but this is simply a reflection of the fact that the outlying charge is smaller when the cavity is larger. Equation (2.45) for $\sigma(\mathbf{s})$ is solved using the same boundary conditions as any other ASC-PCM. By way of nomenclature, the term "COSMO" should probably be reserved for a dual-cavity implementation of Equation (2.45), since the model has been implemented in this way across several different electronic structure programs.[194,204,207–209] The term "C-PCM" can be used for the single-cavity implementation, with $\zeta = 0$ unless otherwise specified. The literature is not always consistent with this convention, however. Whereas the term "C-PCM" almost always implies a single-cavity construction (like other PCMs), "COSMO" has been used for both single- and dual-cavity implementations of Equation (2.45).

The earliest applications of COSMO set $\zeta = 1/2$,[194–196] but much later the value $\zeta = 0$ was recommended for ions.[210] Some justification for these choices can be found in the reaction-field factors that appear in the multipole expansion method, whose form suggests $\zeta = \ell/(\ell+1)$ for an ℓth-order multipole in a spherical cavity [*cf.* Equation (2.21)]. Thus $\tilde{f}_{\varepsilon}(0)$ looks like the ε-dependent factor in the Born ion model [Equation (2.17)] while $\tilde{f}_{\varepsilon}(1/2)$ affords the prefactor for dipole solvation in a spherical cavity [Equation (2.18)]. These are the leading-order multipolar terms for ionic and neutral solutes, respectively. At a pragmatic level, setting $\zeta = 1/2$ for neutral solutes and $\zeta = 0$ for ions works remarkably well in comparison to the IEF-PCM and SS(V)PE methods, even in low-dielectric solvents. This is suggested by the smattering of data for C-PCM (single-cavity construction) in Table 1,[111] and confirmed by calculations on a much larger data set.[210] Statistical difference between these methods are $\lesssim$0.1 kcal/mol for neutral solutes and $\approx$0.5 kcal/mol for ions, even at $\varepsilon_{\text{s}} = 2$.[210] With appropriate choice of ζ, the conductor-like approach is thus little different from SS(V)PE or IEF-PCM in practice, and considerably simpler to implement. It can be extended in a straightforward way to solvents with nonzero ionic strength, with or without ion-size exclusion.[79] For large biomolecular applications in aqueous solvent there would seem to be little reason *not* to use this approach, in lieu of exact but more complicated models and as an alternative to finite-difference solution of Poisson's equation.

Regarding the outlying charge, we note that the total ASC-PCM surface charge ($Q_{\text{surf}} = \int \sigma(\mathbf{s})\, d\mathbf{s}$) satisfies a normalization condition[108,181,211]

$$Q_{\text{surf}} = \int_{\Gamma} \sigma(\mathbf{s})\; d\mathbf{s} = -\left(\frac{1}{\varepsilon_{\text{in}}} - \frac{1}{\varepsilon_{\text{out}}}\right) Q_{\text{in}}. \tag{2.47}$$

This is a consequence of Gauss' law and holds rigorously (up to minor discretization errors) for any PCM.[24] For $\varepsilon_{\text{in}} = 1$ and $\varepsilon_{\text{out}} = \varepsilon_{\text{s}}$, the result is $Q_{\text{surf}} = -[(\varepsilon_{\text{s}} - 1)/\varepsilon_{\text{s}}]Q_{\text{in}}$, therefore rescaling of the surface charge by $\tilde{f}_{\varepsilon}(\zeta)$ helps to correct for outlying charge, at least if $\zeta \approx 0$. In fact, the normalization condition in Equation (2.47) forms the basis of various *ad hoc* attempts to rescale the surface charge.[3,5,10,179,181,196,207,212–215] Tests against exact results, however, suggest that none of these schemes is very satisfactory,[107] and these methods complicate the formulation of analytic energy gradients.[216] It was later pointed out by Chipman[109] that the various conductor-like models already contain an *implicit* correction for volume polarization (i.e., for outlying charge), insofar as they are approximations to the SS(V)PE working equation, without the need for *a posteriori* renormalization of the surface charge.

Finally, it is illustrative to note that C-PCM can be derived in an alternative way that generalizes this method to the Poisson–Boltzmann case, in which the solvent contains a dissolved electrolyte.[79] This can be accomplished by introducing an *ansatz* for the electrostatic potential, of the form[23,79]

$$\varphi(\mathbf{r}) = \begin{cases} \varphi_0^{\rho}(\mathbf{r}) + \varphi_0^{\sigma}(\mathbf{r}) & \text{for } \mathbf{r} \in \Omega \\ \varphi_{\kappa}^{\rho}(\mathbf{r})/\varepsilon & \text{for } \mathbf{r} \notin \Omega \end{cases}, \tag{2.48}$$

where

$$\varphi_{\kappa}^{\rho}(\mathbf{r}) = \int \rho(\mathbf{r}') \frac{\exp(-\kappa \|\mathbf{r} - \mathbf{r}'\|)}{\|\mathbf{r} - \mathbf{r}'\|} d\mathbf{r}'. \tag{2.49}$$

Inside of the cavity, the *ansatz* in Equation (2.48) corresponds to the usual PCM reaction field, whereas outside of the cavity the potential includes the screening effects of dissolved ions, using the same Yukawa potential $e^{-\kappa r}/(\varepsilon_s r)$ that appears in Debye–Hückel theory,[7,68,77,79] with screening length κ^{-1} that is defined in Equation (2.16). For $\kappa = 0$, the C-PCM method is recovered by requiring $\varphi(\mathbf{r})$ in Equation (2.48) to be continuous across the solute cavity surface,[79] but this simple *ansatz* cannot be made to satisfy the jump boundary condition in Equation (2.22) and incurs an error of $\mathcal{O}(1/\varepsilon)$.[23,79] (This is consistent with the observation that C-PCM can be "derived" from IEF-PCM simply by dropping the $\hat{D}$- and $\hat{D}^\dagger$ -dependent terms from IEF-PCM and rescaling the surface charge to compensate.[177,210]) The model in Equation (2.48) is easily modifiable to incorporate the effect of an ion exclusion layer around the solute cavity, as in the size-modified Poisson–Boltzmann Equation (2.12), where the ion accessibility function $\lambda(\mathbf{r})$ serves the same purpose. In homage to GCOSMO, and in recognition of the fact that this approach generalizes Debye–Hückel theory to cavities of arbitrary shape, this approach has been named the *Debye–Hückel-like screening model* (DESMO).[23,79]

3 | IMPLEMENTATION

The topic of this section is numerical implementation of the models introduced in Section 2, beginning with matrix equations for ASC-PCMs (Section 3.1). This requires discretization of the integral equations introduced above, procedures for which are discussed in Section 3.2 with an emphasis on methods that afford smooth potential energy surfaces that are free from discontinuities. This is absolutely vital for exploration of the potential energy surface, for which gradients of the total energy functional $\mathcal{G}_0[\Psi]$ are required. In addition, many spectroscopic observables can be formulated as analytic energy derivatives,[217–219] so a solution-phase theory that encompasses molecular properties also requires a differentiable model. Sections 3.1 and 3.2 focus on PCMs but then the discussion is extended to include methods that solve Poisson's equation in three dimensions (Section 3.3). Linear-scaling implementations, which are necessary for hybrid QM/MM simulations with PCM boundary conditions, are discussed in Section 3.4.

3.1 | Matrix equations for PCMs

In practice, the integral equation that defines any PCM must be discretized to obtain a finite-dimensional matrix equation. For that purpose, it is convenient to rewrite Equation (2.43), which defines SS(V)PE and IEF-PCM, as

$$\hat{K}_\varepsilon \sigma(\mathbf{s}) = \hat{Y}_\varepsilon \varphi^\rho(\mathbf{s}). \tag{3.1}$$

This equation encompasses a whole family of ASC-PCMs, using various definitions for $\hat{K}_\varepsilon$ and $\hat{Y}_\varepsilon$.[23,24,111,155] To discretize this equation, one first generates a surface grid of points $\mathbf{s}_i \in \Gamma$. The surface charge $\sigma(\mathbf{s})$ is thereby replaced by a set of point charges $\{q_i\}$ at the discretization points $\{\mathbf{s}_i\}$. Details of this procedure are discussed in Section 3.2 but for now it suffices to introduce a matrix notation for the discretized form of Equation (3.1):

$$\mathbf{K}_\varepsilon \mathbf{q} = \mathbf{Y}_\varepsilon \mathbf{v}^\rho. \tag{3.2}$$

Given the vector $\mathbf{v}^\rho$ consisting of the molecular electrostatic potential evaluated at the cavity surface, $v_i^\rho = \varphi^\rho(\mathbf{s}_i)$, Equation (3.2) is solved for the vector $\mathbf{q}$ of surface charges. Matrix forms for various PCMs, corresponding to different choices of $\mathbf{K}_\varepsilon$ and $\mathbf{Y}_\varepsilon$, are given in Table 2. In discretized form, surface integrals are replaced by scalar products, so that Equation (2.37) for the electrostatic solvation energy becomes $\mathcal{G}_{\text{elst}} = \frac{1}{2}\mathbf{q}\cdot\mathbf{v}^\rho$, for example.

Equation (3.2) is sometimes rewritten as $\mathbf{q} = \mathbf{Q}_\varepsilon \mathbf{v}^\rho$ where $\mathbf{Q}_\varepsilon = \mathbf{K}_\varepsilon^{-1}\mathbf{Y}_\varepsilon$. Whereas the corresponding operator $\hat{Q}_\varepsilon = \hat{K}_\varepsilon^{-1}\hat{Y}_\varepsilon$ is self-adjoint, this property is generally not preserved upon discretization, except in the special case of C-PCM.[22] This means that the mapping from Equation (3.1) to Equation (3.2) is not unique, because discretization fails to preserve the condition $\hat{D}\hat{S} = \hat{S}\hat{D}^\dagger$.[24] In matrix form, this implies that $\mathbf{DAS} \neq \mathbf{SAD}^\dagger$ (except for spherical cavities),[24,178] where $\mathbf{A}$ is a diagonal matrix consisting of the surface area a_i associated with each discretization point $\mathbf{s}_i$. This leads to an ambiguity in the matrix representation of the operator $\hat{K}_\varepsilon = \hat{S} - (f_\varepsilon/2\pi)\hat{S}\hat{D}^\dagger$ in Equation (2.43), since it can be argued that any matrix of the form

TABLE 2 Matrices that define various PCMs according to $\mathbf{K}_\varepsilon \mathbf{q} = \mathbf{Y}_\varepsilon \mathbf{v}^\rho$.

Method	Matrix $\mathbf{K}_\varepsilon$	Matrix $\mathbf{Y}_\varepsilon$
C-PCM[a]	$\mathbf{S}$	$-\tilde{f}_\varepsilon(0)\mathbf{1}$
DESMO[b]	$\mathbf{S}$	$-\mathbf{1} + (1/\varepsilon)\mathbf{M}$
SS(V)PE[c]	$\mathbf{S} - (f_\varepsilon/4\pi)(\mathbf{DAS} + \mathbf{SAD}^\dagger)$	$-f_\varepsilon[\mathbf{1} - (1/2\pi)\mathbf{DA}]$
IEF-PCM[c]	$\mathbf{S} - (f_\varepsilon/2\pi)\mathbf{DAS}$	$-f_\varepsilon[\mathbf{1} - (1/2\pi)\mathbf{DA}]$

[a] $\tilde{f}_\varepsilon(\zeta) = (\varepsilon - 1)/(\varepsilon + \zeta)$.
[b] $M_{ij} = \delta_{ij}\varphi^\rho_\kappa(\mathbf{s}_i)/\varphi^\rho_0(\mathbf{s}_i)$.
[c] $f_\varepsilon = (\varepsilon - 1)/(\varepsilon + 1)$.

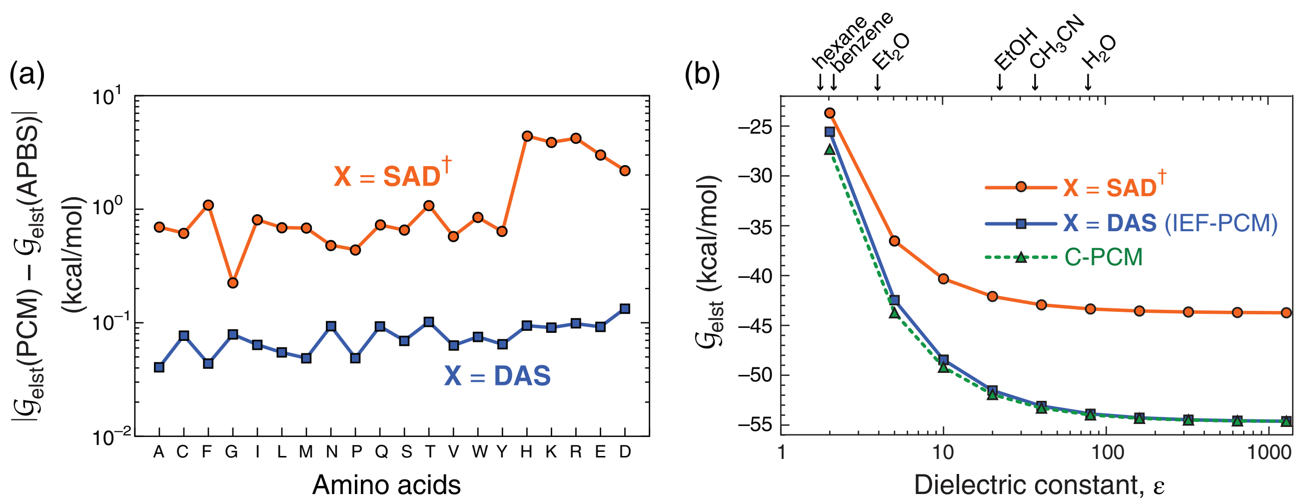

FIGURE 3 (a) Comparison of electrostatic solvation energies in aqueous solution, $|\mathcal{G}_{\text{elst}}(\text{PCM}) - \mathcal{G}_{\text{elst}}(\text{APBS})|$, computed using either an ASC-PCM or else by numerical solution of Poisson's equation using the APBS software. The data set consists of amino acids described using atomic partial charges from a force field, so that there is no outlying charge. The traditional implementation of IEF-PCM corresponds to $\mathbf{X} = \mathbf{DAS}$ (see Table 2) but results are also shown for the transpose $\mathbf{X} = \mathbf{SAD}^\dagger$. (b) Convergence of $\mathcal{G}_{\text{elst}}$ for classical histidine as a function of the solvent's dielectric constant, using the SwiG discretization scheme described in Section 3.2. Adapted from Ref. 24; copyright 2011 Elsevier

$$\mathbf{K}_\varepsilon = \mathbf{S} - \left(\frac{f_\varepsilon}{4\pi}\right)\underbrace{(c_1\mathbf{DAS} + c_2\mathbf{SAD}^\dagger)}_{\mathbf{X}} \tag{3.3}$$

is an equally valid representation, provided that $c_1 + c_2 = 1$.[24] Historically, IEF-PCM has been implemented using $\mathbf{X} = \mathbf{DAS}$ (i.e., $c_1 = 1$ and $c_2 = 0$), whereas SS(V)PE is implemented using the symmetrized matrix $\mathbf{X} = (\mathbf{DAS} + \mathbf{SAD}^\dagger)/2$,[23,111] as indicated in Table 2. Precise definitions of the matrices $\mathbf{S}$ and $\mathbf{D}$ that represent the operators $\hat{S}$ and $\hat{D}$ can be found elsewhere.[10,22–24,144,155] These depend somewhat upon the discretization algorithm that is selected, but generally S_{ij} represents the Coulomb interaction between q_i and q_j (which is straightforward to discretize except when $i = j$), whereas D_{ij} incorporates the effects of the outward-pointing electric field.

In the absence of outlying charge, the IEF-PCM and SS(V)PE models are exact up to discretization errors that can be driven to zero in a controlled way. Although this follows from the derivation in Section 2.3, it is worth emphasizing via numerical calculations. For classical solutes with no outlying charge (described using atomic partial charges from a force field), Figure 3a presents a comparison between PCM solvation energies and those obtained by numerical solution of Poisson's equation,[23,24] using a standard multiresolution algorithm in the APBS program.[220] To examine the ambiguity regarding the choice of $\mathbf{X}$, these calculations test both $\mathbf{X} = \mathbf{DAS}$ (i.e., IEF-PCM) and also $\mathbf{X} = \mathbf{SAD}^\dagger$; the SS(V)PE model is essentially the average of these two choices. Calculations in Figure 3 use dense but finite discretization grids, and a small systematic discrepancy is evident between the two choices of $\mathbf{X}$, indicating a systematic discrepancy between SS(V)PE and IEF-PCM. Numerical values of $\mathcal{G}_{\text{elst}}$ obtained using the IEF-PCM choice agree with APBS results to within

$\lesssim$0.1 kcal/mol, demonstrating the operational equivalence of the ASC-PCM and the volumetric implementation of continuum electrostatics. This equivalence essentially makes the Kirkwood multipolar expansion formulas obsolete, since they are only valid for idealized cavity shapes in the absence of escaped charge. Under those conditions, the ASC-PCM approach furnishes a numerically exact solution to the continuum electrostatics problem,[110,112,211] obviating the need for multipole approximations.

Formally, C-PCM represents the high-dielectric limit of IEF-PCM, and indeed the two models become equivalent as $\varepsilon \to \infty$,[24,79,109] as demonstrated in Figure 3b. In practice there is little difference between them already for moderately polar solvents, and thus little justification for the increased complexity of IEF-PCM for $\varepsilon > 10$. That said, for non-spherical cavities only the $\mathbf{X} = \mathbf{DAS}$ form of $\mathbf{K}_\varepsilon$ achieves the correct conductor limit for finite discretization grids, as demonstrated by both formal and numerical arguments.[24]

Differences between the $\mathbf{X} = \mathbf{DAS}$ and $\mathbf{X} = \mathbf{SAD}^\dagger$ forms of $\mathbf{K}_\varepsilon$ are generally attributable to the fact that $\hat{D}^\dagger\sigma(\mathbf{s})$ proves to be more challenging to implement in a numerically stable way, as compared to $\hat{D}\sigma(\mathbf{s})$,[24,221] specifically in regions near the cusps that appear between interlocking atomic spheres in the vdW cavity construction. These cusps are also present in the SAS cavity, but the use of larger atomic radii in that case tends to mitigate numerical problems associated with the cusps.[25] In fact, numerical differences between the $\mathbf{X} = \mathbf{DAS}$ and $\mathbf{X} = \mathbf{SAD}^\dagger$ forms of $\mathbf{K}_\varepsilon$, and thus between IEF-PCM and SS(V)PE, disappear almost entirely for a "united atom" cavity in which atomic spheres on the hydrogen atoms are omitted, with the remaining atomic radii increased to compensate.[178] Differences between IEF-PCM and SS(V)PE are also negligible when an isodensity contour is used to define the cavity surface (Section 3.3),[155] because the isodensity surface is free of cusps entirely. Thus, differences between the IEF-PCM and SS(V)PE versions of $\mathbf{K}_\varepsilon$ are mostly (if not entirely) limited to the use of vdW cavities. This remains a very common cavity construction, however, so the absence of $\hat{D}^\dagger$ in the IEF-PCM equation is one reason to prefer this form ($\mathbf{X} = \mathbf{DAS}$) as compared to alternatives including the symmetrized SS(V)PE form.

3.2 | Discretization

Having introduced various PCMs in matrix form, we now turn to the details of discretizing the cavity surface. Historically, this has been accomplished using various tessellation schemes in which small, flat surface elements approximate the curved surface of the cavity.[144] The "GePol" ("generate polygons") algorithm[222–226] is a popular version of this finite-element approach, and an example of a molecular surface discretized in this way is presented in Figure 4a. This approach has several limitations, including the fact that the number of tesserae per atomic sphere cannot be increased arbitrarily and therefore the discretization error cannot be systematically driven to zero.[24] Furthermore, the solid

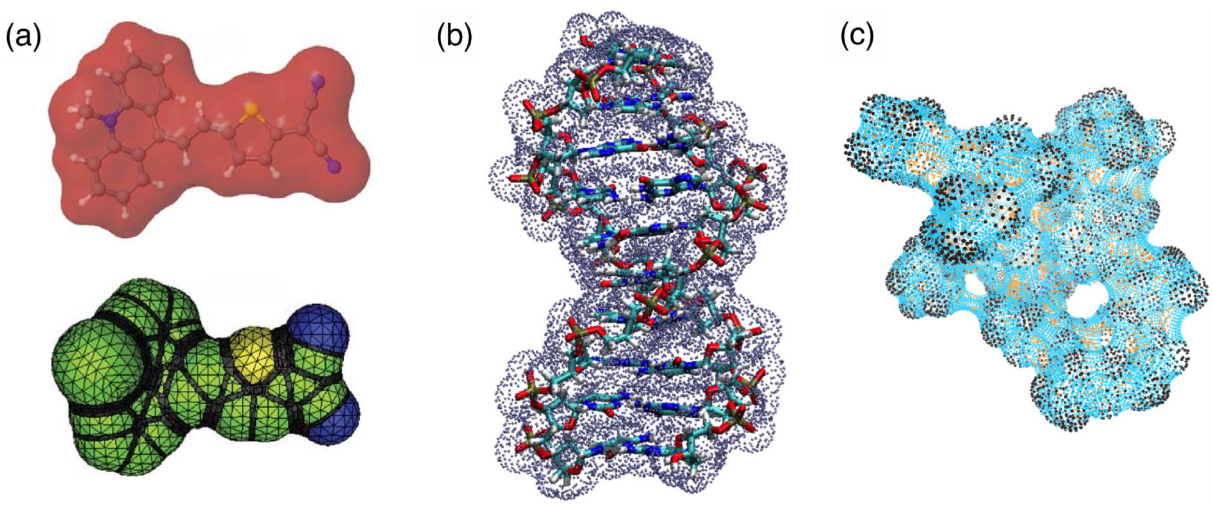

FIGURE 4 Examples of surface discretization for continuum solvation: (a) tessellation of the molecular surface using the GePol algorithm, (b) Lebedev discretization of the van der Waals surface for a segment of double-stranded DNA, and (c) Lebedev discretization of the solvent-excluded (Connolly) surface for a 384-atom protein. Panel (a) is reprinted from Ref. 15; copyright 2012 John Wiley & Sons. Panel (c) is reprinted from Ref. 25; copyright 2020 Taylor & Francis

geometry of the tessellation procedure is complicated, leading to very complex formulas for surface areas[227] and analytic energy gradients.[228] In fact, second derivatives of the tesserae areas a_i were considered sufficiently complicated that they were not originally formulated, and the PCM Hessian was implemented in a semi-analytic way, via finite-difference evaluation of $\partial^2 a_i/\partial x \partial y$.[178]

More recently, these complexities have been overcome by discretizing the surface using atom-centered Lebedev grids,[21–25,229–231] which are widely used in DFT and therefore readily available in quantum chemistry codes.[232–235] Example are depicted in Figure 4b,c, where the outline of the surface is evident even though only the discretization grid points are shown. Relative to GePol and other tessellation schemes, Lebedev grids have the advantage of being systematically improvable so that results can be converged to the infinite-grid limit.[22,24] Fully analytic Hessians have been formulated and implemented.[236]

An important issue faced by both tessellation and quadrature is ensuring that the discretization algorithm produces a smooth potential energy surface as the atoms are displaced. The appearance of discontinuities in some molecular surface area algorithms was noted long ago,[237] and discontinuities are likely the cause of anecdotal complaints about slow convergence of geometry optimizations using PCMs. These discontinuities arise because grid points may disappear into (or emerge from within) the interior of the solute cavity, as displacement of the nuclei modifies the extent to which atomic spheres interpenetrate. An example is shown in Figure 5a, which plots convergence of the energy during geometry optimization of a semicontinuum calculation in which the solute is (adenine)$(H_2O)_{52}$. Two discretization algorithms, the *variable tesserae number* (VTN) method[238] and the *fixed points with variable areas* (FixPVA) approach,[239] are shown to exhibit repeated spikes in the energy.[21] The VTN algorithm uses a fixed surface grid that unceremoniously discards surface elements that are swallowed by the cavity, so it is unsurprising that the corresponding potential surface exhibits discontinuities, although their magnitude (>20 kcal/mol in one case) is disconcerting. The FixPVA algorithm, on the other hand, specifically introduces a switching function to attenuate the surface area of each tesserae within the cavity's interior. Sharp changes in energy along the FixPVA optimization in Figure 5a are actually not discontinuities *per se* but rather near-singularities induced by the switching function, which allows surface discretization charges to approach one another much more closely as compared to the VTN scheme.[21,24] These problems with close approach of the tesserae are most problematic for vdW cavities and may be less troublesome for SAS cavities, where the atomic radii are larger.[240]

These problems can be avoided, even for vdW cavities, using a switching function in conjunction with Gaussian blurring of the surface charges, as illustrated schematically in Figure 5b. This *switching Gaussian* (SwiG) discretization

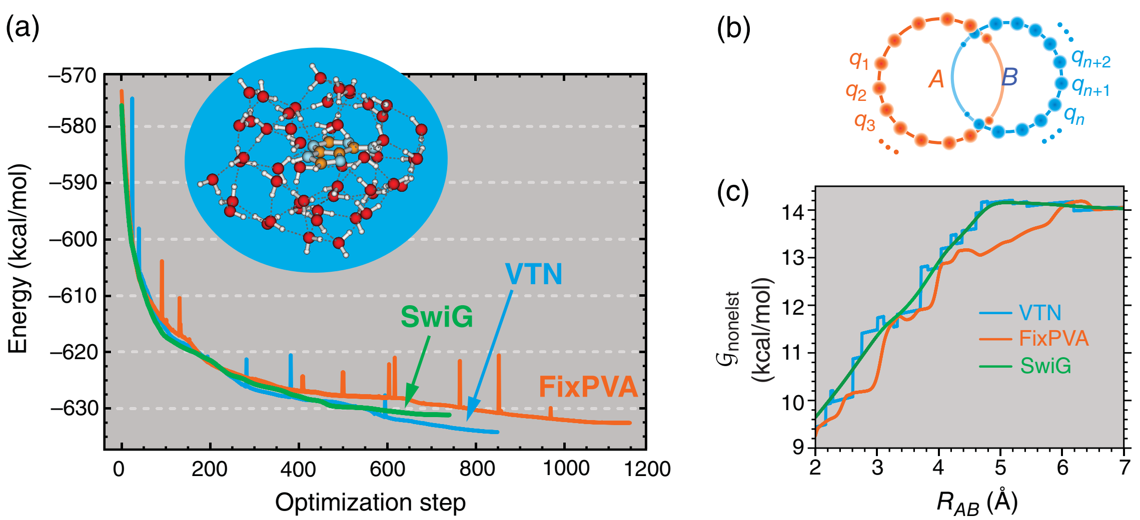

FIGURE 5 Demonstration of the SwiG-PCM discretization approach. (a) Geometry optimization of (adenine)$(H_2O)_{52}$ in a C-PCM representation of bulk water, using several different algorithms to discretize the vdW cavity surface. (The surface itself is not shown, but the atomistic region appears in the inset.) Optimizations are performed in Cartesian coordinates so the total number of steps is large. (b) Schematic of the SwiG discretization algorithm, in which the surface charges $\{q_i\}$ are subject to Gaussian blurring and also to a switching function that attenuates the quadrature weights near the cavity surface. (c) Nonelectrostatic solvation energy ($\mathcal{G}_{\text{nonelst}}$) as spheres A and B are pulled part. The value of $\mathcal{G}_{\text{nonelst}}$ is related to the solvent-exposed surface area and thus inherits any discontinuities in the surface area function. Panels (a) and (c) are adapted from Ref. 21; copyright 2010 American Chemical Society

procedure[21,22] ensures that Coulomb interactions between discretization elements remain finite even as the distance between them approaches zero. Such a procedure was originally introduced by York and Karplus to obtain a smooth version of C-PCM,[229] then later extended by Lange and Herbert to the complete family of PCMs.[21–25] This scheme uses Lebedev quadrature to discretize the surface, rather than tesserae with finite areas, nevertheless the solvent-accessible surface area (SASA) for atom B (whose radius is R_B) is easily defined:

$$\mathrm{SA}_B = R_B^2 \sum_{i \in B}^{\mathrm{grid}} w_i F_i. \tag{3.4}$$

Here, w_i is the quadrature weight for discretization point $\mathbf{s}_i$, and F_i is the switching function associated with that point ($0 \le F_i \le 1$). Thus $a_i = w_i F_i \, R_B{}^2$ is the surface area assigned to quadrature point $\mathbf{s}_i$ on atom B.[21] Equation (3.4) is considerably simpler than geometric algorithms for determining the exposed surface area.[227] Models of the non-electrostatic contributions to the solvation energy (as discussed in Section 4.2) often include terms proportional to the solvent-exposed surface area, so continuity of the potential energy surface demands that the surface area be a continuous function of the nuclear coordinates. For SwiG discretization, it is evident from Figure 5c that this is achieved.

Analytic gradients of SwiG-PCMs are greatly simplified relative to those of the corresponding GePol-discretized models.[22] SwiG-PCM potential energy surfaces are provably continuous and differentiable,[22,229] and are free of the unwanted oscillations that plague the FixPVA approach (see Figure 5).[22,24] SwiG discretization is well-behaved enough to be used for *ab initio* molecular dynamics simulations involving bond-breaking, as shown in Figure 6 for intramolecular proton transfer in glycine. SwiG-PCM forces afford good energy conservation despite significant deformation of the solute cavity as it transforms between two tautomeric forms of the solute. The energy profile in Figure 6b provides a closeup view of energy fluctuations during a time window in which a bond-breaking event occurs.

The SwiG implementation of PCMs first appeared in the Q-Chem program,[241] and was extended recently to discretize not only the vdW and SAS cavities but also the SES.[25] Related discretization schemes have since been adopted in other software.[242,243] While alternative discretization methods have been described subsequently,[244–247] it is unclear whether these have been formulated with gradients in mind. Given the simplicity and success of the SwiG approach, it is also unclear what is to be gained from these formulations.

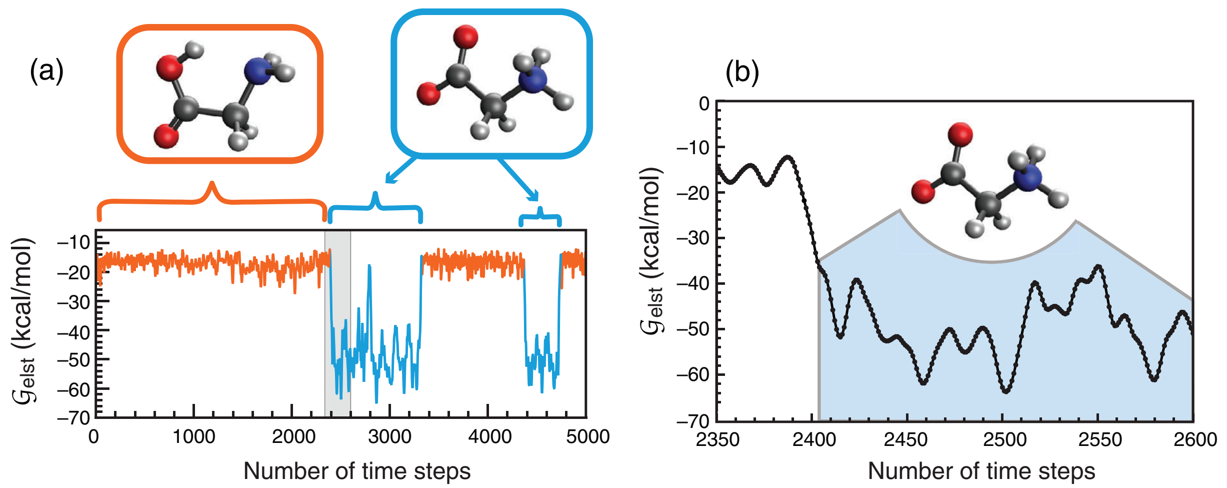

FIGURE 6 (a) Electrostatic solvation energy along an *ab initio* molecular dynamics trajectory of glycine (PBE0/6-31+G* level) in implicit water (SwiG/C-PCM). The simulation starts at $t = 0$ from the amino acid tautomer (energy data in orange), which is the most stable form of gas-phase glycine, but in water this species spontaneously transfers a proton to form the zwitterionic tautomer (energy data in blue). (b) Close-up view of $\mathcal{G}_{\mathrm{elst}}$ in the region where the proton transfer occurs. Energy fluctuations are smooth despite the bond-breaking event. Data are from Ref. 22 and the time step is 0.97 fs

3.3 | Isodensity and self-consistent cavity surfaces

Smooth discretization algorithms solve the practical problem of discontinuities but do not alter what is arguably a more fundamental problem, namely, that construction of the solute cavity itself remains a significant source of arbitrariness. There are good reasons to be skeptical of any "universal" definition based on a set of atomic radii. From a theoretical point of view, careful examination of the Born ion model[46] and the generalized Born (GB) formalism[152,153] suggests that the cavity radius is not strictly a property of the solute but ought to depend on the dielectric constant as well, and probably also on temperature.[248] A universal set of radii cannot capture changes in atomic size with respect to oxidation state, although empirical schemes have been suggested to modify the radii based on atomic charge.[150,151] At a practical level, it is simply a fact that solvation energies[139,249] and other properties[250] can be quite sensitive to the particular atomic radii that are used, and often the atomic radii that work well for small-molecule solvation energies do not work well for proteins.[251] Known differences between properties in protic versus aprotic solvents may be missed unless the atomic radii are adjusted.[252,253]

Both the vdW and SAS cavity constructions consist of atom-centered spheres with radii

$$R_A = \alpha_{\text{vdW}} R_{\text{vdW},A} + R_{\text{probe}}. \tag{3.5}$$

The atomic vdW radii $\{R_{\text{vdW},A}\}$ might be taken from crystal structure data (e.g., Bondi's set of radii and its subsequent extensions),[134–136] or might simply be parameters of the model.[133] For vdW cavities, $R_{\text{probe}} = 0$ and a typical scaling factor is $\alpha_{\text{vdW}} = 1.2$,[9] whereas one generally does not scale the vdW radii for SAS cavities. (Note that the choice $\alpha_{\text{vdW}} = 1.2$ does not result from any kind of elaborate fitting procedure and is intended only as a rough guide;[9] common choices range from $\alpha_{\text{vdW}} = 1.1 - 1.4$.) As an example of just how sensitive $\mathcal{G}_{\text{elst}}$ is to cavity construction, Table 3 reports calculations for the two tautomers of glycine from Figure 6, using various cavity definitions. A change from $\alpha_{\text{vdW}} = 1.2$ to either $\alpha_{\text{vdW}} = 1.1$ or $\alpha_{\text{vdW}} = 1.3$ results in changes of anywhere from 3 to 9 kcal/mol in $\mathcal{G}_{\text{elst}}$.

For solutes described using electronic structure theory, a more satisfying choice is to define the cavity surface using an isocontour of the solute's own electron density.[112,154–156] It is possible to settle on a numerical isocontour value that appears to have some universal validity, typically $\rho_0 \sim 0.001$ a.u.[149,250] Results for glycine using $\rho_0 = 0.001$ a.u. are listed in Table 3 and agree quite well with solvation energies obtained using vdW cavities with $\alpha_{\text{vdW}} = 1.2$. Results from two SAS cavities are reported as well, using either $R_{\text{probe}} = 0.2$ Å or $R_{\text{probe}} = 1.4$ Å. The latter is a realistic estimate of the size of a water molecule,[138] yet the solvation energies obtained from that particular SAS cavity are much too small in comparison to isodensity results. In contrast, $R_{\text{probe}} = 0.2$ Å affords more consistent solvation energies but is much too small to represent the actual size of a water molecule. Nevertheless, this value is commonly used in biomolecular Poisson–Boltzmann calculations,[139] and values in the range $R_{\text{probe}} = 0.2 - 0.3$ Å have been used since the early days of continuum solvation models.[3–5] This is consistent with the idea that the "electrostatic size" of an

TABLE 3 Electrostatic solvation energies in water, computed with the SS(V)PE model for two tautomers of glycine using atomic radii as in Equation (3.5).

Cavity	α_{vdW}	R_{probe} (Å)	$\mathcal{G}_{\text{elst}}$ (kcal/mol)	
			Amino acid	Zwitterion
vdW[a]	1.0	0.0	−26.1	−68.2
vdW[a]	1.1	0.0	−20.2	−56.0
vdW[a]	1.2	0.0	−16.1	−46.8
vdW[a]	1.3	0.0	−12.9	−39.0
vdW[a]	1.4	0.0	−10.6	−32.6
SAS[a]	1.0	0.2	−18.0	−51.4
SAS[a]	1.0	1.4	−4.3	−13.9
Isodensity[b]			−16.4	−48.1

Note: Electronic structure calculations were performed at the B3LYP/6-31+G* level.

[a]Using $R_{\text{vdW}} = 1.10$ Å (H), 1.70 Å (C), 1.55 Å (N), and 1.52 Å (O), discretized using SwiG with 302 points per atom.

[b]Using an isocontour $\rho_0 = 0.001$ a.u. and 1202 grid points.

atom is not the same as its physical size, as discussed in the context of the Born model[46] and also in the GB formalism that is discussed in Section 4.2.

Although the isodensity cavity is an appealing choice on physical grounds, existing algorithms to compute this surface are subject to occasional failure for certain molecular geometries.[155,156] These difficulties could likely be overcome using an implementation based on the "marching cubes" algorithm,[254,255] or variants thereof,[206] which are well-known approaches for surface rendering in computer graphics. A more fundamental problem is that the surface-normal vectors $\mathbf{n}_\mathbf{s}$ become density-dependent,[112,154,155]

$$\mathbf{n}_\mathbf{s} = -\frac{\hat{\boldsymbol{\nabla}}\rho(\mathbf{s})}{\left\|\hat{\boldsymbol{\nabla}}\rho(\mathbf{s})\right\|}. \tag{3.6}$$

The surface area associated with the discretization point $\mathbf{s}_i$ inherits a density dependence as well, which significantly complicates the formulation of analytic energy gradients. To date, these are not available for any isodensity PCM. This complexity could be sidestepped using an analytically differentiable pseudo-density to define the cavity,[23,55,206,256] which has sometimes been used for biomolecular applications. However, although this might remove some arbitrariness from the selection of atomic radii, in QM applications it does not represent a self-consistent determination of the cavity surface that can deform to reflect changes in the molecular electronic structure. Conversely, a pseudo-density that is determined in order to reproduce the molecular electrostatic potential might afford better solvation energies as compared to the use of fixed vdW radii,[257] but reintroduces the problem of how to compute the analytic gradient. As such, it is unclear whether pseudo-density constructions offer genuine advantages relative to the very simple vdW cavity, whereas the isodensity cavity offers clear advantages for single-point calculations but lacks gradients to explore potential energy surfaces. As a workaround, united-atom radii (in which hydrogen atoms are not given atomic spheres) have been parameterized in an effort to reproduce results obtained with an isodensity cavity.[150] Similar to the isodensity construction,[155] the united-atom cavity virtually eliminates differences between symmetric and asymmetric forms of the $\mathbf{K}_\varepsilon$ matrix in IEF-PCM versus SS(V)PE.[178]

Stepping outside of the ASC-PCM formalism, a self-consistent definition of the solute/continuum interface that responds to the electronic structure of the solute has been implemented (with gradients) in the context of Poisson's equation.[28] Originally pioneered by Fattebert and Gygi,[258–260] then later refined by others,[261–264] this approach takes $\varepsilon(\mathbf{r})$ to be a functional of the solute's charge density, with limiting values $\varepsilon = 1$ near the nuclei and $\varepsilon = \varepsilon_\mathrm{s}$ far away. In practice, "near" and "far" are determined not by distance but by comparison of $\rho(\mathbf{r})$ to a pair of parameters ρ_max and ρ_min, the latter of which establishes what constitutes the "tail" of the density. In a sense, this is the QM descendent of the smooth permittivity functions that are typically used in biomolecular electrostatics calculations, which interpolate between limiting values ε_in and ε_out in order to improve convergence of the iterative solver and also to mitigate discontinuities in the forces.[55,265,266] Smooth permittivity functions also facilitate convergence of Poisson's equation in QM applications.[267]

For QM applications, the modern incarnation of this idea defines the *self-consistent continuum solvation* (SCCS) model.[28] At its heart is a permittivity functional,[262]

$$\varepsilon[\rho](\mathbf{r}) = \begin{cases} 1 & \rho(\mathbf{r}) > \rho_\mathrm{max} \\ \exp[t(\ln\rho(\mathbf{r}))] & \rho_\mathrm{min} < \rho(\mathbf{r}) < \rho_\mathrm{max}\,, \\ \varepsilon_\mathrm{s} & \rho(\mathbf{r}) < \rho_\mathrm{min} \end{cases} \tag{3.7}$$

in which $t(x)$ is a switching function that interpolates smoothly between values $t(\ln\rho_\mathrm{min}) = \ln\varepsilon_\mathrm{s}$ and $t(\ln\rho_\mathrm{max}) = 0$, so that $\varepsilon(\mathbf{r})$ achieves the limits indicated in Equation (3.7). Inserting this *ansatz* into Poisson's equation [Equation (2.3)] affords a model in which the dielectric interface is smooth, rather than sharp as it is in PCMs, yet one where the definition of the interface is updated self-consistently as the density $\rho(\mathbf{r})$ is iterated to convergence. The dependence of $\varepsilon(\mathbf{r})$ on the density does mean that the Fock operator $\delta\mathcal{G}/\delta\rho$ acquires an extra term relative to what was discussed in Section 2.1, namely[262]

$$\upsilon_\varepsilon[\rho](\mathbf{r}) = -\frac{1}{8\pi}\left\|\hat{\boldsymbol{\nabla}}\varphi(\mathbf{r})\right\|^2\left(\frac{\delta\varepsilon[\rho]}{\delta\rho(\mathbf{r})}\right). \tag{3.8}$$

The SCCS model is increasingly being used in *ab initio* simulations of materials, for example, to model the aqueous electrolyte/solid-state interfaces relevant in electrochemistry.[28,82,264,268–274] Some of that work points to limitations of the linear dielectric model itself (i.e., a breakdown of the assumption that $\mathbf{P} \propto \mathbf{E}$), which can result either from high field strength ("dielectric saturation"),[275,276] or else because the rotational response of the water molecules saturates at the electrode interface and consequently the susceptibility is smaller than it is in bulk water.[271,272] Limitations in the linearized Poisson–Boltzmann description of electrolyte effects have also been demonstrated.[270–272]

3.4 | Linear-scaling algorithms

The electrostatic solvation energy obtained from IEF-PCM should be *exactly* equivalent to that obtained by solving Poisson's equation, in the case of a classical solute for which there is no outlying charge. (This equivalence holds only up to discretization errors, but those are controllable and can be driven to zero if systematically improvable grids are employed.) It is therefore surprising that the PCM formulation of continuum electrostatics has seen very little use within the protein electrostatics community. Biomolecular calculations are almost always performed in water, meaning that the simpler C-PCM should be essentially exact, and modifications of the PCM formalism are available to treat the linearized Poisson–Boltzmann problem,[79,180,181,189] including modifications to simulate an ion exclusion layer.[79] Nevertheless, it continues to be the case that in nearly all applications of Poisson–Boltzmann theory to proteins, Equation (2.12) is solved in three dimensions using finite-difference evaluation of the Laplacian $\hat{\nabla}^2 \varphi(\mathbf{r})$.[44,277] This poses serious problems for molecular dynamics simulations with implicit solvent, because the forces are generally not continuous when the problem is discretized in this way. Although significant effort has gone into obtaining high-quality forces,[186–188,265,278–281] from a certain point of view this looks like engineering an elaborate means of escape from the very deep hole created by a numerical framework that admits discontinuities. A better strategy is not to get trapped in that hole in the first place. The SwiG discretization procedure for PCMs (Section 3.2) was designed as a starting point that is free of discontinuities.

All of this suggests that SwiG-PCMs could be very attractive replacements for the finite-difference Poisson–Boltzmann solvers that are commonplace in biomolecular electrostatics calculations. Efforts to do so, however, will quickly run up against the size of the PCM matrix equation, which is equal to the number of discretization grid points, itself proportional to the number of solvent-exposed atoms. This means that a straightforward solution of Equation (3.2), based on construction of $\mathbf{Q}_\varepsilon = \mathbf{K}_\varepsilon^{-1}\mathbf{Y}_\varepsilon$ or its equivalent, incurs a CPU cost of $\mathcal{O}(N_{\text{atoms}}^3)$ and a memory footprint of $\mathcal{O}(N_{\text{atoms}}^2)$, with significant prefactors in both cases that reflect the number of discretization points per atom. In QM/MM/PCM calculations (i.e., QM/MM with implicit solvent), it is the size of the MM region that dictates the matrix dimension; for small QM regions with large MM environments, one can easily encounter scenarios where the cost of the classical electrostatics calculation exceeds the cost of the QM calculation![23]

A straightforward solution to this problem is to introduce iterative solvers that do not require storage or inversion of $\mathbf{K}_\varepsilon$,[23,282,283] such as conjugate gradient (CG) or biconjugate gradient algorithms.[23] In these iterative approaches, the bottleneck step becomes the calculation of Coulomb interactions between surface discretization points, which can be accelerated using the fast multipole method (FMM),[283] in either its original formulation or using a simpler tree-code approach.[23,166,284] Parallelization strategies have also been discussed.[23] Data for polyalanine helices $(\text{Ala})_n$ show that wall times for iterative solution of the PCM linear equations can be reduced to a few seconds for $(\text{Ala})_{250}$ (Figure 7a). For $(\text{Ala})_{4000}$, with 5.6×10^6 surface discretization points, wall times can be reduced to less than a minute on modest hardware (Figure 7b). Proof-of-concept MM/PCM molecular dynamics simulations have been reported involving ≈22,000 classical atoms in the MM solute, with ≈124,000 point charges used to discretize the surface.[23]

An alternative algorithm for fast iterative solution of the PCM equations is based on a domain decomposition procedure.[190–193,285–288] Here, the solute cavity is divided into overlapping domains, each consisting of a single atomic sphere, and single-sphere solutions form the basis for an iterative solution of the PCM equation for the full domain. This can be formulated in terms of sparse matrix equations that can be solved in $\mathcal{O}(N_{\text{atoms}})$ time. This method was originally developed for C-PCM and called "ddCOSMO,"[190–193,286,287] although it has since been extended to arbitrary PCMs ("ddPCM").[288] The name ddPCM is used here to avoid confusion with COSMO's dual-cavity construction that was described in Section 2.4. Timing data on just a single compute node (Figure 7c) show that the method is competitive with a parallelized CG-FMM solver. The ddPCM algorithm has been implemented for MM/PCM molecular dynamics in the Tinker-HP code,[289] using a switching function eliminate discontinuities.[290] This method seems promising as a replacement for finite-difference Poisson–Boltzmann solvers.

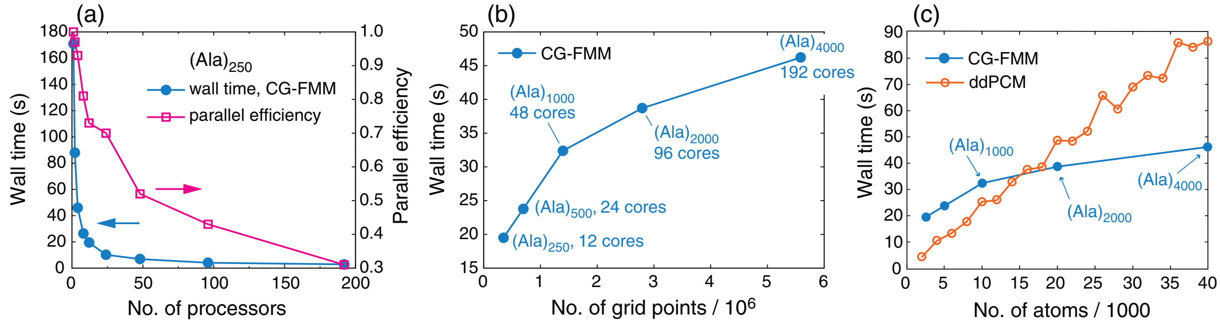

FIGURE 7 Timings and parallel scalability data for $\mathcal{O}(N)$ PCM solvers applied to polyalanine helices, using a classical force field description of the solute. (a) Strong-scaling data for a CG-FMM algorithm applied to $(\text{Ala})_{250}$, running on 12 shared-memory cores per node. (b) Weak-scaling data for $(\text{Ala})_n$ helices of increasing length, versus the number of Lebedev grid points used to discretize the cavity surface. (c) Comparison of timing data for CG-FMM versus the ddPCM algorithm, for $(\text{Ala})_n$. The CG-FMM data in (c) are the same as those in (b), but all ddPCM calculations were run on a single 12-core node. Data in (a) and (b) are from Ref. 23 and ddPCM data in (c) are from Ref. 190

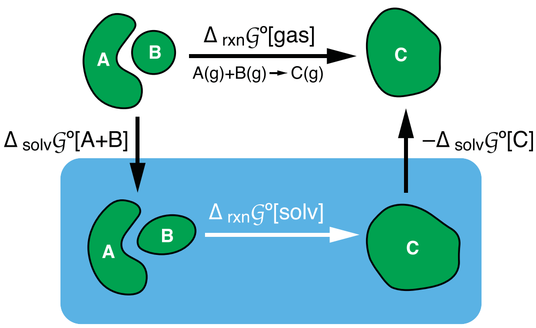

FIGURE 8 Thermodynamic cycle connecting gas- and solution-phase reaction energies for A + B → C. Changes in shape signify that geometries of A, B, and C may be different in solution than they are in the gas phase, in which case the solvation energies $\Delta_{\text{solv}}\mathcal{G}^\circ$ should include a term representing the gas-phase deformation energy

4 | SOLVATION ENERGIES

Perhaps the single most important property afforded by a solvation model is the free energy of solvation, $\Delta_{\text{solv}}\mathcal{G}^\circ$. This can be used to compute solution-phase reaction energies ($\Delta_{\text{rxn}}\mathcal{G}^\circ$) and reaction barrier heights ($\Delta\mathcal{G}^\ddagger$), by performing reactant, product, and/or transition state optimizations with implicit solvent. This is sometimes called the "isodesmic approach" (especially in the context of pK_a calculations),[291–293] in order to distinguish it from an alternative that is based on the thermodynamic cycle shown in Figure 8. In the latter approach, the gas-phase reaction energy might be computed at a high level of quantum theory and then combined with solvation energies for reactants and products, computed at a different (usually lower) level of theory, in order to estimate the solution-phase reaction energy $\Delta_{\text{rxn}}\mathcal{G}^\circ[\text{solv}]$. This strategy can be used, for example, if no appropriate solvation model is available at the target level of theory. The method based on thermodynamic cycles has long been considered to be more accurate (especially for pK_a calculations) as compared to the direct (isodesmic or "absolute pK_a") approach,[294] although it is no longer clear that this is true when the best-available solvation models are used.[295,296] Furthermore, the use of a thermodynamic cycle is predicated on the assumption that neither reactants nor products undergo major conformational changes or isomerization upon solvation; if this assumption is questionable or invalid then the direct approach should be employed instead.[292,296]

A subtle point concerns vibrational and rotational contributions to the reaction entropy.[293,297,298] The reaction free energy $\Delta_{\text{rxn}}\mathcal{G}^\circ$ is related to the internal energy change $\Delta_{\text{rxn}}\mathcal{U}^\circ$ via partition functions Z for reactants and products,

$$\Delta_{\text{rxn}}\mathcal{G}^\circ = \Delta_{\text{rxn}}\mathcal{U}^\circ - RT\ln\left(\frac{Z_{\text{products}}}{Z_{\text{reactants}}}\right). \tag{4.1}$$

These partition functions might be evaluated within the harmonic oscillator and rigid rotor approximations, or with more sophisticated approaches.[299] However, thermal corrections are seldom included in the parameterization of solvation models, which are typically fit to reproduce experimental values of $\Delta_{\text{solv}}\mathcal{G}^\circ$ for small molecules and ions using rigid gas-phase geometries. In principle, this leads to an inconsistency when rovibrational entropies are included via Equation (4.1),[297] though it appears that this inconsistency is numerically small in practice (~0.2 kcal/mol for molecules in typical training sets),[298] meaning that intramolecular entropic contributions to $\Delta_{\mathrm{solv}}\mathcal{G}^{\circ}$ largely cancel in the parameterization of solvation models. (This is consistent with parameterization based mostly on small molecules, as in the Minnesota Solvation Database of experimental solvation energies,[300–303] which is widely used to parameterize solvation models.) These observations suggest that the best strategy for including vibrational contributions to $\Delta_{\mathrm{rxn}}\mathcal{G}^{\circ}[\mathrm{solv}]$ is to compute partition functions (vibrational frequencies) in the presence of the solvent model,[298] which also sidesteps the need to account for translational and rotational contributions in the gas phase. When using a composite level of theory and a thermodynamic cycle such as that shown in Figure 8, this means that the higher-level electronic structure method is used only to compute $\Delta_{\mathrm{rxn}}\mathcal{U}^{\circ}[\mathrm{gas}]$, bypassing the need for vibrational frequency calculations at the higher level of theory.

4.1 | There is more to solvation than electrostatics

The dielectric continuum formalism that has been described up to this point defines only the electrostatic contribution to the free energy, and thus only the electrostatic contribution to $\Delta_{\mathrm{solv}}\mathcal{G}^{\circ}$. *This is generally insufficient to predict accurate solvation energies*. A vivid example is provided by statistical errors in C-PCM solvation energies, which are presented in Table 4 alongside results from the "SMD" model,[302] which is described in Section 4.2 and which contains both electrostatic and nonelectrostatic contributions to $\Delta_{\mathrm{solv}}\mathcal{G}^{\circ}$. In water, for which differences between C-PCM and IEF-PCM should be inconsequential, mean unsigned errors (MUEs) with respect to experimental solvation energies are ≈2 kcal/mol for charge-neutral solutes but ≈8 kcal/mol for ions. In nonaqueous solvents, especially for ions (in acetonitrile, dimethyl sulfoxide, and methanol), the errors are even larger. These errors should be compared to the data labeled SMD(C-PCM) in the same table, as this model is built upon C-PCM electrostatics but includes nonelectrostatic contributions as well. Errors for the same data set are <1 kcal/mol for neutral solutes and ≈4 kcal/mol for ions.

To do better than the C-PCM error statistics in Table 4, electrostatics-only models (including sophisticated ones such as IEF-PCM) need to be augmented to include nonelectrostatic interactions,

$$\mathcal{G} = \mathcal{G}_{\mathrm{elst}} + \mathcal{G}_{\mathrm{nonelst}}. \tag{4.2}$$

It is the quantity $\mathcal{G}$ in Equation (4.2) that is used to compute $\Delta_{\mathrm{solv}}\mathcal{G}^{\circ} = \mathcal{G}^{\circ}[\mathrm{solv}] - \mathcal{G}^{\circ}[\mathrm{gas}]$, but only $\mathcal{G}_{\mathrm{elst}}$ is included in PCM or Poisson–Boltzmann calculations. The nonelectrostatic term $\mathcal{G}_{\mathrm{nonelst}}$ is a catch-all that includes

TABLE 4 Mean unsigned errors (MUEs) versus experiment, for solvation energies ($\Delta_{\mathrm{solv}}\mathcal{G}^{\circ}$) computed using various models.

		MUE (kcal/mol)		
			SMD[c]	
Data set[a]	N_{data}	**C-PCM[b]**	**C-PCM**	**IEF-PCM**
Aqueous neutrals	274	1.6	0.9	0.9
Aqueous cations	52	7.3	2.9	2.8
Aqueous anions	60	8.1	3.9	3.9
Nonaqueous neutrals	666	2.8	0.7	0.7
Nonaqueous cations[d]	72	12.0	5.4	5.4
Nonaqueous anions[d]	148	6.6	4.1	4.1
All neutrals	940	2.5	0.8	0.8
All ions	332	8.1	4.1	4.1

Note: All QM calculations are performed at the HF/6-31G* level and all data are from Ref. 302.
[a]Reference data are from the Minnesota Solvation Database.[300–303] Estimated errors in the reference data are ±0.2 kcal/mol for neutral solutes[300,301] and ±3 kcal/mol for ions.[301]
[b]Using a vdW cavity with GAMESS atomic radii (see Ref. 304), which are close to Bondi radii scaled by 1.2.
[c]Using SMD-optimized radii to construct the vdW cavity for $\mathcal{G}_{\mathrm{elst}}$.
[d]In acetonitrile, methanol, and dimethyl sulfoxide.

- *cavitation*, meaning the energy required to carve out a space in the continuum solvent;
- *Pauli repulsion*, that is, short-range repulsive interactions with the solvent molecules;
- *dispersion*, which is nonspecific but attractive; and finally
- *hydrogen-bonding* between solute and solvent.

Harder-to-define entropic (structural) changes to the solvent make a contribution to $\Delta_{\text{solv}}\mathcal{G}^{\circ}$ as well,[305] although this effect could also be classified as part of the cavitation free energy. Indeed, the phenomena on the list above are not wholly independent; short-range repulsion is related to cavitation, and hydrogen bonding has contributions from electrostatics, repulsion, and dispersion. Furthermore, because cavitation stems from nonelectrostatic repulsion yet cavity size has a tremendous effect on electrostatic interactions, the separation of $\Delta_{\text{solv}}\mathcal{G}^{\circ}$ into electrostatic and nonelectrostatic contributions is difficult to make in a model-free way that would, for example, define a universal electrostatic model for solvation energy calculations.[306]

Further confusing these issues is the fact that some versions of the GAUSSIAN software compute nonelectrostatic interactions by default when a PCM calculation is requested, while other versions implement the same electrostatic model without $\mathcal{G}_{\text{nonelst}}$. This has led to significant confusion on the part of users, with regard to what precisely constitutes a "PCM" calculation.[302,306–309] In the opinion of this author (and some others[306]), the term "PCM" ought to refer to the electrostatics model *only*, which may or may not be augmented by some model of $\mathcal{G}_{\text{nonelst}}$. Absent some treatment of nonelectrostatic interactions, PCMs should not be expected to produce accurate solvation energies although they can still be useful as a simple means to incorporate electrostatic boundary conditions into a quantum chemistry calculation. This can significantly modify frontier orbital energy levels, as compared to vacuum boundary conditions, so even an electrostatics-only model can provide a useful starting point for spectroscopic applications, where solvent-polarized MOs are used in a post-SCF step to compute excitation energies. (Models that go beyond this "zeroth-order" treatment of solvation effects on excitation energies are discussed in Section 5.)

For the purpose of computing absolute solvation energies $\Delta_{\text{solv}}\mathcal{G}^{\circ}$, however, the PCM free energy $\mathcal{G}_0$ in Equation (2.7) should not be used as the solution-phase energy. Nevertheless, there are numerous instances in the literature where a particular solvation model is compared against "PCM" in order to demonstrate its competitive advantage, and it is often difficult to tell what physics is (or is not) included in "PCM," because the term is so often used imprecisely. Furthermore, any model that does not contain nonelectrostatic contributions should not be held up as a standard against which other methods intended to compute solvation energies are compared; such comparisons are fundamentally disingenuous. It is incumbent upon users of electronic structure software to define precisely what *physical model* is being used in any calculations that they report, and this specification should be independent of any software-specific keywords or nomenclature. A software version number is not sufficient because access to that software may be restricted.[310]

Models for $\mathcal{G}_{\text{nonelst}}$, which can be combined with a PCM or other treatment of $\mathcal{G}_{\text{elst}}$, are described below. Before introducing that material, however, let us first survey the overall performance of the best models. Error statistics for hydration energies ($\Delta_{\text{hyd}}\mathcal{G}^{\circ}$) are listed in Table 5 for six different solvation models, each containing both $\mathcal{G}_{\text{elst}}$ and $\mathcal{G}_{\text{nonelst}}$ These models are discussed individually in Sections 4.2 and 4.3, but for now it suffices to note that each significantly outperforms the electrostatics-only approach (C-PCM in Table 4), especially for ions. Specifically for the case of ionic solutes, several of the methods actually approach the accuracy of the reference data themselves, which has been estimated to be no better than 2–3 kcal/mol,[300,301,311] as compared to ≈0.2 kcal/mol for neutral solutes.[300,301]

The uncertainties in the reference data warrant some discussion. The much larger uncertainties for ions reflect the fact that $\Delta_{\text{solv}}\mathcal{G}^{\circ}$ cannot be measured directly for a single ion (although it can be extrapolated from gas-phase cluster ion data),[316–319] and extra-thermodynamic assumptions are required in order to obtain single-ion solvation energies from thermodynamic data for ion pairs.[319–323] Typically, cluster extrapolations and/or semicontinuum calculations are used to establish the proton's solvation energy, $\Delta_{\text{solv}}\mathcal{G}^{\circ}[\text{H}^+]$,[324–328] from which solvation energies for other ions can be obtained from ion-pair data using appropriate thermodynamic cycles.[319,329–331] However, convergence of the cluster extrapolations is slow and not monotonic,[318,331] and it has been suggested that errors in theoretical solvation energies for ions may lie partly (or perhaps mostly) in the reference values,[318] especially for pK_a calculations.[309] Indeed, several different "reference" values of $\Delta_{\text{solv}}\mathcal{G}^{\circ}[\text{H}^+]$ (in various solvents) are available,[319,326,327,332] and these estimates sometimes differ by nontrivial amounts. The worst cases are acetonitrile and dimethyl sulfoxide, for which recent estimates of $\Delta_{\text{solv}}\mathcal{G}^{\circ}[\text{H}^+]$ span ranges of 5 and 7 kcal/mol, respectively.[319,327,333,334] (Although the decision to use H^+ as an extra-thermodynamic reference is defensible in view of the importance of acid/base chemistry, proton quantum effects make this a challenging choice for computations and Li^+ has been suggested as an alternative.[333,335]) Complicating the calculations is the much-debated role of the surface potential of the liquid.[336–340] At least for water, a recent literature review

TABLE 5 Mean unsigned errors (MUEs) relative to experiment, for hydration energies $\Delta_{\text{hyd}}\mathcal{G}^\circ$ computed using various solvation models. The method used for electrostatic interactions is indicated in parenthesis but all models contain nonelectrostatic contributions as well.

		MUE (kcal/mol)					
Data set[a]	N_{data}	SM12[b,c] (GB)	SMD[b,d] (IEF-PCM)	SMVLE[b,e] (SVPE)	CMIRS[f] [SS(V)PE]	SCCS[g] (Poisson)	Soft-sphere[b,h] (Poisson)
Neutrals	274	1.3	0.8	0.6	0.8	1.1	1.1
Cations	52	3.5	3.4	2.6	1.8	2.3	2.1
Anions	60	3.8	6.3	3.2	2.8	5.5	3.0
All ions	112	3.7	4.9	2.9	2.4	4.0	2.6

[a]Reference data are from the Minnesota Solvation Database.[300–303] Estimated errors in the reference data are ±0.2 kcal/mol for neutral solutes[300,301] and ±3 kcal/mol for ions.[301]
[b]Of the 112 ionic solutes, 31 of them include a single explicit H_2O molecule.[301,302]
[c]B3LYP/6-31G* level using ChElPG charges, from Ref. 303.
[d]B3LYP/6-31G* level, from Ref. 302.
[e]HF/6-31+G* level using an isodensity cavity with $\rho_0 = 0.001$ a.u., from Ref. 312.
[f]B3LYP/6-31G* level using an isodensity cavity with $\rho_0 = 0.001$ a.u., from Ref. 313.
[g]PBE in a plane-wave basis, from Ref. 314.
[h]PBE in a wavelet basis, from Ref. 315.

and new calculations suggest that convergence to a consistent reference for $\Delta_{\text{hyd}}\mathcal{G}^\circ[\text{H}^+]$ has finally been achieved.[319,323,334]

Especially for reactions involving ions in protic solvents, including transitions states with significant ionic character, specific hydrogen-bonding effects may be critical to obtaining accurate energetics. In such cases, one or more explicit solvent molecules is often included as part of the atomistic solute. Semicontinuum or "cluster-continuum" approaches of this kind are common, especially for calculating hydration energies of ions.[8,301,324,331,341,342] An important special case is pK_a calculations,[8,343–350] corresponding to the ionization reaction

$$\text{HA(aq)} \rightarrow \text{H}^+\text{(aq)} + \text{A}^-\text{(aq)}, \tag{4.3}$$

for which errors in solvation energies are often the largest source of uncertainty.[294,309,351] Several of the methods assessed in Table 5 for aqueous solvation energies include a single explicit water molecule, in cases where an electronegative atom on the solute exhibits a partial charge exceeding that of oxygen in H_2O.[301,312] For the SMD model in Table 5, this monohydration approach reduces the MUE for ions by ≈1.4 kcal/mol.[312] That said, the C-PCM calculations in Table 4 also include these explicit water molecules yet the errors remain quite large for ions, underscoring the need for nonelectrostatic contributions even in cluster-continuum calculations.

It is also important to realize that in cluster-continuum calculations, convergence of $\Delta_{\text{hyd}}\mathcal{G}^\circ$ is not guaranteed as the number of explicit water molecules is increased,[296,342,351–354] at least not in the absence of sampling over the explicit solvent degrees of freedom. Absent such sampling, the semicontinuum approach fundamentally treats entropic contributions in an unbalanced way. For a single explicit H_2O molecule, or perhaps even one H_2O per hydrogen-bonding site, this inconsistency is likely to be much smaller than the error engendered by omitting the explicit water(s), but if convergence is desired then a theoretically consistent semicontinuum approach must include thermal sampling. A rigorous statistical-mechanical version of the cluster-continuum approach can be formulated in the guise of the *quasi-chemical theory*, developed (in its modern form) by Pratt and coworkers,[355–363] which partitions the solvation energy into "inner shell" (explicit solvent) and "outer shell" (continuum) contributions.

Nonelectrostatic models appropriate for use with PCMs have been developed over the years on an *ad hoc* basis.[9,13] Much of this work has been driven by Luque, Orozco, and coworkers,[116,364–370] who use the name "Miertuš-Scrocco-Tomasi" (MST) solvation model in acknowledgement of the original authors of the model that is now known as D-PCM [Equation (2.25)].[3] The MST-PCM approach combines a PCM (to compute $\mathcal{G}_{\text{elst}}$) with a SASA-type model for $\mathcal{G}_{\text{nonelst}}$, along the lines of what will be discussed in Section 4.2. However, this particular approach has retained something of a do-it-yourself aesthetic insofar as "canned" or "black-box" implementations and parameter sets are not readily available in most electronic structure programs.

Section 4.2 examines several other SASA-type models for $\mathcal{G}_{\rm nonelst}$ that have seen more widespread adoption. Among these, the SM*x* models developed by Cramer, Truhlar, and coworkers are especially popular,[301–305] and for many years have defined the state-of-the-art in solvation modeling within quantum chemistry, although some competitive alternatives have emerged recently and will be discussed. As a counterpoint to the highly empirical SASA-type approach, Section 4.3 introduces "minimally parameterized" models for $\mathcal{G}_{\rm nonelst}$, which attempt to move closer to a first-principles description of nonelectrostatic interactions. Among these, only the *composite method for implicit representation of solvent* (CMIRS), developed by Pomogaeva and Chipman,[371–375] can legitimately be called a black-box model. CMIRS rivals the accuracy of the best SM*x* methods but uses fewer parameters, although it is available only for a few solvents.

As compared to these methods, an even blacker-box approach that is sometimes encountered in chemistry applications (but more often in the chemical engineering literature) is "COSMO-RS,"[197,376–380] a model developed by Klamt and coworkers based on COSMO electrostatics (Section 2.4) but designed for "real solvents." As its basic ingredient, COSMO-RS uses a coarse-grained version of the COSMO surface charge density $\sigma(\mathbf{s})$, averaged over segments of the cavity surface to define a "σ-profile." Solution-phase activities are then parameterized in terms of the σ-profile, and this constitutes a QM-based alternative to other parameterized activity coefficient models that are widely used in engineering thermodynamics.[381–384] However, modern versions of COSMO-RS are available only in the proprietary COSMOTHERM software,[378] and attempts by other groups to implement (or sometimes even to use) COSMO-RS and related models outside of the COSMOTHERM program have been met with harsh criticism from Klamt.[385–414] The tenor of those discussions strongly suggests that insufficient details are available in the literature that would allow others to implement COSMO-RS.[306,387,390,393,396,405,408,411,414,415] Because COSMO-RS appears to be a black box that cannot be opened, it will not be discussed any further in this review.

4.2 | SM*x* and other SASA-based models

To compute free energies of solvation, the most successful and popular models within quantum chemistry are the "SM*x*" models.[305] These have version numbers through $x = 12$ but the comparison in Table 5 is limited to the most recent version (SM12),[303] along with SMD[302] (where the "D" stands for "density") and SMVLE.[312] Together, these three models are representative of the SASA-type parameterization of $\mathcal{G}_{\rm nonelst}$ upon which all of the SM*x* models are built, combined with three different treatments of $\mathcal{G}_{\rm elst}$. A statistical comparison of SM12, SMD, and SMVLE can be found in Table 5 and similar assessments for earlier models such as SM6[301] and SM8[304] can be found elsewhere.[416,417] Given the favorable performance of the versions considered here, however, there is little compelling reason to use these earlier versions.

To understand how these models work, we first take a step back to discuss implicit solvation in classical biomolecular simulations. Owing in no small part to difficulties in obtaining stable numerical forces for Poisson–Boltzmann electrostatics,[186–188,281] the most popular implicit solvation models in that context are *not* based directly on solution of the Poisson–Boltzmann equation but instead are methods known as GB models.[418,419] The GB formalism for electrostatics is used in most of the SM*x* models as well,[420] with the exception of SMD and SMVLE. The GB approach uses the Born ion formula of Equation (2.17) as a pairwise *ansatz* to compute the total electrostatic solvation energy according to

$$\mathcal{G}_{\rm elst}^{\rm GB} = -\frac{1}{2}\left(\frac{1}{\varepsilon_{\rm in}} - \frac{1}{\varepsilon_{\rm out}}\right) \sum_{A,B>A}^{\rm atoms} \frac{Q_A Q_B}{f_{AB}}. \tag{4.4}$$

The quantity f_{AB}^{-1} is a parameterized, effective Coulomb potential, the canonical example of which is[418,419,421]

$$f_{AB} = \left[R_{AB}^2 + \bar{R}_A \bar{R}_B \exp\left(-R_{AB}^2/4\bar{R}_A\bar{R}_B\right)\right]^{1/2}, \tag{4.5}$$

where $R_{AB} = \|\mathbf{R}_A - \mathbf{R}_B\|$ is the interatomic distance. The quantity Q_A^2/f_{AA} constitutes a Coulomb self-energy, with an effective cavity radius $f_{AA} \equiv \bar{R}_A$. As such, the quantities $\{\bar{R}_A\}$ are a set of effective radii that measure the "electrostatic size" of each atom, in the environment created by the other atoms and the continuum boundary conditions.[422–424] For a classical solute, in which $\rho(\mathbf{r})$ is a collection of atom-centered point charges $\{Q_A\}$, these radii can be computed exactly by solving either Poisson's equation,[423] or else its PCM analogue,[152] once per atomic charge Q_A, in a cavity representing the entire molecule. This procedure effectively forces the pairwise GB *ansatz* in Equation (4.4) to reproduce the exact electrostatic energy defined by the continuum electrostatics problem, and the values of $\bar{R}_A$ determined in this way have been called the "perfect" Born radii.[419,423] However, the procedure just described is not a practical one, although it can be used to generate data sets of exact pairwise interactions,[23,152,153] which might suggest new analytical forms to replace Equation (4.5).[23,152,153,425,426]

For practical purposes the radii $\{\bar{R}_K\}$ are usually determined using surface integration procedures, the most popular of which is[418,419,422,424]

$$\bar{R}_K = \left(\frac{1}{R_{\mathrm{vdW},K}} + \frac{1}{4\pi} \int_{\mathbf{r}\in\Omega} \frac{\theta(\|\mathbf{r}-\mathbf{R}_K\| - R_{\mathrm{vdW},K})}{\|\mathbf{r}-\mathbf{R}_K\|^4} d\mathbf{r} \right)^{-1}. \tag{4.6}$$

Here, θ is a step function such that $\theta(x) = 1$ for $x > 0$ and $\theta(x) = 0$ for $x \le 0$. This limits the integration domain to the region of the solute cavity ($\mathbf{r}\in\Omega$) that lies outside of the vdW sphere for atom K, which is centered at $\mathbf{R}_K$. The formula in Equation (4.6) comes from the so-called Coulomb-field approximation, a charge-in-a-sphere model for the reaction-field potential.[72,418,419,422] This is thought to overestimate electrostatic size, especially for charges close to the cavity surface, and alternatives have been suggested,[419,424] but Equation (4.6) is the form used in the SM*x* models such as SM6, SM8, and SM12. The requisite integral can be evaluated numerically using concentric atomic radial shells,[427] but its gradient with respect to nuclear displacements (needed to obtain $d\mathcal{G}^{\mathrm{GB}}_{\mathrm{elst}}/dx$) is complicated when defined in terms of the solid geometry of interpenetrating vdW spheres.[227] Both the integral in Equation (4.6) and its gradient would be straightforward to evaluate using SwiG discretization (Section 3.2), but this has not been implemented.

The GB *ansatz* in Equation (4.4) specifies only the electrostatic component of the solvation energy. The model is completed by adding a nonelectrostatic term $\mathcal{G}_{\mathrm{nonelst}}$, typically using one of two forms. The first option consists of a term proportional to the volume of the solute cavity (V_{cavity}), to model the cavitation energy, along with a second term proportional to the total SASA, which serves to model dispersion:

$$\mathcal{G}_{\mathrm{nonelst}} = \beta V_{\mathrm{cavity}} + \gamma \cdot \mathrm{SASA}. \tag{4.7}$$

The total SASA can be written in terms of atomic contributions [*cf.* Equation (3.4)],

$$\mathrm{SASA} = \sum_K^{\mathrm{atoms}} \mathrm{SA}_K, \tag{4.8}$$

where SA_K is the solvent-exposed surface area of atom K. The quantities β and γ in Equation (4.7) are empirical parameters. An alternative form for $\mathcal{G}_{\mathrm{nonelst}}$ that is also widely used is

$$\mathcal{G}_{\mathrm{nonelst}} = \sum_K^{\mathrm{atoms}} \gamma_K \mathrm{SA}_K, \tag{4.9}$$

with atomic parameters $\{\gamma_K\}$ having units of surface tension. Note that there is no volumetric term in Equation (4.9). It has been argued, based on the scaled-particle theory of hard-sphere fluids,[428] that for small molecules the cavitation energy ought to be parametrizable in terms of the solvent-exposed surface area.[116,174,429,430] This is borne out by comparison to classical atomistic simulations,[429,431] which demonstrate that both surface and volume parameterizations can fit the dispersion–repulsion interactions about equally well.[431] That said, the model in Equation (4.9) has been used not just for small solutes in QM calculations but also for macromolecules in implicit solvent.[432] Models that combine GB electrostatics [Equation (4.4)] with force-field charges to represent the solute, using either Equation (4.7) or Equation (4.9) for $\mathcal{G}_{\mathrm{nonelst}}$, are known as "MM/GBSA" methods.[433–441] There is an analogous set of "MM/PBSA" methods that substitute Poisson–Boltzmann electrostatics in place of the GB model.[433–442] The MM/GBSA approach is the most widely-used implicit solvation model in biomolecular simulations,[419] and both MM/GBSA and MM/PBSA are popular in drug-discovery applications, for calculating ligand–protein binding affinities.[442–445] In that context, these methods are often used as low-resolution screening tools representing a level of sophistication that is intermediate between "knowledge-based" (but largely physics-free) docking or scoring-function methods, and much more expensive atomistic free energy simulations in explicit solvent.

The "numbered" versions of SM*x* (i.e., SM6, SM8, and SM12 but not SMD or SMVLE) each use GB electrostatics, with radii obtained from Equation (4.6) and with atomic charges $\{Q_A\}$ that are derived from the QM charge density by means of certain charge models, CM*x*.[301,446–449] The latter are built upon standard atomic partial charge prescriptions (Mulliken, Hirshfeld, etc.) but include additional empirical parameters designed to improve agreement with the dipole moment of the original charge density from which they were obtained.[450] However, CM*x* charges inherit the basis-set sensitivity of the underlying wave function-derived charges, and therefore these GB-based SM*x* models are each parameterized for use with particular small basis sets (e.g., 6-31G*), and even the use of diffuse functions (e.g., 6-31+G*) can sometimes degrade their performance.[312] The SMD model was introduced to overcome this limitation, by substituting IEF-PCM electrostatics in place of a GB model.[302] As a result, SMD can be used with arbitrary basis sets, as can be the SM12 model based on Hirshfeld charges. Earlier SM*x* models should only be used in conjunction with the basis sets for which they were parameterized. Along similar lines, the SMVLE model uses exact SVPE electrostatics [Equation (2.39)],[312] so should also be stable in arbitrary basis sets, although this model has not seen widespread use.

In the nomenclature preferred by Cramer and Truhlar,[305] $\mathcal{G}_{\text{elst}}$ is the "ENP" term representing electronic, nuclear, and polarization interactions (i.e., electrostatics plus polarization), whereas $\mathcal{G}_{\text{nonelst}}$ is the "CDS" contribution representing cavitation, dispersion, and changes to solvent structure. (Solvent structure is primarily an entropic effect. Notably, only in SM8 are changes in $\mathcal{G}_{\text{nonelst}}$ parameterized as a function of temperature.[451,452]) In practice, each of the SM*x* models (including SMD and SMVLE) uses Equation (4.9) for $\mathcal{G}_{\text{nonelst}}$, although the atomic surface tension parameters $\{\gamma_K\}$ (one per atomic number) are not fit directly but are themselves modeled in a way that includes a coupling between nearby atoms:

$$\gamma_K = \tilde{\gamma}_K + \sum_{J \neq K} \tilde{\gamma}_{JK} t_{\text{sw}}(\|\mathbf{R}_J - \mathbf{R}_K\|). \tag{4.10}$$

The switching function t_{sw} attenuates the coupling as a function of distance, and only a limited subset of the atomic numbers are coupled. (See Ref. 301 for details.) The fitting parameters are $\{\tilde{\gamma}_K\}$ and $\{\tilde{\gamma}_{JK}\}$, which are subsequently expressed as empirically-fitted functions of certain "solvent descriptors" including surface tension, refractive index (which is related to polarizability), and certain Lewis acidity parameters.[453] The result is a "universal" model,[305] in the sense that once the fitting procedure is completed, the nonelectrostatic term is defined for any solvent whose descriptors are known. This is quite a wide range; for example, there are 92 solvents in the training set for SM12.[303]

Altogether the SM*x* fitting parameters include $\{\tilde{\gamma}_K\}$ and $\{\tilde{\gamma}_{JK}\}$ in Equation (4.10) along with the atomic radii $\{R_{\text{vdW},K}\}$ in Equation (4.6). (The optimized radii are used to evaluate $\mathcal{G}_{\text{elst}}$ whereas an SAS surface is used for $\mathcal{G}_{\text{nonelst}}$.[301]) These parameters are fit together, in order to reproduce experimental solvation energies and "transfer energies," that is, aqueous/organic partition coefficients. The resulting nonelectrostatic model need not be transferrable between different treatments of electrostatics,[302,306,454] and each SM*x* model should therefore be taken as an inseparable unit. That said, SMD appears to be less sensitive in this capacity; results in Ref. 302 (and Table 4) show that other treatments of $\mathcal{G}_{\text{elst}}$ can be substituted for IEF-PCM with little effect on the errors, provided that the SMD-optimized atomic radii are used to construct the solute cavity. That caveat underscores the difficulty in separating $\mathcal{G}_{\text{elst}}$ from $\mathcal{G}_{\text{nonelst}}$.[306] Note also that data from several different density functionals were used to train SMD, in an effort to obtain a transferrable parameterization;[302] nevertheless, comprehensive testing for ions suggests that Hartree–Fock-based SMD calculations consistently outperform common density functionals such as B3LYP and M06-2X.[302,455]

Table 5 compares the performance of several different models for small-molecule hydration free energies. For SM12, the MUEs for ions are ≈4 kcal/mol, which is only slightly larger than the estimated uncertainty of the reference data.[301] (Similar errors for other ionic data sets have also been reported.[455] Errors for ions are slightly larger for SM8 than for SMD.[305]) Especially revealing is the comparison in Table 4 between electrostatics-only C-PCM calculations and SMD calculations that use C-PCM for $\mathcal{G}_{\text{elst}}$ but augment this with $\mathcal{G}_{\text{nonelst}}$. For charge-neutral solutes, the electrostatics-only model affords errors that are larger by modest (albeit chemically-significant) amounts, for example, ≈2 kcal/mol larger in nonaqueous solvents. The impact for ions is dramatic, however: SMD reduces the C-PCM errors by ≈4 kcal/mol in both aqueous and nonaqueous solvents. Given the importance of ionic solutes (e.g., for pK_a calculations) and ionic transition states (e.g., for S_N2 reactions), electrostatics-only models cannot be considered acceptable for calculation of $\Delta_{\text{solv}}\mathcal{G}^{\circ}$. The use of PCMs as a metric to gauge the success of new solvation models therefore represents a disingenuous comparison. On the other hand, for properties that depend on only a single geometry (e.g., vertical transition energies for spectroscopic applications), the nonelectrostatic contributions may be less important or may cancel altogether. To compute a reaction profile, however, one should worry that changes in geometry along the reaction coordinate may affect $\mathcal{G}_{\text{nonelst}}$ differently for the various chemical species that are involved.

SM*x* error statistics for nonaqueous solvents are on par with results for aqueous solvation, with MUEs of $\lesssim$1 kcal/mol for neutral solutes and 3–5 kcal/mol for ions. Prediction of $\Delta_{\text{solv}}\mathcal{G}^{\circ}$ in nonaqueous solvents is necessary in order to predict partition coefficients between different solvents. The octanol/water partition coefficient (equilibrium constant K_{ow}), in particular, is a common measure of lipophilicity (or conversely, hydrophobicity),[456–458] and is related to solvation energies according to

$$\Delta_{\text{solv}}\mathcal{G}^{\circ}[\text{octanol}] - \Delta_{\text{solv}}\mathcal{G}^{\circ}[\text{water}] = -RT\ \ln K_{\text{ow}}. \tag{4.11}$$

The value of K_{ow} is widely used in drug-discovery applications,[458–460] and atomic decomposition of terms contributing to $\Delta\Delta\mathcal{G}^{\circ}$ in Equation (4.11) has been used to determine similarity indices for predicting quantitative structure–activity relationships.[458] For environmental toxicology purposes, K_{ow} is an important physical parameter to determine for any new compound.[461] The octanol/water partition coefficient was the subject of a recent blind challenge for theoretical methods,[462] with the SM*x* models emerging as amongst the best performers with a root-mean-square error of 0.44 in units of $\log_{10} K_{\text{ow}}$.[463]

Note that by using Equation (4.9) for $\mathcal{G}_{\text{nonelst}}$, the SM*x* models do not contain any term proportional to the cavity volume, as is often present in MM/GBSA and MM/PBSA models [*cf.* Equation (4.7)]. Volumetric cavitation effects are therefore included by means of *area*-dependent parameters. This can be formally justified by appeal to scaled-particle theory,[116] although the argument is perhaps most convincing for small-molecule solutes. As such, the success of SM*x* may partly reflect the fact that it was parameterized using experimental solvation energies of mostly small molecules. (The largest molecules in the training set are *n*-hexadecane and ethyloctadecanoate, at 51 and 63 atoms, respectively, but most of the solutes are much smaller.[302,417]) Limitation of the reference data to small molecules was intentional, as it minimizes the need to account for thermal effects (vibrational entropy) in the parameterization.[298] Because small solutes have limited conformational flexibility, however, there may not be too much difference in the volumes of different conformers, such that a term that explicitly accounts for cavitation may be largely redundant and therefore not required to obtain accurate solvation energies. In contrast, MM/GBSA and MM/PBSA methods are usually parameterized for (or at least tested on) proteins and other macromolecular solutes, using solvation energies obtained from molecular dynamics simulations in explicit solvent. For a macromolecule, cavity volume may depend sensitively on conformation, as for example in a folded versus an unfolded protein. Since the SM*x* models have not been scaled up to macromolecules, it is unclear how they would perform in that context.

For many years the SM*x* methods have been the go-to quantum chemistry models for solvation energies, even if there are other models that exhibit similar (or occasionally smaller) statistical errors.[370] Focusing on approaches with parameters sets that are openly available, there are a few alternatives to SM12 and SMD whose overall error statistics are comparable (Table 5). One such method is actually a little-used variant of SM*x* called SMVLE.[312] It is based on the same SASA-type model for $\mathcal{G}_{\text{nonelst}}$ that is used in other SM*x* models [Equation (4.9)], but uses the exact SVPE method [Equation (2.39)] for $\mathcal{G}_{\text{elst}}$. In addition, this model includes a "local electrostatics" term based on the extremal values of the normal electric field at the cavity surface, inspired by the observation that those values correlate very well with hydration energies for ions.[464,465] As indicated by the statistics in Table 5, the accuracy of SMVLE is comparable to that of SM12 and SMD for neutral solutes and for cations, but significantly better for anions. It is worth noting that anions are the most challenging case: like cations, their solvation energies are quite large in polar solvents, yet the volume polarization for anions is likely to be much larger since the tails of the anion's wave function extend farther into the continuum. Moreover, with SMVLE the use of explicit water molecules proves to be unnecessary, and the error increases by <0.2 kcal/mol when bare ions are used instead. (For other SM*x* models, the increase is >1 kcal/mol.[312]) The SMVLE approach is therefore an improvement upon the accuracy of other SM*x* models for what feels like the right reasons. However, the underlying SVPE electrostatic model uses an isodensity contour to define the cavity surface and for that reason no analytic gradient of SMVLE is available, as discussed in Section 3.3. This probably explains its lack of widespread use.

A more recent model, which is somewhat similar in form to SMD but developed independently, is the so-called "easy solvation estimation" (ESE) approach of Voityuk and Vyboishchikov.[466,467] This method was designed for rapid screening of large numbers of molecules and for that reason it employs an approximate, non-self-consistent C-PCM calculation to obtain $\mathcal{G}_{\text{elst}}$. Specifically, CM5 atomic charges are computed from the gas-phase QM charge density, and the electrostatic potential from these charges is used to polarize the continuum in a one-shot, *a posteriori* fashion.[466] To this is added a nonelectrostatic term

$$\mathcal{G}_{\text{nonelst}} = \sum_{B}^{\text{atoms}} \left(\gamma_B + \gamma'_B \sigma_B + \gamma''_B \sigma_B^2\right) \text{SA}_B, \tag{4.12}$$

whose first term is identical to the SASA-type model used in SM*x*. Additional terms, with additional parameters $\{\gamma'_B\}$ and $\{\gamma''_B\}$, depend on the solvent-exposed surface charge density on each atom:

$$\sigma_B = \frac{1}{\text{SA}_B} \sum_{b \in B} q_b. \tag{4.13}$$

This is reminiscent of the segmented surface charge densities (or "σ-profiles") that are used to parameterize COSMO-RS.[376,377] An "extended" (xESE) model for ions includes in addition a term that depends on the minimum and maximum values of $|\sigma_K|$,[467] similar in spirit to the "local electrostatics" correction in SMVLE but inspired in this case by a functional form developed by Pomogaeva and Chipman,[372] which is described in Section 4.3. With this addition, xESE achieves MUEs of 2.9 kcal/mol for cations and 3.1 kcal/mol for anions, on par with the estimated uncertainties in the reference data.[301] Further testing is needed to evaluate the robustness of this model and whether its lack of self-consistency will be problematic for prediction of relative energies. (It will almost certainly be problematic for analytic gradient theory.) As a quick-and-dirty screening method to estimate $\Delta_{\text{hyd}}\mathcal{G}^\circ$, however, this method seems quite promising.

Returning to self-consistent models, new approaches based on Poisson's equation also appear quite promising.[314,315,468] One is the SCCS model that was described in Section 3.3, which uses a density-dependent permittivity functional $\varepsilon[\rho](\mathbf{r})$ to determine the continuum interface self-consistently, alongside the charge density $\rho(\mathbf{r})$. Poisson's equation is solved in three-dimensional space to obtain $\mathcal{G}_{\text{elst}}$, which is then combined with the simple two-parameter model for $\mathcal{G}_{\text{nonelst}}$ in Equation (4.7). More precisely, the nonelectrostatic model is

$$\mathcal{G}_{\text{nonelst}} = (\alpha + \gamma)\text{SASA} + \beta V_{\text{cavity}}, \tag{4.14}$$

in which $\text{SASA} = \sum_K \text{SA}_K$ is the total surface area. The quantity γ is the actual surface tension of the solvent, whereas α and β are adjustable parameters. The latter are fit, along with two other parameters that define $\varepsilon[\rho](\mathbf{r})$, in order to reproduce aqueous solvation energies.[314] Despite having just four adjustable parameters, the SCCS model achieves a statistical accuracy that is comparable to SM12 or SMD (see Table 5); notably, it does so for ions *without* using explicit H_2O molecules. Further improvements for aqueous anions are obtained using a "soft-sphere" cavity model,[315] which constructs the cavity from vdW spheres but then interpolates the dielectric function (from $\varepsilon = 1$ to $\varepsilon = 78$) over a narrow switching region centered on the vdW radius.[315] When combined with the nonelectrostatic model in Equation (4.14), the soft-sphere solvation model affords a MUE of 3.0 kcal/mol for anion hydration energies, improving upon both SM12 and SMD and (like SMVLE) on par with the accuracy of the experimental data themselves.[301]

The SM*x* models employ a considerably larger number of empirical parameters as compared to the SCCS-based approaches, although the former are designed to be "universal" models for all solvents whereas the SCCS model was originally parameterized only for water.[314] Recently the SCCS parameterization has been extended to 67 nonaqueous solvents, simply by refitting α in Equation (4.14) for each solvent.[468] (The same volumetric parameter β was used for all solvents, and the two parameters that define the interface functional were fixed as well.) The overall average error in $\Delta_{\text{solv}}\mathcal{G}^\circ$, for neutral solutes in all nonaqueous solvents, is 0.8 kcal/mol,[468] comparable to the accuracy of the SM*x* methods despite the use of only four parameters per solvent. These results seem to defy the notion that continuum electrostatics cannot be separated from nonelectrostatic interactions and made universal. The difference, when it comes to the SCCS approach, may be the self-consistent determination of the solute/continuum interface without resort to atomic radii as parameters, which naturally allows the electrostatic size of an atom to change in response to its environment and in response to the electronic structure of the solute. The next section describes another minimally-parameterized model that also uses a self-consistent cavity surface (based on an isodensity contour) and attempts to separate $\mathcal{G}_{\text{elst}}$ from $\mathcal{G}_{\text{nonelst}}$ and to parameterize the latter separately.

4.3 | Physics-based models

Occasionally there have been attempts to put the nonelectrostatic contributions to the solvation energy on a more rigorous footing,[371–375,469–474] or at least to develop parameterized models that are more closely connected to the physics of intermolecular interactions as compared to the wholly empirical SASA-type approaches.[431,475–478] These physics-based approaches are considered next.

As a simple example, one might borrow from QM/MM methodology and assume classical intermolecular interaction potentials (e.g., of Lennard-Jones type), centered on the solute atoms. An r^{-6} interaction potential provides a model for solute–solvent dispersion, but the explicit solvent molecules need to be replaced with parameters. One such model takes the detailed form[431,476–478]

$$\mathcal{G}_{\text{disp}} = \sum_{A}^{\text{solvent}} \bar{\rho}_A \sum_{B}^{\text{solute}} \gamma_{AB} \sum_{i \in B}^{\text{grid}} a_i \left(\frac{\mathbf{r}_{iB} \cdot \mathbf{n}_{\mathbf{s}_i}}{3 r_{iB}^6} \right), \tag{4.15}$$

where $\bar{\rho}_A$ is the average number density of solvent atom A (e.g., oxygen or hydrogen in aqueous solution), and the parameters $\{\gamma_{AB}\}$ come from a force field. A similar model can be developed to describe the repulsive contribution ($\mathcal{G}_{\text{rep}}$), with r_{iB}^{-6} replaced by r_{iB}^{-12} or perhaps $\exp(-r_{iB})$.[431,477] The quantity $\mathcal{G}_{\text{disp-rep}} = \mathcal{G}_{\text{disp}} + \mathcal{G}_{\text{rep}}$ is usually then combined with a cavitation energy of the form

$$\mathcal{G}_{\text{cav}} = \sum_{B}^{\text{solute}} \left(\frac{\text{SA}_B}{4\pi R_B^2} \right) \Delta G_{\text{HS}}(R_B), \tag{4.16}$$

in which $\Delta G_{\text{HS}}(R_B)$ is the solvation energy for a hard sphere of radius R_B, obtained from scaled-particle theory.[428] Typically the atomic radii used in these nonelectrostatic terms are SAS radii, that is, they include a probe radius representing the assumed size of a solvent molecule. This makes sense from the point of view that r_{iB} represents a first-shell solute–solvent distance. On the other hand, numerical results for electrostatic energies in Table 3 suggest that atomic radii $R_B = 1.2 R_{\text{vdW},B}$ afford results that are closer to the isodensity cavity construction, as compared to SAS radii $R_B = R_{\text{vdW},B} + R_{\text{probe}}$, at least when R_{probe} is a realistic estimate of the size of a solvent molecule. Therefore it is not unusual to employ scaled vdW radii to evaluate $\mathcal{G}_{\text{elst}}$ but SAS radii for $\mathcal{G}_{\text{nonelst}}$. The same is done in the SM*x* models,[301] and similarly in the present case the radii used to define $\mathcal{G}_{\text{elst}}$ need to be optimized in the presence of the electrostatics term in order to obtain useful solvation energies.[200] Some applications of this "QM/MM"-style approach to $\mathcal{G}_{\text{nonelst}}$ are reviewed in Ref. 478, but these models never achieved either the accuracy or the universality of the approaches discussed in Section 4.2.

Equation (4.15) is a classical model for dispersion but there have also been attempts to derive QM dispersion and dispersion-repulsion models, within a continuum framework. One such model, due to Amovilli,[469,470] starts from the generalized Casimir–Polder expression for the dispersion energy of a supramolecular complex A· · ·B:[479–484]

$$\mathcal{U}_{\text{disp}}^{\text{A}\cdots\text{B}} = -\frac{\hbar}{2\pi} \left(\frac{e^2}{4\pi\varepsilon_0} \right)^2 \int_0^\infty d\omega \int_{\mathbb{R}^3} d\mathbf{r}_1 d\mathbf{r}_2 d\mathbf{r}_1' d\mathbf{r}_2' \left(\frac{\chi^{\text{A}}(\mathbf{r}_1, \mathbf{r}_1' | i\omega) \chi^{\text{B}}(\mathbf{r}_2, \mathbf{r}_2' | i\omega)}{\|\mathbf{r}_1 - \mathbf{r}_1'\| \, \|\mathbf{r}_2 - \mathbf{r}_2'\|} \right). \tag{4.17}$$

The quantity $\chi(\mathbf{r}, \mathbf{r}'|\omega)$ is the frequency-dependent density susceptibility (also known as the polarization propagator),[483,484] evaluated in Equation (4.17) at imaginary frequencies. When the monomer separation R_{AB} is large, second-order perturbation theory affords the "uncoupled" approximation,[480,485–489] first derived by London:[490,491]

$$\mathcal{U}_{\text{disp}}^{\text{A}\cdots\text{B}}(R_{\text{AB}}) = -\left[\frac{3\hbar}{\pi}\int_0^\infty \bar{\alpha}^{\text{A}}(i\omega)\ \bar{\alpha}^{\text{B}}(i\omega)\ d\omega\right]\frac{1}{R_{\text{AB}}^6}. \tag{4.18}$$

The quantity $\bar{\alpha}(\omega)$ is the frequency-dependent isotropic polarizability and the term in brackets provides a microscopic formula for the C_6 coefficient. Components α_{ab} of the polarizability tensor, in the spectral representation, are

$$\alpha_{ab}(\omega) = \frac{1}{\hbar}\sum_{n>0}\left[\frac{\langle 0|\hat{\mu}_a|n\rangle\langle n|\hat{\mu}_b|0\rangle}{\omega-\omega_{n0}} + \frac{\langle 0|\hat{\mu}_b|n\rangle\langle n|\hat{\mu}_a|0\rangle}{\omega+\omega_{n0}}\right], \tag{4.19}$$

where $\omega_{n0} = (E_n - E_0)/\hbar$.[492] In early work by Rösch and Zerner,[493] a sum-over-states formalism (at the level of configuration interaction with single substitutions) was used to explicitly evaluate the dispersion, essentially along the lines of Equation (4.19) and its analogue for excited states, in the interest of understanding dispersion-induced shifts in excitation energies. This approach is expensive, as hundreds of states are required for convergence, but it does correctly model trends in solvatochromic shifts for nonpolar chromophores in nonpolar solvents (e.g., naphthalene in cyclohexane). However, these shifts are generally <0.1 eV and this work has not been pursued further.

Returning to $\mathcal{U}_{\text{disp}}^{\text{A}\cdots\text{B}}$ in Equation (4.17), a sum-over-states expression (Lehmann representation) can be introduced for the requisite density susceptibilities, writing them in terms of transition densities $\rho_{0n}(\mathbf{r})$:[482,484]

$$\chi(\mathbf{r},\mathbf{r}'|i\omega) = -\frac{2}{\hbar}\sum_{n>0}\frac{\omega_{0n}\ \rho_{0n}(\mathbf{r})\ \rho_{0n}(\mathbf{r}')}{\omega_{n0}^2+\omega^2}. \tag{4.20}$$

Inserting this formula in place of $\chi^{\text{A}}(\mathbf{r}_1,\mathbf{r}_1'|i\omega)$ in Equation (4.17) affords an expression for the dispersion (free) energy of "A-in-B," that is, solute A interacting with an implicit representation of B:[469]

$$\mathcal{G}_{\text{disp}}^{\text{A-in-B}} = \frac{1}{\pi}\int_0^\infty d\omega\sum_{n>0}\frac{\omega_{n0}^{\text{A}}}{(\omega_{n0}^{\text{A}})^2+\omega^2}\int_{\mathbb{R}^3}d\mathbf{r}\int_\Gamma d\mathbf{s}\left(\frac{\rho_{0n}^{\text{A}}(\mathbf{r})\ \sigma_{\text{B}}\left[\varepsilon^{\text{B}}(i\omega),\rho_{0n}^{\text{A}}\right](\mathbf{s})}{\|\mathbf{r}-\mathbf{s}\|}\right). \tag{4.21}$$

In writing this equation, the susceptibility χ^{B} in Equation (4.17) has been eliminated by first introducing a polarization density

$$\rho_{\text{pol}}^{\text{B}}(\mathbf{r}_2) = \int_{\mathbb{R}^3}d\mathbf{r}_1'd\mathbf{r}_2'\left(\frac{\chi^{\text{B}}(\mathbf{r}_2,\mathbf{r}_2'|i\omega)\ \rho^{\text{A}}(\mathbf{r}_1')}{\|\mathbf{r}_1'-\mathbf{r}_2'\|}\right), \tag{4.22}$$

induced on B by the presence of A. This quantity is then replaced with a surface charge $\sigma_{\text{B}}(\mathbf{s})$, in the spirit of the ASC-PCM formulation of continuum electrostatics, except that in the present case the surface charge depends on the frequency-dependent dielectric function $\varepsilon(i\omega)$ evaluated at imaginary frequencies. The function $\varepsilon(i\omega)$ is the central quantity in the Lifshitz theory of the Casimir force and the dispersion energy.[479,494–496] In a separate approach, Ninham and coworkers[473,474] use the frequency-dependent dipole- and higher-order (hyper)polarizabilities for the solute, $\bar{\alpha}(i\omega)$, and so on, in conjunction with models for $\varepsilon(\omega)$, to model solute–solvent dispersion.

Models for $\mathcal{G}_{\text{disp}}$, the dispersion contribution to $\mathcal{G}_{\text{nonelst}}$, can now be constructed based on Equation (4.21) by modeling the function $\varepsilon(i\omega)$ as well as the surface charge density $\sigma_{\text{B}}(\mathbf{s})$ that is induced by various excited states of solute A. The transition densities $\rho_{0n}^{\text{A}}(\mathbf{r})$ and excitation frequencies ω_{n0}^{A} that appear in Equation (4.21) could be computed explicitly, since the solute A is described by quantum chemistry,[469] or perhaps modeled using SCF eigenvalues.[470,471] A suggested model for the surface charge is[470]

$$\sigma_{\text{B}}\left[\rho_{0n}^{\text{A}}\right](\mathbf{s}) = -\frac{1}{4\pi}\left(\frac{\bar{\Omega}^2}{\bar{\Omega}^2+\omega^2}\right)\left(\frac{\varepsilon_\infty-1}{\varepsilon_\infty}\right)E_\perp\left[\rho_{0n}^{\text{A}}\right](\mathbf{s}), \tag{4.23}$$

where $E_{\perp}\left[\rho_{0n}^{\mathrm{A}}\right](\mathbf{s})$ is the normal electric field generated by $\rho_{0n}^{\mathrm{A}}(\mathbf{r})$. Modulo a factor of $\bar{\Omega}/(\bar{\Omega}+\omega^2)$, Equation (4.23) looks just like the ASC in the D-PCM method [Equation (2.25)], albeit generated by the transition density $\rho_{0n}^{\mathrm{A}}(\mathbf{r})$ rather than the ground-state density and with the "optical" dielectric constant ε_∞ replacing the static dielectric constant ε_s. (As will be discussed in Section 5, ε_∞ is the appropriate dielectric constant for polarization upon sudden or vertical excitation, without orientational contributions from the solvent.) The quantity $\hbar\bar{\Omega}$ is the characteristic ionization energy of the solvent, which comes from the approximation of setting every ω_{n0} equal to $\bar{\Omega}$.[491] [In practice, $\hbar\bar{\Omega} = \varepsilon_\infty \times (\mathrm{IE})_{\mathrm{solvent}}$ has been used.[470,471]] The integral over ω in Equation (4.21) remains to be evaluated and the factor of $\bar{\Omega}^2/(\bar{\Omega}^2+\omega^2)$ interpolates between limits of unity for $\omega = 0$, for which the solute sees the full induced polarization response, and zero as $\omega \to \infty$ because when $\omega \gg \bar{\Omega}$ the excitation frequency is so large that the response averages to zero. These models have interesting possibilities for the description of solute–environment dispersion in excited states, which are only starting to be explored.[471,472]

A rather different formulation of $\mathcal{G}_{\mathrm{disp}}$ has been put forward by Pomogaeva and Chipman,[373] who borrow from the nonlocal correlation energy functional developed by Vydrov and Van Voorhis.[497–500] This functional, usually known as VV10,[501] represents an attempt to incorporate dispersion interactions into DFT in a rigorous way, and is itself a simplified form of the nonlocal functional developed by Langreth and Lundqvist.[502–505] (In a mildly annoying bit of physicist reductionism, the Langreth–Lundqvist functional is often known as "the" vdW functional, as if such a designation could possibly be unique.) These nonlocal correlation functionals are already based on a pairwise *ansatz*,[501] and to use them in conjunction with a continuum representation of the solvent one simply replaces the density of one interacting partner with the bulk solvent density, $\bar{\rho}$. The functional form is then[313,373]

$$\mathcal{G}_{\mathrm{disp}} = A\int_{\mathbf{r}\in\Omega}\left(\frac{\rho(\mathbf{r})\ I(\mathbf{r})}{w[\rho](\mathbf{r})\left(w[\rho](\mathbf{r}) + \bar{\rho}_{\mathrm{solvent}}^{1/2}\right)}\right)d\mathbf{r}, \tag{4.24}$$

where

$$I(\mathbf{r}) = \int_{\mathbf{r}'\notin\Omega}\left(\frac{d\mathbf{r}'}{\|\mathbf{r}-\mathbf{r}'\|^6+\delta^6}\right) \tag{4.25}$$

and

$$w[\rho](\mathbf{r}) = \left(\rho(\mathbf{r}) + \frac{3C}{4\pi}\frac{\left\|\hat{\boldsymbol{\nabla}}\rho(\mathbf{r})\right\|^4}{\rho(\mathbf{r})^4}\right)^{1/2}. \tag{4.26}$$

The parameter C in Equation (4.26) is taken without modification from VV10,[498,499] but a parameter δ is introduced in Equation (4.25) to prevent the integral from diverging. Aside from that, the only additional parameter that has been introduced (beyond those already present in VV10) is an overall scaling factor A in Equation (4.24). The density $\rho(\mathbf{r})$ is the solute's electron density and the integral in Equation (4.24) is evaluated over the solute cavity ($\mathbf{r}\in\Omega$). However, the integration domain in Equation (4.25) is the region $\mathbf{r}'\notin\Omega$ that is *outside* of the cavity, which requires integration of three-dimensional space. (In practice, the discretization need not extend very far beyond the cavity, since the integrand decays rapidly.) It is worth noting that analytic gradients have not been implemented for any of the QM-based dispersion models described in this section, although they have been implemented for the QM/MM-style approach of Equation (4.15).[478] The functional form for $\mathcal{G}_{\mathrm{disp}}$ in Equation (4.24) may better lend itself to analytic gradients as compared to other approaches, insofar as the analytic gradient of VV10 has already been reported.[499]

In contrast to dispersion, a functional form for Pauli repulsion is rather straightforward. This effect arises from interpenetration of the tails of two nonbonded densities, and one functional form that has been suggested is simply

$$\mathcal{G}_{\mathrm{exch}} = B'\int_{\mathbf{r}\notin\Omega}\rho(\mathbf{r})\ d\mathbf{r}, \tag{4.27}$$

where B' is an empirical parameter.[470] (Note also that the integration domain is over the solvent, $\mathbf{r}\notin\Omega$.) An alternative is[373]

$$\mathcal{G}_{\text{exch}} = B\int_{\mathbf{r}\notin\Omega}\left\|\hat{\boldsymbol{\nabla}}\rho(\mathbf{r})\right\|\,d\mathbf{r}. \tag{4.28}$$

The latter form is suggested by an exact result for the exchange-repulsion between two hydrogen atoms,[506] but both models have been used in practice. For example, the model in Equation (4.27) has been used to develop an "extreme pressure" (XP-)PCM,[507,508] based on the thermodynamic relation $p = -(\partial\mathcal{G}/\partial V)_T$ and calculation of analytic derivatives of $\mathcal{G}_{\text{exch}}$ and $\mathcal{G}_{\text{elst}}$ with respect to the cavity volume. XP-PCM has been used to study how pressures $p > 1$ GPa affect both molecular geometries and the equilibrium positions of chemical reactions.[509,510] The model in Equation (4.28) has been used as part of a black-box solvation model that is described next.

In an attempt to develop a first-principles implicit solvation model that can compete with SM*x*, Pomogaeva and Chipman[371–375] combined SS(V)PE electrostatics (using an isodensity cavity construction) with a "minimally parameterized" nonelectrostatic model of the form

$$\mathcal{G}_{\text{nonelst}} = \mathcal{G}_{\text{disp}} + \mathcal{G}_{\text{exch}} + \mathcal{G}_{\text{FESR}}. \tag{4.29}$$

The components $\mathcal{G}_{\text{disp}}$ and $\mathcal{G}_{\text{exch}}$ are modeled as in Equations (4.24) and (4.28), respectively, and $\mathcal{G}_{\text{FESR}}$ is "field-effect short-range" (FESR) term for hydrogen bonding.[372] The latter takes as inputs the maximum and minimum values of the normal electric field at the cavity surface, and has the form

$$\mathcal{G}_{\text{FESR}} = C(\min|E_\perp|)^\xi + D(\max|E_\perp|)^\xi. \tag{4.30}$$

This form is inspired by the observation that ion hydration energies correlate well with local electric field strength.[464,465] Further evidence comes from a correlation between hydrogen bond strength and local electric fields in water (as noted in classical molecular dynamics simulations),[511–513] as well as an observed correlation between PCM surface charge densities (which themselves correlate with electric field strength) and hydrogen bond energies for small solutes that form a single hydrogen bond.[514,515] Indeed, the *ansatz* in Equation (4.30) would only seem to accommodate a single hydrogen-bond donor site and a single acceptor site. Nevertheless, this simple form is remarkably effective in reducing errors for ionic species. As discussed in Section 4.2, both the SMVLE[312] and xESE[467] solvation models use a local electric field correction, albeit not precisely the same as the one in Equation (4.30), and these two models both exhibit rather small errors for ion hydration energies, approaching the accuracy limits of the data. A downside to using $\min|E_\perp|$ and $\max|E_\perp|$ (or $\min\{q_k\}$ and $\max\{q_k\}$, as suggested in Ref. 514) is that these are not differentiable with respect to nuclear positions. The SMVLE model introduces a modified form of the field-dependent local electrostatics term, with a switching function to ensure continuity as the nuclei are displaced.[312]

It is often considered that the separation $\mathcal{G} = \mathcal{G}_{\text{elst}} + \mathcal{G}_{\text{nonelst}}$ is difficult to accomplish in a rigorous manner,[306] leading to nonelectrostatic models that cannot be used interchangeably with different treatments of continuum electrostatics,[454] although recent results with SCCS suggest this may not be entirely true,[468] as discussed in Section 4.2. It appears that the worst aspects of nontransferability are related to cavity construction, as SMD works well with various models for $\mathcal{G}_{\text{elst}}$ provided that the atomic radii used in the electrostatics calculation were optimized together with the nonelectrostatic parameters.[302] Using an isodensity implementation of SS(V)PE to define $\mathcal{G}_{\text{elst}}$, Pomogaeva and Chipman[373–375] have attempted to make a universal separation between electrostatic and nonelectrostatic interactions, with $\mathcal{G}_{\text{nonelst}}$ given by Equation (4.29), in a model they call CMIRS. This model contains five empirical parameters for a given solvent: the linear coefficients A, B, C, and D that appear in $\mathcal{G}_{\text{disp}}$, $\mathcal{G}_{\text{exch}}$, and $\mathcal{G}_{\text{FESR}}$, as well as the exponent ξ in $\mathcal{G}_{\text{FESR}}$. The FESR term is omitted for nonpolar solvents, leaving just two parameters. These parameters were originally determined for benzene,[373] cyclohexane,[373] water,[374] dimethyl sulfoxide,[375] and acetonitrile,[375] by fitting to experimental solvation energies, but were later adjusted to fix an error in the original implementation of the model.[313] Parameters for methanol have also been reported, based on the original implementation.[516] As with the SCCS approach, this is considerably fewer parameters (for any given solvent) as compared to the SM*x* models, although the latter are designed as "universal" models in which the nonelectrostatic parameters are determined only once, and then the model is available for any solvent whose macroscopic descriptors are available.[305] For example, the training set for SM12 contains

92 solvents,[303] as compared to the six for which CMIRS parameters are currently available. As noted above, however, the SCCS model has recently been extended to 67 nonaqueous solvents by refitting just a single parameter per solvent,[468] and it would be straightforward to attempt something similar with CMIRS, adjusting only the A and B parameters that appear in $\mathcal{G}_{\text{disp}}$ and $\mathcal{G}_{\text{exch}}$.

Water is the solvent to have if you are only having one, and error statistics versus experimental hydration energies (Table 5) demonstrate that CMIRS is somewhat more accurate than SM12 or SMD, especially for ions, despite fewer parameters in the model. It is also more accurate than SCCS, especially for anions. Given the 2–3 kcal/mol uncertainties in the reference data for ions,[300,301,311] CMIRS has achieved the practical lower limit for any solvation model trained on these data. Correlation with experimental hydration energies is excellent; see Figure 9.

However, despite all of the physical considerations that went into the CMIRS approach to modeling $\mathcal{G}_{\text{nonelst}}$, and despite the limited number of parameters used per solvent, an error in the original implementation of $\mathcal{G}_{\text{disp}}$ went unnoticed despite the fact that it modifies dispersion energies in the training set by up to 8 kcal/mol.[313] This was able to escape notice because the B parameter in $\mathcal{G}_{\text{exch}}$ [Equation (4.28)] absorbs the discrepancy, rendering $\mathcal{G}_{\text{exch}}$ even more repulsive in order to offset a dispersion energy that is too attractive.[313] A similar cancellation between cavitation and dispersion has been noted elsewhere,[474,517] and in fact $\mathcal{G}_{\text{disp}} + \mathcal{G}_{\text{exch}}$ is often parameterized together as a single entity in empirical models, including SM*x* and others that use the atomic surface tension *ansatz* of Equation (4.9). This may hide certain subtleties, such as the fact that cavitation effects are more important than dispersion to explain binding affinities of rare-gas guest atoms to cucurbituril host molecules,[518] or that the unfavorable hydration energies of small nonpolar polymers are well approximated by the cavitation energy ($\Delta_{\text{hyd}}\mathcal{G} \approx \mathcal{G}_{\text{cav}}$),[519] suggesting near-cancellation of other effects.

5 | NONEQUILIBRIUM SOLVATION

5.1 | Conceptual overview

How does a continuum solvent respond to a sudden change in the solute's charge distribution? This question must be considered for electronic spectroscopies, including absorption to (or emission from) an excited electronic state, or photoelectron spectroscopy that removes an electron. The general theory of time-dependent processes in dielectric materials introduces a frequency-dependent dielectric function $\varepsilon(\omega)$, such that the induction field $\mathbf{D}$ responds to a frequency-dependent electric field $\mathbf{E}$ according to $\mathbf{D}(\mathbf{r}, \omega) = \varepsilon(\omega)\mathbf{E}(\mathbf{r}, \omega)$.[520–523] In the presence of a time-dependent field, the frequency-dependent permittivity is complex-valued, in order to describe the phase lag between $\mathbf{E}$ and

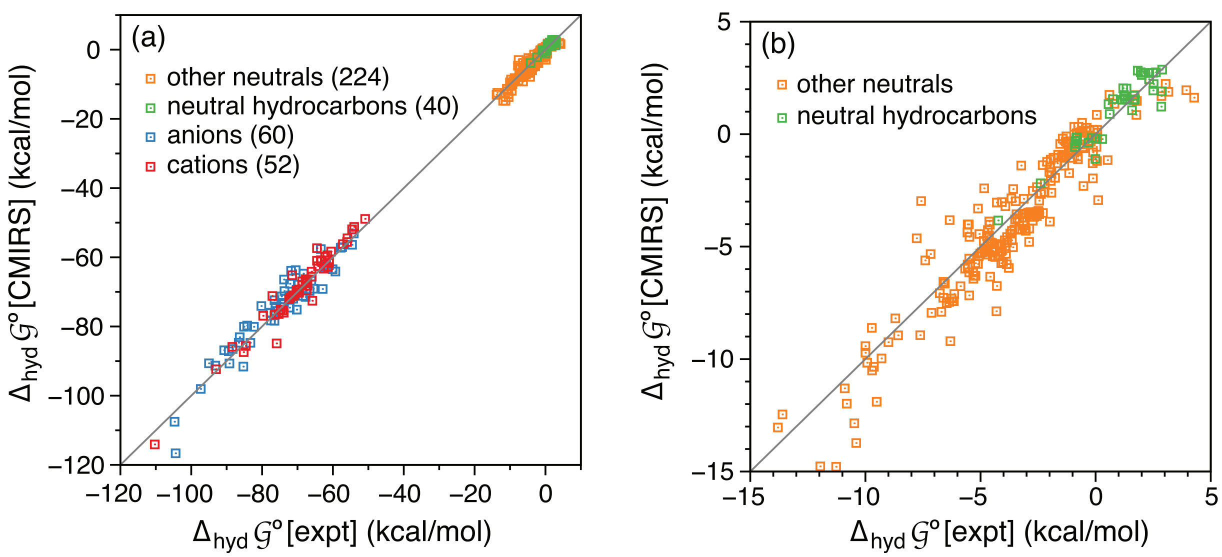

FIGURE 9 Comparison of experimental hydration energies (Minnesota solvation database[300–303]) with values computed using CMIRS: (a) all solvation energies, including both neutral molecules as well as ions (with the number of data points indicated in each case), versus (b) results for charge-neutral solutes only. Reprinted from Ref. 313; copyright 2016 American Chemical Society

D.[520,523] This complex-valued permittivity is often denoted $\hat{\varepsilon}$ or ε^* but we will not do so here. Where needed, we will simply indicate the frequency dependence explicitly.

The permittivity is real-valued in two important limits, namely, $\varepsilon_s \equiv \varepsilon(0)$, which is the static (zero-frequency) limit, and also in the high-frequency limit, where the limiting value $\varepsilon_\infty = \lim_{\omega \to \infty} \varepsilon(\omega)$ is known as the *optical dielectric constant*, for reasons that are described below. That $\varepsilon_\infty > 0$ describes the fact that there is always some part of the polarization that is able to remain in phase with the applied field. Switching to the time domain and labeling that part of the medium's response as "fast" polarization,

$$\mathbf{P}_{\text{fast}}(t) = \left(\frac{\varepsilon_\infty - 1}{4\pi}\right)\mathbf{E}(t), \tag{5.1}$$

the remaining ("slow") component is then defined by a time-dependent analogue of Equation (2.1):[520]

$$\mathbf{D}(t) = \varepsilon_\infty \mathbf{E}(t) + 4\pi \mathbf{P}_{\text{slow}}(t). \tag{5.2}$$

The frequency components of $\mathbf{P}_{\text{slow}}(t)$ depend on $\varepsilon(\omega)$, but generally speaking the slow polarization response consists of vibrational contributions with timescales of 10^{-12}–10^{-14} s, along with even slower orientational components. (The primary relaxation timescale for neat liquid water is 8–10 ps under ambient conditions.[89,524–526])

It is possible to model the frequency dependence of $\varepsilon(\omega)$ directly.[527–531] A phenomenological model is

$$\varepsilon(\omega) = \varepsilon_\infty + (\varepsilon_s - \varepsilon_\infty)\sum_k \frac{c_k}{1 + i\omega\tau_k}, \tag{5.3}$$

in which the parameters $\{\tau_k\}$ represent characteristic time constants for microscopic relaxation processes, with $\sum_k c_k = 1$.[520] (The version with only a single timescale was originally introduced by Debye and usually bears his name.[89,523,532]) When such a model is used in the context of continuum solvation theory, the polarization charge becomes explicitly time-dependent and the permittivity for "fast" polarization is the real part of $\varepsilon(\omega)$ for frequencies larger than the perturbation of interest. Such models have been used to simulate the time-dependent Stokes shift in the fluorescence energy,[527–529] and to simulate the combined response of the molecule and the medium to an external field that is resonant with an excited state of the solute.[531,533] The latter application makes the most sense when combined with electronic structure methods that simulate time-dependent electron dynamics,[534,535] but these explicitly time-dependent approaches are not considered in this work.

The focus here is on the nonequilibrium response to a sudden change in the solute density, that is, a vertical or Franck–Condon process. For vertical absorption, emission, or ionization, the nuclei are fixed and the continuum solvent "molecules" cannot vibrate or reorient. This limits the continuum response to the fast component of the polarization, which is electronic in nature and remains in equilibrium with the sudden change in $\rho(\mathbf{r})$. The slow component is dictated by the solute's initial electronic state and cannot respond on the timescale of vertical excitation or ionization, and is therefore out of equilibrium with the final electronic state. Phenomenologically, this picture reduces $\varepsilon(\omega)$ to its limiting values ε_s and ε_∞.

The value of ε_∞ can be related to the polarizability of the solvent molecules (Lorenz–Lorentz equation),[520] but in the present context is simply a measurable property of the solvent, determined from the index of refraction $n(\omega) = \sqrt{\varepsilon(\omega)}$.[520,536] Formally, ε_∞ should be determined in the limit $\omega \to \infty$, but at the same time $n(\omega)$ needs to be measured away from any resonances and therefore optical wavelengths are often used, hence the "optical" dielectric constant. Values are often measured at the sodium D-line (λ = 589 nm),[537] and for water the value obtained is $\varepsilon_\infty(\lambda) = 1.78$ at λ = 589 nm, as compared to $\varepsilon_\infty(\lambda) = 1.95$ at λ = 200 nm.[538] In older literature (and sometimes repeated more recently),[539,540] values such as $\varepsilon_\infty = 4.0 - 5.5$ are reported for water,[89,541] and these larger values were originally thought to agree better with predictions from Onsager's reaction-field theory.[541] In fact, these larger values were based on a false extrapolation using Debye's model of a single relaxation timescale ($\tau_1 = 8 - 10$ ps), whereas permittivity data that extend to terahertz frequencies reveal at least two distinct relaxation timescales,[526,542–545] including a faster process $\tau_2 < 1$ ps.[526,542,543] (The microscopic explanation for these timescales remains a topic of current debate.[546,547]) The data therefore appear to approach a limiting value $\varepsilon_\infty \approx 5$ in the microwave regime,[89,548] but decay to $\varepsilon_\infty \approx 2$ at terahertz frequencies.[543,545] The latter value is consistent with $n^2(\lambda)$ measured at optical wavelengths.[538]

Looking at a modern tabulation of the data for common solvents, one finds little variation in refractive indices at visible wavelengths, which generally range from $n \approx 1.3$–1.5.[537] Consequently, there is considerable uniformity in the optical dielectric constants ($\varepsilon_\infty = 1.7 - 2.3$), despite the fact that the static dielectric constants for these solvents range from $\varepsilon_s = 2 - 110$; see Table 6. The narrow range of ε_∞ reflects the fact that typical solvents are closed-shell, small-molecule insulators with band gaps in the vacuum ultraviolet, and which therefore possess roughly similar molecular polarizabilities. Inorganic solids may have considerably larger indices of refraction,[551] for example, $n = 2.43$ at 589 nm (and therefore $\varepsilon_\infty = 5.90$) for $BaTiO_3(s)$,[552] a material used in nonlinear optical applications. These larger values are attributable to low-lying excited states that facilitate more substantial electronic polarization and therefore significant dispersion of light, but this behavior is simply not found in common solvents.

Before introducing a modern computational formalism for nonequilibrium polarization, we first consider two historical examples. The first is a well-known result in electronic spectroscopy that relates the Stokes shift ($\Delta\nu = \nu_{\text{abs}} - \nu_{\text{fluor}}$) to the change in the solute's dipole moment upon excitation ($\Delta\mu$), and which is known as the *Lippert-Mataga equation*,[45,553–555]

$$hc\Delta\nu = \text{constant} + \frac{2(\Delta\mu)^2}{\bar{R}^3} \underbrace{\left[\frac{\varepsilon_s - 1}{\varepsilon_s + 1} - \frac{\varepsilon_\infty - 1}{2\varepsilon_\infty + 1}\right]}_{F(\varepsilon_s, \varepsilon_\infty)}. \tag{5.4}$$

In practice, this equation is used to determine excited-state dipole moments (assuming that the ground-state dipole moment is known) by measuring the Stokes shift in solvents of differing polarity. In fact, a variety of alternative formulas for this purpose have been suggested,[556–564] along the lines of Equation (5.4) but differing somewhat in their treatment of excited-state polarization, which leads to differences in the form of the "solvent polarity function" $F(\varepsilon_s, \varepsilon_\infty)$. These models (including the Lippert-Mataga one) are so crude that often experimental data can be fit equally well to any one of them.[565–571] More important is the basic molecular physics that underlies this approach. Comparison to the model of a dipole in a spherical cavity [Equation (2.18)] shows that the physical content of Equation (5.4) is to take the difference dipole moment $\Delta\mu$ and solvate it using permittivity ε_∞ rather than ε_s.

The solvent parameter ε_∞ also makes an appearance in Marcus' theory of electron transfer,[572–577] in which the "outer-sphere" reorganization energy is given by

$$\lambda_{\text{outer}} = (\Delta Q)^2 \left(\frac{1}{\varepsilon_\infty} - \frac{1}{\varepsilon_s}\right)\left(\frac{1}{2R_D} + \frac{1}{2R_A} - \frac{1}{\|\mathbf{r}_D - \mathbf{r}_A\|}\right). \tag{5.5}$$

This formula is derived from what is essentially a nonequilibrium formulation of the Born ion model [Equation (2.17)], combined with a Coulomb interaction between charges centered in a donor sphere (radius R_D centered at $\mathbf{r}_D$) and an

TABLE 6 Static dielectric constants[a] (ε_s) and optical dielectric constants[b] (ε_∞) for some common solvents.

Solvent	ε_s	ε_∞	Solvent	ε_s	ε_∞
n-Hexane	1.9	1.89	Ethanol	24.3	1.85
Cyclohexane	2.0	2.03	Ethylene glycol	30.9	2.05
Benzene	2.3	2.25	Methanol	33.0	1.77
Toluene	2.4	2.24	Nitrobenzene	34.7	2.41
Diethyl ether	4.2	1.83[c]	Acetonitrile	36.0	1.81
Chloroform	4.7	2.08	Dimethyl acetamide	39.6	2.07
Dichloromethane	8.9	2.03	Dimethyl sulfoxide	46.6	2.18
2-Propanol	18.2	1.92	Water	78.4	1.78[d]
Acetone	20.8	1.85	Formamide	109.6	2.10

Note: Values are given as dimensionless numbers relative to vacuum permittivity, ε_0.
[a]At 25°C, from Ref. 549.
[b]At 20°C except where noted, based on refractive indices $n(\lambda)$ measured at $\lambda = 589$ nm, from Ref. 537.
[c]At 16.5°C.
[d]Valid for 20–25°C, from Ref. 550.

acceptor sphere (radius R_A centered at $\mathbf{r}_A$). The electron transfer is assumed to occur instantaneously—before the orientational motion of the solvent molecules can respond—hence the change in $\mathcal{G}_{\text{elst}}$ involves ε_∞ in addition to ε_s. The prefactor of $\left(\varepsilon_\infty^{-1} - \varepsilon_s^{-1}\right)$ in Equation (5.5) is sometimes called the *Pekar factor*,[540,578] and replaces the prefactor of $(1 - \varepsilon_s^{-1})$ in the equilibrium version of the Born model. For water, ε_s is large due to the sizable H_2O dipole moment, lending a large orientational component to the dielectric screening effect, but for nonpolar solvents most or all of the solvent response is electronic since $\varepsilon_\infty \approx \varepsilon_s$ (Table 6). The electronic contribution comes from the intrinsic polarizability of the solvent molecules, and for this reason ε_∞ has sometimes been called the "dielectric constant for induced polarization."[520] Onsager calls n^2 the "internal" (to the molecule) dielectric constant.[84]

5.2 | State-specific approach

The phenomenology introduced above can be generalized to a rigorous description of electrostatics,[579,580] affording a continuum theory of nonequilibrium solvation.[539,576,578–582] Several variants have been formulated for use with PCMs,[221,583–587] as well as for continuum solvation based on Poisson's equation.[44,588] Operationally, a charge density $\rho_0(\mathbf{r})$ corresponding to the initial electronic state $|\Psi_0\rangle$ is first equilibrated with a continuum whose dielectric constant is ε_s. Then, following excitation (or ionization) from state $|\Psi_0\rangle$ to state $|\Psi_k\rangle$, the difference density $\Delta\rho_k(\mathbf{r}) = \rho_k(\mathbf{r}) - \rho_0(\mathbf{r})$ is allowed to polarize a continuum whose dielectric constant is ε_∞, representing the change in the fast polarization. We now consider this in detail.

Consistent with the appearance of the zero- and infinite-frequency dielectric constants in Equations (5.4) and (5.5), a general nonequilibrium theory of continuum electrostatics is based upon a partition $\mathbf{P} = \mathbf{P}_{\text{slow}} + \mathbf{P}_{\text{fast}}$ in which the fast component of the polarization remains in equilibrium with the solute even upon sudden change in its charge density. The slow polarization is frozen on this timescale, at the value determined by equilibrium solvation of the initial state. This is accomplished via a partition of the (linear) electric susceptibility, $\chi(\omega) = [\varepsilon(\omega) - 1]/4\pi$. Separating the susceptibility $\chi = \chi_f + \chi_s$ into fast and slow contributions, the form of χ_f is suggested by Equation (5.1). This affords[221,564,580,589,590]

$$\chi_f = (\varepsilon_\infty - 1)/4\pi, \tag{5.6a}$$

$$\chi_s = (\varepsilon_s - \varepsilon_\infty)/4\pi. \tag{5.6b}$$

This has been called the "Marcus partition" of the polarization response,[221] although it was actually formalized by Brady and Carr.[564] It embodies the phenomenological concepts introduced above, for example, that $\mathbf{P}_{\text{fast}}$ originates with molecular polarizability while $\mathbf{P}_{\text{slow}}$ is orientational.

An alternative to Equation (5.6) is the so-called "Pekar partition,"[221,590] which was originally introduced to describe self-trapped polarons,[591,592] then subsequently adapted for optical spectroscopy,[554,558,593] and still later adopted for use in ASC-type continuum solvation models.[5,13,594–596] Its use is prevalent in older literature so the distinction is worth pointing out even though Equation (5.6) will be used in practice. Within the Pekar approach, the induced surface charge is partitioned into "inertial" and "dynamic" components, $\mathbf{P} = \mathbf{P}_{\text{in}} + \mathbf{P}_{\text{dyn}}$. The total surface charge $\sigma(\mathbf{s})$ is given by Equation (2.25) and the dynamical part by the analogous expression that is obtained by replacing ε_s with ε_∞, namely[5]

$$\sigma_{\text{dyn}}(\mathbf{s}) = \frac{1}{4\pi}\left(\frac{\varepsilon_\infty - 1}{\varepsilon_\infty}\right)\left(\frac{\partial\varphi}{\partial\mathbf{n}_\mathbf{s}}\right)_{\mathbf{s}=\mathbf{s}^-}. \tag{5.7}$$

The inertial charge is $\sigma_{\text{in}}(\mathbf{s}) = \sigma(\mathbf{s}) - \sigma_{\text{dyn}}(\mathbf{s})$.

The difference between these two partitions can readily be understood by examining the reaction field for a dipole $\boldsymbol{\mu}_0$ in a spherical cavity. The slow contribution to the reaction field is[590]

$$\mathbf{E}_{\text{rxn}}^{s} = \begin{cases} g_1(\varepsilon_s, \bar{R})\left(\dfrac{\varepsilon_s - \varepsilon_\infty}{\varepsilon_s - 1}\right)\boldsymbol{\mu}_0 & \text{(Marcus-Brady-Carr)} \\ [g_1(\varepsilon_s, \bar{R}) - g_1(\varepsilon_\infty, \bar{R})]\boldsymbol{\mu}_0 & \text{(Pekar)} \end{cases}, \tag{5.8}$$

where $g_1(\varepsilon,\bar{R})$ is the "Onsager factor" defined in Equation (2.21). The Marcus-Brady-Carr result follows from the fact that the slow polarization constitutes a fraction $\chi_s/\chi = (\varepsilon_s - \varepsilon_\infty)/(\varepsilon_s - 1)$ of the total polarization, according to Equation (5.6), whereas the Pekar result is set by fiat. Both partitions afford the *same* total reaction field,[590] $\mathbf{E}^{s}_{rxn} + \mathbf{E}^{f}_{rxn}$, and therefore the same nonequilibrium free energy,[221,590,597] up to some minor issues involving discretization along the lines of what was discussed in Section 3.1.[221] However, the partition between fast and slow components is different in the two schemes. Noting that $g_1(\varepsilon_s,\bar{R}) \approx 1/\bar{R}^3$ for high-dielectric solvents, Brady and Carr[564] observed that the Pekar result for $\mathbf{E}^{s}_{rxn}$ seems oddly small (and also decoupled from the value of ε_s) in this limit. To wit, for water one obtains $\mathbf{E}^{s}_{rxn} = 0.97\boldsymbol{\mu}_0/\bar{R}^3$ for the Marcus-Brady-Carr case and $\mathbf{E}^{s}_{rxn} = 0.63\boldsymbol{\mu}_0/\bar{R}^3$ for the Pekar partition. For that reason, the Marcus-Brady-Carr partition is the more common choice in modern literature although the Pekar partition has not vanished.[597] (The Marcus partition is also not free of criticism, and some alternatives have been suggested.[540]) Side-by-side expressions for the free energy $\mathcal{G}_{elst}$ in the Marcus-Brady-Carr versus the Pekar partition are provided by Tomasi *et al.*[13] As those authors note, there is some confusion in the literature regarding the names, for example, Equation (5.6) is called Pekar partition by Chipman.[585] As such, Tomasi *et al.* designate these schemes as "partition I," meaning Equation (5.6), and "partition II," meaning Equation (5.7). Although this notation has been adopted in a few places,[581,597] the names "Marcus" (for partition I) and "Pekar" (for partition II) remain common.

Having settled on the Marcus-Brady-Carr partition given in Equation (5.6), the basic idea of nonequilibrium polarization is that the susceptibility χ_s should be used to induce polarization for the initial state ("0"), whose solute charge density is $\rho_0(\mathbf{r})$, and then χ_f should be used in conjunction with the difference density $\Delta\rho(\mathbf{r})$ in order to adjust the polarization in the final state. To realize this in practice, one first computes the surface charge $\sigma_0(\mathbf{s})$ that is induced by $\rho_0(\mathbf{r})$ in a medium whose dielectric constant is ε_s, according to a normal (equilibrium) solvation calculation. Next, $\sigma_0(\mathbf{s})$ is partitioned into fast and slow contributions,[539,580,586]

$$\sigma_0^{f}(\mathbf{s}) = \left(\frac{\varepsilon_\infty - 1}{\varepsilon_s - 1}\right)\sigma_0(\mathbf{s}), \tag{5.9a}$$

$$\sigma_0^{s}(\mathbf{s}) = \left(\frac{\varepsilon_s - \varepsilon_\infty}{\varepsilon_s - 1}\right)\sigma_0(\mathbf{s}). \tag{5.9b}$$

The quantity $\sigma_0^{s}(\mathbf{s})$ is retained, whereas $\sigma_0^{f}(\mathbf{s})$ is replaced by a surface charge induced by the excited-state charge distribution, in a medium whose dielectric constant is ε_∞.

In order to derive rigorous formulas for the electrostatic free energy of the final state, introduce a Schrödinger equation of the form

$$\underbrace{\left(\hat{\mathscr{H}}_{vac} + \hat{\mathscr{R}}_0^{s} + \hat{\mathscr{R}}_k^{f}\right)}_{\hat{\mathscr{H}}_k^{SS}}|\Psi_k\rangle = \mathscr{E}_k^{SS}|\Psi_k\rangle \tag{5.10}$$

with $k = 0$ indicating the ground state. The quantity $\hat{\mathscr{H}}_{vac}$ is the vacuum Hamiltonian and the reaction-field operator $\hat{\mathscr{R}}_k = \hat{\mathscr{R}}_0^{s} + \hat{\mathscr{R}}_k^{f}$ consists of a slow component $\hat{\mathscr{R}}_0^{s}$ that originates with the ground-state density ρ_0 and susceptibility χ_s, along with a fast component $\hat{\mathscr{R}}_k^{f}$ based on the final-state density $\rho_k(\mathbf{r})$ and susceptibility χ_f. Because $\hat{\mathscr{R}}_k^{f}$ depends on the wave function $|\Psi_k\rangle$ that is needed to compute the final state's electrostatic potential, the Hamiltonian $\hat{\mathscr{H}}_k^{SS} = \hat{\mathscr{H}}_{vac} + \hat{\mathscr{R}}_k$ that is introduced in Equation (5.10) is state-specific (SS), and straightforward attempts to solve this equation encounter significant complications including convergence difficulties and ambiguous formulas for transition moments.[598] These problems can be circumvented by treating $\hat{\mathscr{R}}_k^{f}$ as a perturbation to zeroth-order states that are eigenfunctions of $\hat{\mathscr{H}}_0^{SS}$, as discussed below.

First, let us consider an expression for the free energy in an excited state. Equation (2.8) for the ground-state free energy $\mathcal{G}_0$ could be written in terms of a Hamiltonian

$$\hat{\mathscr{H}}_0 = \hat{\mathscr{H}}_{vac} + \hat{\mathscr{R}}_0^{s+f}, \tag{5.11}$$

however $\mathcal{G}_0$ differs from $\langle \Psi_0 | \hat{\mathscr{H}}_0 | \Psi_0 \rangle$ by an amount equal to the work $\mathcal{W}_0 = \frac{1}{2}\langle \Psi_0 | \hat{\mathscr{R}}_0 | \Psi_0 \rangle$ that is required to polarize the continuum. For an arbitrary state $|\Psi_k\rangle$, the polarization work is

$$\mathcal{W}_k = \frac{1}{2}\langle \Psi_k | \hat{\mathscr{R}}_k | \Psi_k \rangle = \frac{1}{2}\int_\Gamma \sigma_k(\mathbf{s})\; \varphi^{\rho_k}(\mathbf{s}) d\mathbf{s}. \tag{5.12}$$

In what follows, superscripts "f" or "s" will be added to $\sigma_k(\mathbf{s})$ in Equation (5.12), and thus to $\hat{\mathscr{R}}_k$ and $\mathcal{W}_k$, to signify the partition into fast or slow charge according to Equation (5.9). With this notation, the excited-state generalization of $\mathcal{G}_0$ is[221]

$$\mathcal{G}_k^{\mathrm{SS}} = \mathscr{E}_k^{\mathrm{SS}} - \mathcal{W}_0^{\mathrm{s}} - \mathcal{W}_k^{\mathrm{f}} + \mathcal{W}_{0,k}, \tag{5.13}$$

where

$$\mathscr{E}_k^{\mathrm{SS}} = \left\langle \Psi_k \middle| \hat{\mathscr{H}}_k^{\mathrm{SS}} \middle| \Psi_k \right\rangle = \left\langle \Psi_k \middle| \hat{\mathscr{H}}_{\mathrm{vac}} + \hat{\mathscr{R}}_0^{\mathrm{s}} + \hat{\mathscr{R}}_k^{\mathrm{f}} \middle| \Psi_k \right\rangle \tag{5.14}$$

and

$$\mathcal{W}_{0,k} = \frac{1}{2}\int_\Gamma \varphi^{\sigma_0^{\mathrm{s}}}(\mathbf{s}) \left[\sigma_k^{\mathrm{f}}(\mathbf{s}) - \sigma_0^{\mathrm{f}}(\mathbf{s})\right] d\mathbf{s}. \tag{5.15}$$

Equation (5.13) has a straightforward interpretation. To obtain the free energy $\mathcal{G}_k^{\mathrm{SS}}$ for state k, which includes the effects of averaging over implicit solvent degrees of freedom, the eigenstate energy $\mathscr{E}_k^{\mathrm{SS}}$ that is obtained from the Schrödinger equation must be reduced by the work $\mathcal{W}_0^{\mathrm{s}} + \mathcal{W}_k^{\mathrm{f}}$ that is required for the ground- and excited-state polarization processes. The final term, $\mathcal{W}_{0,k}$, accounts for the Coulomb interaction between initial- and final-state surface charge. This term has sometimes been omitted from similar treatments,[529,599] however its presence is necessary when the Marcus partition of the polarization is used.[13,221,580,589,590,597] The nonequilibrium expression for the excitation energy is $\hbar\omega_k = \mathcal{G}_k^{\mathrm{SS}} - \mathcal{G}_0$, or

$$\mathcal{G}_k^{\mathrm{SS}} - \mathcal{G}_0 = \Delta\mathscr{E}_k^{\mathrm{SS}} - \mathcal{W}_k^{\mathrm{f}} + \mathcal{W}_0^{\mathrm{f}} + \mathcal{W}_{0,k}, \tag{5.16}$$

where $\Delta\mathscr{E}_k^{\mathrm{SS}} = \mathscr{E}_k^{\mathrm{SS}} - \mathscr{E}_0$.[221] Equation (5.16) also has a straightforward interpretation. The quantity $\Delta\mathscr{E}_k^{\mathrm{SS}}$ is the difference between ground- and excited-state eigenvalues of the SS Hamiltonian [Equation (5.10)], but must be corrected by the difference in the work required to polarize either state, which is restricted to the fast part of the response ($\mathcal{W}_k^{\mathrm{f}} - \mathcal{W}_0^{\mathrm{f}}$) since only the fast polarization is modified upon vertical excitation.

As a simple example of the nonequilibrium formalism, we consider calculation of VIEs in aqueous solution. These can be measured using liquid microjet photoelectron spectroscopy[600–602] and may be quite different from gas-phase values,[600] especially for singly-charged anions X^-(aq) where the initial state is solvated much more strongly than the final state. Although equilibrium solvation models might be appropriate for computing *adiabatic* ionization energies, for which the solvent has the opportunity to re-equilibrate following ionization, such models do a poor job of predicting VIEs.[600,603] From a computational perspective, the change in charge upon photoionization means that long-range polarization effects are significant, requiring hundreds of explicit solvent molecules (with concomitant sampling) to obtain a converged result.[604–608] Convergence is significantly accelerated by continuum boundary conditions, using an atomistic solute $X^-(H_2O)_n$ that contains approximately two solvation shells of explicit water.[44,588] The limited size of the atomistic region not only reduces the cost of the quantum chemistry calculation for any one structure, but also reduces the sampling that is required in order to obtain converged averages. PCM boundary conditions have also been shown to accelerate convergence of absorption spectra with respect to inclusion of explicit water,[609] although the effects (in absolute energy shifts) are not as dramatic as they are for ionization.

Table 7 shows aqueous VIEs computed for several small solutes using a cluster-continuum approach with an atomistic region extending to a radius of 5.5 Å around the solute, containing ≈30 explicit water molecules. Shown side-by-side are VIEs computed using vacuum boundary conditions (including the explicit water molecules but absent any continuum model), versus results using equilibrium and nonequilibrium PCMs. In the latter case, results are shown using either a SAS cavity or else a cavity that consists of a single sphere around the atomistic region, which affords VIEs that are essentially identical to the SAS values. The nonequilibrium PCM results are ≈1 eV too large for Li^+(aq) and Na^+(aq) but significantly more accurate for the aqueous halide ions. For the halides, these calculations are also significantly more accurate than previous QM/MM or equilibrium PCM calculations.[603] For neat liquid water, these calculations represent the most accurate VIE to date, in line with new experiments,[611] and are also one of the most accurate VIE calculations to date for the challenging e^-(aq) system.[613]

More germane to the present discussion is the comparison of various boundary conditions. Using vacuum boundary conditions, results for $X^-(H_2O)_{30}$ and $M^+(H_2O)_{30}$ are in serious error relative to experiment, with VIEs that are too small for the anions and too large for the cations. This is consistent in both cases with understabilization of the state having larger charge. Addition of equilibrium PCM boundary conditions modifies VIEs for these systems by up to 3 eV for the cations, which is perhaps unsurprising given that the divalent ion M^{2+} incurs very long-range polarization effects in the final state, but even when the solute is neutral H_2O, one observes a shift of 3 eV when continuum boundary conditions are activated. While the application of an equilibrium PCM pushes the VIE substantially in the right direction with respect to experiment, results remain far from quantitative until the nonequilibrium correction is added, which ranges in magnitude up to ≈0.6 eV. Other calculations for aqueous nucleobases find nonequilibrium corrections to VIEs of ≈1 eV.[614] For the nucleobases, the calculations suggest that the solvent response upon ionization is the most important part of the difference between vertical and adiabatic ionization energies, more so than geometric relaxation of the ionized solute.[614]

The nonequilibrium formalism is relatively straightforward for ionization, assuming that the final state is the ground state of the ionized species, but is more complicated for excited states. In the presence of near-degeneracies, the SS nature of the Hamiltonian in Equation (5.10) can lead to convergence problems,[598,615] and even when the states are well-separated, properties such as oscillator strengths are ill-defined because the final-state wave functions are not eigenfunctions of a common Hamiltonian and are therefore not orthogonal.[598] These problems are not unique to continuum solvation methods and arise for any kind of polarizable model of the environment, including QM/MM methods that employ polarizable force fields.[598,616,617] A solution to this conundrum is to treat $\hat{\mathscr{R}}_k^{\mathrm{f}}$ in Equation (5.10) as a perturbation.[221,529,586,587,599,618] To do so, first introduce a set of orthonormal zeroth-order states,

$$\hat{\mathscr{H}}_0\left|\Psi_k^{(0)}\right\rangle = \mathscr{E}_k^{(0)}\left|\Psi_k^{(0)}\right\rangle, \tag{5.17}$$

TABLE 7 Vertical ionization energies (VIEs) for aqueous ions, comparing experimental results to calculations using nonequilibrium MP2 + PCM calculations, from Ref. 610

Solute	Experimental VIE (eV)	Computed VIE (eV)				
		Noneq. PCM		Equil. PCM		
		Spherical[a]	SAS[b]	Spherical[a]	SAS[b]	No PCM
Li^+	60.4[c]	61.8	61.6	61.3	61.0	64.2
Na^+	35.4[c]	36.5	36.3	36.0	35.8	38.9
H_2O	11.7[d]	11.6	11.6	11.1	10.9	13.8
e^-	3.7[e]	3.2	3.2	2.6	2.6	1.8
F^-	11.6[f]	11.4	11.5	10.8	10.9	10.0
Cl^-	9.6[c]	9.4	9.4	8.8	8.8	7.9

Note: Each system contains ≈30 explicit water molecules and each calculated VIE represents an average over ≈100 snapshots from a simulation.

[a]Single spherical cavity for the entire atomistic region, $R = 7.525$ Å.

[b]Equation (3.5) with $\alpha_{\mathrm{vdW}} = 1.0$ and $R_{\mathrm{probe}} = 1.4$ Å, with atomic radii from Ref. 136.

[c]Ref. 603.

[d]Ref. 611.

[e]Ref. 612.

[f]Ref. 602.

such that the eigenvalue $\mathscr{E}_k^{(0)}$ includes the effects of the ground-state reaction field, $\hat{\mathscr{R}}_0$. As a convenient approximation for $\mathcal{G}_k^{\mathrm{SS}}$ in Equation (5.13), substitute $\mathscr{E}_k^{(0)}$ in place of $\mathscr{E}_k^{\mathrm{SS}}$ and use $|\Psi_k^{(0)}\rangle$ to evaluate the electrostatic potential for state k. This avoids the complexities of the SS approach, and is equivalent to first-order perturbation theory with respect to a perturbation $\hat{W} = \hat{\mathscr{R}}_k^{\mathrm{f}} - \hat{\mathscr{R}}_0^{\mathrm{f}}$, obtained from a partition

$$\hat{\mathscr{H}}_k^{\mathrm{SS}} = \underbrace{\hat{\mathscr{H}}_{\mathrm{vac}} + \hat{\mathscr{R}}_0^{\mathrm{s+f}}}_{\hat{\mathscr{H}}_0} + \underbrace{\hat{\mathscr{R}}_k^{\mathrm{f}} - \hat{\mathscr{R}}_0^{\mathrm{f}}}_{\hat{W}}. \tag{5.18}$$

This approximation has been called the *perturbation theory state-specific* (ptSS) approach to nonequilibrium solvation.[221,586,587] (In principle, it could be extended to higher-order perturbation theory but it is not clear that this is warranted.) Note that a widely used "corrected linear response" (cLR) procedure,[529] introduced for excited-state PCM calculations at the level of time-dependent (TD-)DFT, is fundamentally a ptSS approach. (The "linear response" in cLR refers to TDDFT, not to the LR-PCM formalism that is discussed in Section 5.3.) In the context of the ptSS or cLR approach, it is best to view TDDFT as a form of configuration interaction with single substitutions (CIS), which provides an eigenvalue equation of the form in Equation (5.17). This is consistent with the idea that the SS version of TDDFT, as implemented by Improta *et al.*,[619,620] is a fully iterative realization of Equation (5.10) within a CIS-style *ansatz*. Both the ptSS and the full SS approaches to TDDFT do require construction of the "relaxed" density for the TDDFT excited state in question,[621–623] in order to compute its electrostatic potential.

To obtain practical formulas for ASC-PCMs, let us introduce a vector notation for surface integrals. As an example, we rewrite Equation (2.37) for $\mathcal{G}_{\mathrm{elst}}$ in the form

$$\mathcal{G}_{\mathrm{elst}} = \frac{1}{2}\int_\Gamma \sigma(\mathbf{s})\ \varphi^{\rho}(\mathbf{s})\ d\mathbf{s} = \frac{1}{2}\mathbf{q}\cdot\mathbf{v}^{\rho}. \tag{5.19}$$

The quantities $\mathbf{q}$ and $\mathbf{v}^{\rho}$ were introduced in Equation (3.2) and the dot-product notation represents how ASC-PCM surface integrals are evaluated in practice, upon discretization of the cavity surface. Using this notation, an expression for the nonequilibrium free energy for excited state k can be manipulated into the form[529]

$$\mathcal{G}_k^{\mathrm{neq}} = \mathscr{E}_k^{(0)} + \frac{1}{2}\mathbf{v}_0\cdot\mathbf{q}_0 + \frac{1}{2}(\mathbf{v}_k - \mathbf{v}_0)\cdot\left(\Delta\mathbf{q}_k^{\mathrm{f}}\right) + \mathcal{W}_{0,k}, \tag{5.20}$$

where $\mathbf{v}_0$ and $\mathbf{v}_k$ represent the electrostatic potentials for states $|\Psi_0^{(0)}\rangle$ and $|\Psi_k^{(0)}\rangle$, and $\Delta\mathbf{q}_k^{\mathrm{f}} = \mathbf{q}_k^{\mathrm{f}} - \mathbf{q}_0^{\mathrm{f}}$ is the difference in the fast polarization charges for the two states. The latter quantity is computed according to

$$\Delta\mathbf{q}_k^{\mathrm{f}} = \mathbf{Q}_{\varepsilon_\infty}(\mathbf{v}_k - \mathbf{v}_0) = \mathbf{Q}_{\varepsilon_\infty}\mathbf{v}^{\Delta\rho} \tag{5.21}$$

for a reaction field ($\mathbf{Q}_\varepsilon = \mathbf{K}_\varepsilon^{-1}\mathbf{Y}_\varepsilon$) involving the optical dielectric constant. The second equality in Equation (5.21) recognizes that $\mathbf{v}^{\Delta\rho} = \mathbf{v}_k - \mathbf{v}_0$ is the electrostatic potential corresponding to the difference density $\Delta\rho_k(\mathbf{r}) = \rho_k(\mathbf{r}) - \rho_0(\mathbf{r})$. Somewhat similar expressions to Equation (5.20) can be found elsewhere,[584,619,620] but the connection to the actual free energy of the excited state is most explicit in the work of Caricato *et al.*[529] For cases where the solvent polarization has time to fully equilibrate with respect to the excited-state density, an analogous expression for the *equilibrium* free energy $\mathcal{G}_k^{\mathrm{eq}}$ is obtained from Equation (5.20) by replacing $\Delta\mathbf{q}_k^{\mathrm{f}}$ with $\mathbf{q}_k - \mathbf{q}_0$, where both ground- and excited-state charges are equilibrium values.[529] In the equilibrium case, $\mathbf{q}_k = \mathbf{Q}_{\varepsilon_s}\mathbf{v}_k$.

The solvent-corrected, nonequilibrium excitation energy is simply the difference between ground- and excited-state free energies,[529,624]

$$\hbar\omega_{0k}^{\mathrm{neq}} = \mathcal{G}_k^{\mathrm{neq}} - \mathcal{G}_0 = \Delta\mathscr{E}_k^{(0)} + \frac{1}{2}(\mathbf{v}_k - \mathbf{v}_0)\cdot\left(\Delta\mathbf{q}_k^{\mathrm{f}}\right) + \mathcal{W}_{0,k}. \tag{5.22}$$

The quantity $\Delta\mathscr{E}_k^{(0)} = \mathscr{E}_k^{(0)} - \mathscr{E}_0$ is the excitation energy computed in the presence of the ground-state reaction field, which is then corrected in Equation (5.22) for the change in the fast polarization upon excitation. These equations remain valid for the Pekar partition if $\mathcal{W}_{0,k}$ is omitted from Equations (5.20) and (5.22). As noted by Cammi *et al.*,[618] Equation (5.22) is the detailed analogue of the heuristic theories of excited-state solvation developed much earlier by McRae,[558,593,625] by Lippert,[554] and by Mataga.[553,555] This becomes clear upon considering the special case of a polarizable dipole in a spherical cavity.[618,619]

Although presented here in the notation of ASC-PCMs, an analogous theory of nonequilibrium solvation can be developed based directly on Poisson's equation.[44,588] In that context, the total charge density $\rho_{\text{tot}}(\mathbf{r}) = \rho(\mathbf{r}) + \rho_{\text{pol}}(\mathbf{r})$ includes an induced polarization $\rho_{\text{pol}}(\mathbf{r})$ [as in Equation (2.6)], in addition to the solute's charge density $\rho(\mathbf{r})$. The reaction-field potential is the electrostatic potential arising from $\rho_{\text{pol}}(\mathbf{r})$, and surface integrals such as the ones in Equations (5.12) and (5.15) are replaced by volumetric integration. Conveniently, the dot product notation introduced in Equation (5.19) is ambivalent to this distinction and a formula analogous to Equation (5.20) can be derived,[44] with the dot product signifying volumetric integration.

In the interest of brevity, the notation introduced above omits a subscript "elst" on both $\mathcal{G}_k^{\text{SS}}$ [Equation (5.13)] and $\mathcal{G}_k^{\text{neq}}$ [Equation (5.20)], and for that matter on $\mathcal{G}_0$ in Equation (2.8) as well. In each case, these quantities represent only the electrostatic contribution to the free energy. Some of the earliest theoretical work on solvatochromatic shifts was concerned not just with changes in the chromophore's dipole moment, as in the Onsager-style treatment leading to the Lippert-Mataga equation, but also with the role of dispersion effects.[625–628] In modern formulations of continuum theory, however, there have been only preliminary efforts to incorporate nonelectrostatic interactions (as described in Section 4) into excited-state calculations.[471,472,493,629,630] This is an interesting problem insofar as solute–solvent dispersion is likely more attractive in an excited state, whose wave function is probably more polarizable than the ground state wave function, but at the same time Pauli repulsion will likely increase in the excited state due to the larger spatial extent of the wave function. To an extent, favorable results for solvatochromic shifts that are obtained with electrostatics-only models[586,597,615,631] likely rely on some error cancellation along these lines. (That said, early attempts to model excited-state dispersion afford shifts <0.1 eV,[493] and it is likely that electrostatics remains the dominant effect.) Models that introduce SS nonelectrostatic interactions also do well for solvatochromic shifts.[630]

There is one remaining source of complexity when the nonequilibrium theory is applied to excited states, in that the Schrödinger equation in Equation (5.10) leaves open the question of what level of self-consistency should be sought in obtaining the excited-state reaction-field operator, $\hat{\mathscr{R}}_k^{\text{f}}$, which depends on $|\Psi_k\rangle$. The multiple-choice answer to this question leads to several categories of methods that are mapped out in Figure 10, and which are called "perturbation to energy" (PTE), "perturbation to density" (PTD), and "perturbation with self-consistent energy and density" (PTED).[48] This nomenclature derives from efforts to use perturbation theory to include correlation in the ground-state calculation (e.g., MP2 + SCRF),[632–635] where one must decide whether (and how) electron correlation should be included in the density that is used to polarize the continuum. The same notation has been adopted for PCM calculations using nonperturbative models such as coupled-cluster theory,[636,637] and is used here in a discussion that is formulated specifically with excited-state calculations in mind. As illustrated in Figure 10a, the PTE scheme involves self-consistent solution of the SCF + SCRF problem followed by a single-shot post-SCF calculation using solvent-polarized MOs. This represents a kind of "zeroth-order" inclusion of solvation effects in the correlated calculation.[586] This approach has obvious advantages in terms of cost: assuming that the post-SCF step dominates the cost of the gas-phase calculation, then addition of SCRF boundary conditions adds little to the overall cost of a PTE calculation. Alternatively, in the PTD scheme the correlated calculation is performed in the gas phase and then the correlated density (rather than the SCF density) is used to polarize the solvent. This introduces solvation effects beyond zeroth-order in perturbation theory,[634] at marginally increased cost: it is still a single-shot correlation calculation but the relaxed density is required, which entails computational effort along the lines of a gradient calculation at the correlated level of theory. A slightly better-performing variant of the traditional PTD approach is the PTE-PTD scheme (Figure 10a),[587] in which the SCF + SCRF calculation is solved self-consistently and those MOs are used in the post-SCF calculation, but then the correlated density is used in a final, single-shot PCM calculation to compute the solvation energy, $\mathcal{G}_{\text{elst}}$. None of these schemes constitutes a fully self-consistent treatment of post-SCF correlation effects, which can be accomplished using the PTED scheme that is mapped out in Figure 10a. Here, the correlated density is used to obtain the PCM surface charge and this procedure is iterated to self-consistency. This is significantly more expensive because the correlated calculation is performed at each SCRF iteration.

These ideas have been extended beyond their perturbation theory origins and represent the available options for self-consistency in any calculation that combines an SCRF method with a quantum-chemical model that requires a post-SCF calculation,[582,586,587,615,636–640] including TDDFT.[586] An alternative pictorial representation of the simplest method (PTE) and most complete scheme (PTED) is provided in Figure 10b, which furnishes a flowchart for an excited-

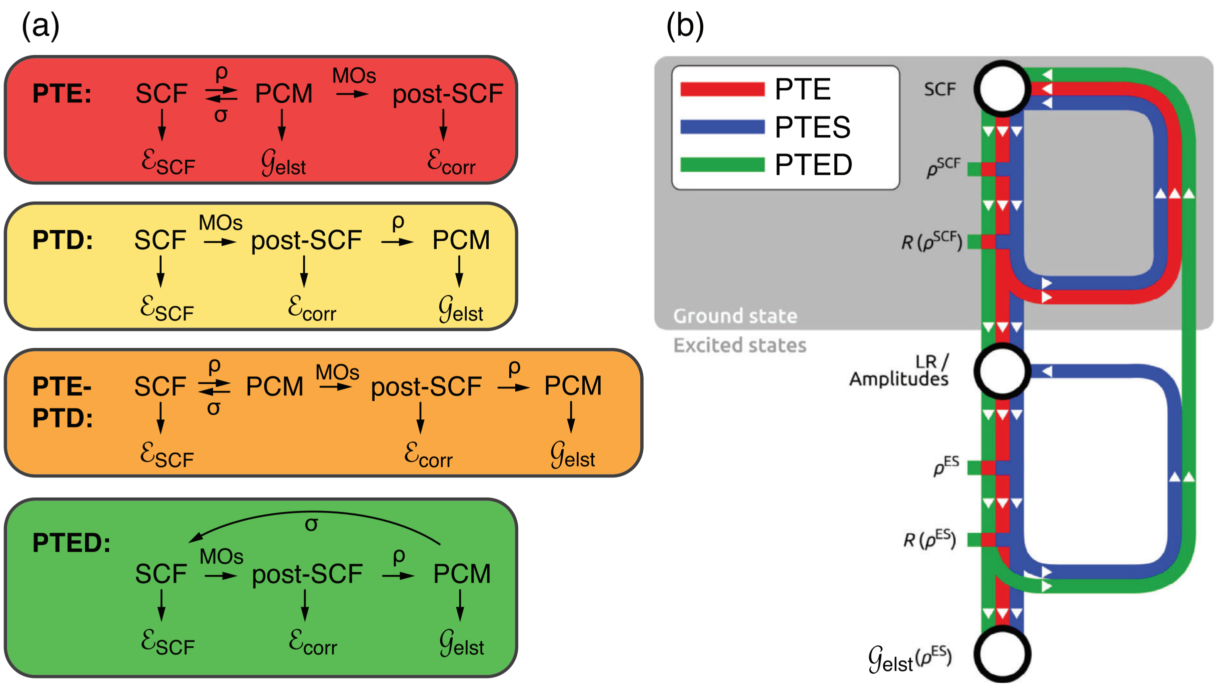

FIGURE 10 Flowcharts representing various state-specific procedures for combining a polarizable continuum model (PCM) or other self-consistent reaction-field (SCRF) procedure with a quantum chemistry method that requires a post-self-consistent field (SCF) step. (a) Illustration of the perturbation to energy (PTE) and perturbation to density (PTD) schemes, and two different combinations thereof. Forward-backward arrows (⇄) indicate where the solute density (ρ) and the polarization charge (σ) are iterated to self-consistency, whereas downward arrows indicate the points at which various contributions to the energy are extracted. (b) Schematic representation of the PTE and perturbation with self-consistent energy and density (PTED) procedures for an excited-state (ES) calculation, along with the PTES procedure designed as a lower-cost approximation to PTED. Panel (a) is adapted from Ref. 587; copyright 2017 The PCCP Owner Societies. Panel (b) is adapted from Ref. 582; copyright 2019 John Wiley & Sons

state calculation indicating which densities are used to construct the various reaction-field operators $\hat{\mathcal{R}}$. Due to the expense associated with the fully self-consistent PTED approach, approximations have been developed in which both the ground- and excited-state calculations are iterative but those two iterative sequences are uncoupled.[635,638–641] This scheme, which Caricato calls "PTES" and has implemented at the coupled-cluster level of theory,[638–640] is analogous to a "vertical excitation model" introduced for TDDFT.[629] At the TDDFT level, the PTED scheme in Figure 10 is essentially equivalent to the SS-TDDFT + PCM method introduced by Improta *et al.*[619,620]

Figure 11 presents solvatochromic shifts for a set of nitrobenzene derivatives,[586] with excitation energies computed at the level of the second-order algebraic diagrammatic construction [ADC(2)],[642] which is something of an excited-state analogue of MP2. Solvent contributions in Figure 11 are incorporated using either the PTE or PTD variant of the ptSS approach. Differences between the two variants are negligible, and both approaches show good agreement with experimental shifts, without the need to invoke the more expensive PTED scheme. For many of these molecules, the first-order ptSS contribution to the solvatochromic shift (representing fast polarization) is 0.10–0.15 eV, in total shifts ranging up to 0.6 eV. The remainder comes from the zeroth-order contribution of simply inserting solvent-polarized MOs into the correlated part of the calculation.[586] Tests on a more diverse set of systems do reveal a small systematic error in the PTE approach,[615] but the mean error with respect to experiment remains <0.1 eV and the systematic error can be eliminated by intermediate approaches that do not require the full self-consistency of PTED.[615] In particular, the PTE-PTD scheme (see Figure 10a) works well in this regard;[587] it requires the correlated density but is not iterative at the correlated level of theory. Other benchmark studies, comparing continuum approaches to large QM calculations with explicit QM solvent molecules, have suggested that QM/PCM excitation energies may agree better with full-QM result as compared to QM/MM calculations, but explicit water molecules in the QM/PCM calculation are required to obtain good agreement for oscillator strengths.[643] Simulation of band shapes requires thermal sampling, which cannot be accomplished without at least some explicit solvent.

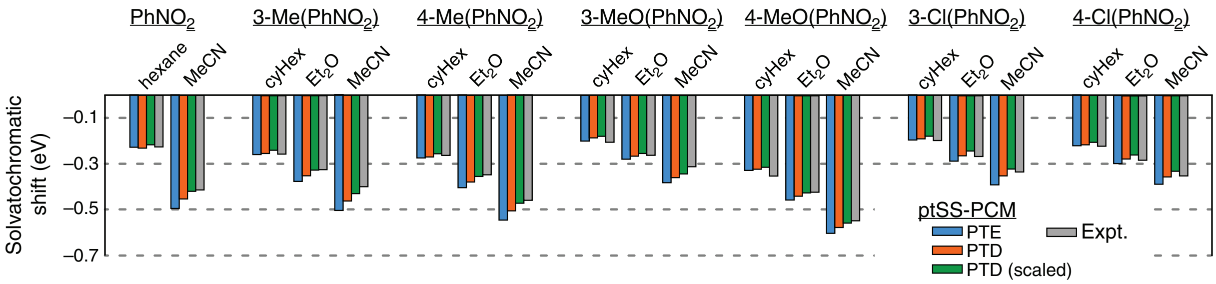

FIGURE 11 Solvatochromic shifts in the lowest $^1\pi\pi^*$ state for derivatives of nitrobenzene ($PhNO_2$) in different solvents, comparing experimental values to ADC(2)/C-PCM calculations. Solvent effects are described using perturbation to energy (PTE) and perturbation to density (PTD) variants of the perturbation theory state-specific (ptSS) approach. Also shown are results for an empirically-scaled version of the nonequilibrium PTD correction. Adapted from Ref. 586; copyright 2015 American Chemical Society

5.3 | Linear response approach

Despite its computational complexities, the SS approach to excited-state solvation is conceptually straightforward. An alternative to the state-by-state approach, which has fewer moving parts at the computational level, is based on LR quantum chemistry methods in which excitation energies are computed from the poles of the frequency-dependent response to a perturbation, rather than from a Schrödinger equation. To formulate a LR-PCM approach to excitation energies, first write the PCM electrostatic energy in the form

$$\mathcal{G}_{\text{elst}} = \frac{1}{2}\int_\Gamma\int_\Gamma \varphi(\mathbf{s})\ Q_\varepsilon(\mathbf{s},\mathbf{s}')\ \varphi(\mathbf{s}')\ d\mathbf{s}\ d\mathbf{s}', \tag{5.23}$$

in which $Q_\varepsilon(\mathbf{s},\mathbf{s}')$ is the kernel of the solvent-response operator $\hat{Q}_\varepsilon = \hat{K}_\varepsilon^{-1}\hat{Y}_\varepsilon$. The solvent model contributes only a one-electron potential to the Hamiltonian, $v^{\text{PCM}}(\mathbf{r}) = \delta\mathcal{G}_{\text{elst}}/\delta\rho(\mathbf{r})$. The matrix elements of this potential are[644]

$$v_{\mu\nu}^{\text{PCM}} = \int_\Gamma\int_\Gamma \varphi(\mathbf{s})\ Q_\varepsilon(\mathbf{s},\mathbf{s}')\ \varphi_{\mu\nu}(\mathbf{s}')\ d\mathbf{s}\ d\mathbf{s}' = (\mathbf{v}^\rho)^\dagger \mathbf{Q}_\varepsilon \mathbf{v}^{\mu\nu}, \tag{5.24}$$

in which $\varphi_{\mu\nu}(\mathbf{s}')$ is the electrostatic potential generated by the function pair $\mu\nu$ at the point $\mathbf{s}'$. The second equality in Equation (5.24) demonstrates how the Fock matrix contribution from $v^{\text{PCM}}(\mathbf{r})$ is evaluated in practice, and analogous expressions exist for three-dimensional Poisson approaches.[44] The quantities $\mathbf{v}^\rho$ and $\mathbf{v}^{\mu\nu}$ involve only one-electron integrals, so incorporating the PCM contribution into a LR calculation incurs negligible overhead with respect to the cost of the gas-phase calculation, meanwhile this approach is free of the iterative complexities of the SS method. A general LR-PCM formulation has been given by Cammi *et al.*,[618,645] and specific formulations for different excited-state methods are available as well, including for TDDFT and other single-excitation theories,[644–648] following on earlier implementations of the coupled-perturbed SCF + PCM procedure for response properties;[216,649] for multi-configurational SCF wave functions;[98] for ADC;[599,641] and for the *GW*/Bethe-Salpeter equation formalism.[650] Finally, LR-PCM has been implemented for coupled-cluster theory,[651–655] based on the coupled-cluster response formalism.[637]

For isolated-molecule quantum chemistry, the LR formalism for excitation energies is generally equivalent to solving the corresponding Schrödinger equation,[656] but the LR- and SS-PCM formalisms are *not* equivalent.[618,657] The general form of the LR-PCM result for excitation energies is[618]

$$\hbar\omega_{0k}^{\text{neq,LR}} = \hbar\omega_k^{(0)} + \underbrace{\langle\Psi_k|\hat{\mathcal{V}}|\Psi_0\rangle\left\langle\Psi_0\middle|\hat{\mathcal{Q}}^{\text{f}}\middle|\Psi_k\right\rangle}_{\Delta\mathscr{R}^{\text{f}}(\mu_{0k})}, \tag{5.25}$$

where $\langle\Psi_k|\hat{\mathcal{V}}|\Psi_0\rangle$ is the electrostatic potential generated by the *transition* density $\rho_{k0}(\mathbf{r})$, and $\left\langle\Psi_0\middle|\hat{\mathcal{Q}}^{\text{f}}\middle|\Psi_k\right\rangle$ is the ASC induced by $\rho_{k0}(\mathbf{r})$. For comparison, the SS-PCM result in Equation (5.22) can be rewritten in similar notation:

$$\hbar\omega_{0k}^{\mathrm{neq,SS}} = \hbar\omega_k^{(0)} + \underbrace{\frac{1}{2}\left[\langle\Psi_k|\hat{\mathcal{V}}|\Psi_k\rangle - \langle\Psi_0|\hat{\mathcal{V}}|\Psi_0\rangle\right]\cdot\left[\left\langle\Psi_k\middle|\hat{\mathcal{Q}}^{\mathrm{f}}\middle|\Psi_k\right\rangle - \left\langle\Psi_0\middle|\hat{\mathcal{Q}}^{\mathrm{f}}\middle|\Psi_0\right\rangle\right]}_{\Delta\mathscr{R}^{\mathrm{f}}(\Delta\rho_k)}. \tag{5.26}$$

In both cases, the quantity $\hbar\omega_{0k}^{(0)} \equiv \Delta\mathscr{E}_k^{(0)}$ is the zeroth-order approximation to the solution-phase excitation energy, calculated in the static reaction field of the ground state. The quantity $\Delta\mathscr{R}^{\mathrm{f}}$ represents the change in the dynamical part of the reaction field, which is a function of the transition dipole moment $\mu_{0k} = \langle\Psi_0|\hat{\mu}|\Psi_k\rangle$ in the LR case but a function of the difference density $\Delta\rho_k(\mathbf{r})$ in the SS case. A detailed analysis of the two formalisms suggests that their differences arise from the nonlinear nature of the SS Hamiltonian combined with the lack of entanglement between the atomistic wave function and its continuum environment.[657]

Whatever the origin of the discrepancy, the form of the LR-PCM correction in Equation (5.25) is problematic because the correction vanishes for optically forbidden transitions, as is readily seen from a model of a dipole in a spherical cavity, for which $\Delta\mathscr{R}^{\mathrm{f}} = -g_1(\varepsilon_\infty, \bar{R})\mu_{0k}$.[619] For the same reason, the LR-PCM correction $\Delta\mathscr{R}^{\mathrm{f}}(\mu_{0k})$ will be rather small for any excitation involving significant displacement of charge, whereas intuitively (and in the SS formalism) one expects a significant solvent effect for a charge-transfer excitation in a polar solvent. Indeed, SS-PCM results are consistently superior to LR-PCM calculations for excited states with charge-transfer character.[658–663] (As discussed in Section 5.2, the cLR formalism encountered in some of these studies is really a ptSS-PCM approach, and typically outperforms true LR methods for excitations with charge-transfer character.) Even for states that are not dominated by charge transfer, the SS-PCM approach generally affords smaller errors for solvatochromatic shifts in the absorption spectrum as compared to LR-PCM calculations,[586,597,631] although it is worth bearing in mind that the experimental $\lambda_{\max}$ need not correspond to the origin (0–0) transition, due to vibrational structure.[664–666] The ptSS-PCM approach also affords more accurate results for emission energies,[667] though it is found that the accuracy is largely unaffected if the LR-PCM procedure is used for the excited-state geometry optimization, followed by a ptSS-PCM single-point calculation, which simplifies the procedure.[667] It has also been argued that the LR correction $\Delta\mathscr{R}^{\mathrm{f}}(\mu_{0k})$ constitutes a solute–continuum dispersion interaction,[582,657,668] insofar as it has the form of the solute charge distribution oscillating at the Bohr frequency $\omega_{0k}^{(0)}$ and coupling to the dynamical response of the environment. As such, some studies have opted to include both the LR- and ptSS-PCM corrections to $\omega_{0k}^{(0)}$.[586]

6 | ANISOTROPIC SOLVATION

Up to this point we have assumed that the continuum environment is isotropic, which is usually the case in a bulk liquid environment although there are certain exceptions (notably, liquid crystals) where polarization of the medium depends upon the orientation of the electric field vector. This can be described by allowing ε to take the form of a 3×3 matrix, with orientation-dependent permittivities ε_{xx}, ε_{yy}, and ε_{zz}. The ASC-PCM formalism, and in particular IEF-PCM, has been formulated to handle a permittivity tensor,[180–182,669,670] but this will not be considered here.

A more general class of anisotropic solvation problems are interfacial phenomena. An example is shown in Figure 12a, in which an atomistic solute consisting of ClO_3^- with approximately two solvation shells of explicit water is situated at a continuum representation of the air/water interface. The atomistic region experiences a dielectric environment characterized by $\varepsilon = 78$ on one side but $\varepsilon = 1$ on the other. The basic PCM formalism is not equipped to handle such a situation, as it is predicated on a sharp dielectric interface between $\varepsilon_{\mathrm{in}} = 1$ inside the cavity and a bulk solvent value outside, although it can be accomplished piecewise if the medium is divided into separate domains, each with its own value of ε.[671] Modified versions of IEF-PCM to describe the interface between an aqueous electrolyte and the surface of an electrode have been developed,[672–674] as have methods to describe the liquid/vapor interface, in which the PCM matrix elements interpolate between different values of ε.[675–682] Treatment of nonelectrostatic effects proves to be crucial at the interface. For example, it is a commonly held view that continuum models are incapable of describing the interfacial affinity exhibited by soft ions,[683,684] because (so the logic goes) the ion in a continuum solvent ought to be repelled from the interface by its own image charge.[684,685] Despite this conventional wisdom, however, continuum models that include nonelectrostatic interactions have been shown to predict interfacial free energy minima for dragging a soft ion through the air/water interface.[675,677,686,687]

Fundamentally, however, the interfacial solvation problem seems to cry out for a permittivity function $\varepsilon(\mathbf{r})$ that assumes different values in different regions of space, that is, a method that solves the generalized Poisson equation

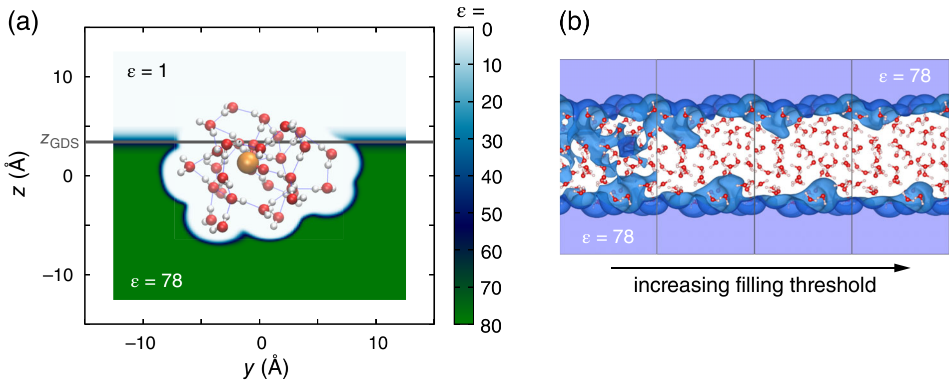

FIGURE 12 Illustrations of anisotropic permittivity functions $\varepsilon(\mathbf{r})$ for use in Poisson's equation. (a) A semicontinuum description of chlorate ion at the air water interface, in which the atomistic solute is $ClO_3^-(H_2O)_{30}$. The background color shows the function $\varepsilon(\mathbf{r})$, interpolating between $\varepsilon_{\text{out}} = 1$ above the Gibbs dividing surface (GDS) and $\varepsilon_{\text{out}} = 78$ below it, with $\varepsilon_{\text{in}} = 1$ inside of the solute cavity. The horizontal line indicates the position of the dividing surface, $z_{\text{GDS}} = 3.5$Å. (b) Periodic water slab bounded on either side by continuum water ($\varepsilon = 78$, shown in purple), with regions characterized by $\varepsilon > 15$ shown in blue. From left to right, the interpolating function is modified (using a "filling threshold" parameter), in order to exclude pockets of high permittivity that encroach into the interstices between the atomistic water molecules. Panel (b) is adapted from Ref. 269; copyright 2019 American Chemical Society

with an anisotropic permittivity function, $\varepsilon(\mathbf{r})$. Such a strategy has been pursued to describe the interface between a solid-state electrode and an aqueous electrolyte,[28,82,264,268–274] as well as host/guest systems where the guest experiences a low-dielectric environment despite the fact that the host is dissolved in water.[688] Finally, anisotropic models have been used to compute VIEs of solutes at the air/water interface,[44,588] in order to connect with liquid microjet photoelectron spectroscopy.

The setup for an interfacial calculation of this type is illustrated in Figure 12a, which depicts an atomistic (semicontinuum) model of ClO_3^-(aq) at the air/water interface and shows how the function $\varepsilon(\mathbf{r})$ is defined. In this particular example, two solvation shells of explicit water molecules are included in the atomistic region in order to account for hydrogen bonding, and the continuum model takes care of long-range polarization upon ionization of ClO_3^-. Calculations based on a nonequilibrium formulation of Poisson's equation suggest that the VIEs of common inorganic anions are very nearly the same at the air/water interface as they are in bulk water.[44,610] Even for an exotic anion like e^-(aq),[613,689] it appears that the interfacial VIE that is no more than 0.2–0.4 eV different from its bulk value.[44,588,610]

In cluster-continuum calculations such as these, one must be careful to parameterize the function $\varepsilon(\mathbf{r})$ to avoid artificial penetration of high-dielectric regions into the interstices between molecules. This admonition extends not just to methods based on Poisson's equation but also to PCM calculations that use explicit solvent molecules, as in pK_a calculations or other applications involving ions. Oddly, the dielectric penetration problem in semicontinuum calculations has received scant attention in the quantum chemistry literature,[44,269] although there is an analogous problem in classical biomolecular Poisson–Boltzmann calculations that is widely discussed, namely, that standard cavity construction algorithms (based on intersecting atomic spheres) may leave pockets of high-dielectric "solvent" within the hydrophobic interior of a protein.[59,139,251,690–693] This can be mitigated by appropriate adjustment of the interpolating function that defines the dielectric boundary. A spatially varying permittivity function has been suggested as a solution to the problem that there is no single optimal value for the dielectric "constant" inside of a protein.[59]

Figure 12b presents an example using the SCCS approach. This example is driven by the desire to perform *ab initio* molecular dynamics simulations of liquid water, using continuum boundary conditions in order to limit the size of the atomistic simulation cell that is required. The solute/continuum interface is defined by a functional $\varepsilon[\rho](\mathbf{r})$, but care must be taken to ensure that high-dielectric regions do not appear between the explicit water molecules, as they do on the left side of Figure 12b. That situation is physically incorrect because the QM calculation is based on Coulomb operators that assume vacuum permittivity. The undesirable dielectric penetration is eliminated by introducing "solvent awareness" into the definition of the permittivity function, so that $\varepsilon(\mathbf{r})$ depends on the coordinates in the atomistic region *directly*, not just implicitly via the functional $\varepsilon[\rho]$.[269] Moving from left to right in Figure 12b, this solvent awareness is activated and removes the spurious high-dielectric regions.

An important aspect of interfacial phenomena are "specific-ion" or "Hofmeister" effects at the air/water interface,[683,684] and it is common in that context to encounter blanket dismissals of continuum models based on the fact that the Born ion model [Equation (2.17)] cannot distinguish between cations and anions. As such, this model cannot describe "charge hydration asymmetry," that is, the fact that hydration energies for monovalent atomic anions are significantly larger in magnitude than those for cations.[694–699] This asymmetry, which also affects polar but charge-neutral solutes,[700] is partly attributable to water's surface potential,[701,702] however a primary origin of this effect is simply the fact that an anion sees a much different facet of a water molecule as compared to a cation,[701,702] leading to a very different electrostatic size for cations versus anions. Indeed, it has been understood for a long time that the Born model can produce reasonable hydration energies for monatomic ions of either charge, but the requisite atomic radii are quite different for anions versus cations.[46,703] Charge hydration asymmetry therefore does not reflect a failure of continuum electrostatics *per se*, and is arguably better ascribed to the effects of short-range repulsion rather than electrostatics.[320,702] This can be modeled in an *ad hoc* way by modifying the atomic radii based on the charge state of the atom,[704,705] but a more satisfying approach is to modify the jump boundary condition $\varepsilon_{\text{in}} E_\perp(\mathbf{s}^-) = \varepsilon_{\text{out}} E_\perp(\mathbf{s}^+)$ in Equation (2.22), replacing it with

$$\left[\varepsilon_{\text{in}} - (\varepsilon_{\text{out}} - \varepsilon_{\text{in}}) h\left(E_\perp^-\right)\right] E_\perp(\mathbf{s}^-) = \left[\varepsilon_{\text{out}} - (\varepsilon_{\text{out}} - \varepsilon_{\text{in}}) h\left(E_\perp^-\right)\right] E_\perp(\mathbf{s}^+), \tag{6.1}$$

where $E_\perp^- \equiv E_\perp(\mathbf{s}^-)$. In this "solvation-layer interface condition,"[701,706–709] a parameterized function $h\left(E_\perp^-\right)$ serves to enhance or diminish the local permittivity based on the value of the surface-normal electric field. This is consistent with the idea that the local permittivity is different around an aqueous cation than it is around an anion, a fact that is borne out by molecular dynamics simulations in explicit water.[710] Note that the original boundary condition in Equation (2.22) is recovered if $h = 0$, and since $E_\perp^-$ is a signed quantity this modification is sufficient to capture charge hydration asymmetry.[706] A numerical complication is that the boundary condition in Equation (6.1) is nonlinear, meaning that the integral equation derived from Poisson's equation is also nonlinear, yet there still exists a (nonlinear) ASC-type integral equation formulation wherein the basic variable is the surface charge $\sigma(\mathbf{s})$.[706] Along similar lines (but perhaps easier to execute in practice), the SCCS approach has recently been modified to use a "field-aware" definition of the cavity surface,[711] which might describe the same physics.

7 | CLOSING REMARKS

With the contents of this review serving as a detailed guide to what continuum solvation models can do, in closing it feels *a propos* to comment on their limitations. These are very crude models. That is not inconsistent with being *useful* models, but one should not demand too much of something so simple. Perhaps the primary manner in which most users will encounter the crudeness of these models is in the fact that there is considerable arbitrariness in construction of the solute cavity, for which there is no "right" choice, although there are certainly plenty of wrong ones. In particular, there is no "magical" cavity construction or scaling factor for the vdW radii that will make these quantities universal. Small tweaks that might provide better answers for one system may very well degrade the accuracy in other cases. That said, the least arbitrary choices are isodensity cavity constructions and smooth interfaces based on permittivity functionals $\varepsilon[\rho](\mathbf{r})$, though the former lack analytic gradients and the latter are not yet widely available in Gaussian-orbital-based electronic structure programs. Nevertheless, evidence is beginning to emerge that these particular constructions may yield transferrable models of electrostatics that can be separated from the manner in which nonelectrostatic interactions are parameterized.

The electrostatic part of a dielectric continuum method is perhaps best viewed as an improved boundary condition for condensed-phase electronic structure calculations, as compared to vacuum boundary conditions. With that in mind, differences between how $\mathcal{G}_{\text{elst}}$ is computed amongst different PCMs seem inconsequential in comparison to the overall quality of these models, to the point where these differences can likely be parameterized away, or are simply washed out, by minor changes in cavity construction. The COSMO method, for example, performs well in comparison to more exact formulations of the continuum electrostatics problem, even in low-dielectric solvents.[210] For the SS(V)PE approach, discretization of $\hat{D}^\dagger \sigma(\mathbf{s})$ proves to be challenging when vdW cavities are used,[24,221] but these problems disappear for cavity constructions in which interatomic cusps are absent or less severe,[155,178] or can be avoided by reordering the operators to obtain the IEF-PCM method.[24]

In view of this, there would seem to be little room to further improve the electrostatic part of continuum solvation models. A corollary is that efforts to make the solvation model fully consistent with correlated wave function methods, either in the ground or excited states, seem misguided. For spectroscopic applications the "zeroth-order" solvation model, in which solvent-polarized MOs are inserted into a post-SCF correlation calculation, likely recovers the most important effects, and a ptSS-style correction for the fast polarization response affords a simple-to-use estimate for the excited-state (ε_∞-dependent) polarization correction to excitation energies.[586] Differences with respect to a fully self-consistent model are likely considerably smaller than errors introduced by the introduction of implicit solvent in the first place. Keeping those caveats in mind, the continuum solvation approach can be highly effective in situations where vacuum boundary conditions are dubious, for example, due to significant charge rearrangement in a polar solvent (including redox chemistry), or to modulate the energy levels of the frontier, solvent-exposed orbitals that control the electronic and valence photoelectron spectroscopy.

For calculation of solvation energies, which is arguably the most important application of continuum solvation models in chemistry, electrostatics alone is insufficient but a variety of black-box solvation models are available that incorporate nonelectrostatic contributions such as cavitation, dispersion, Pauli repulsion, and hydrogen bonding. The best contemporary models afford errors (with respect to experimental values of $\Delta_{\text{solv}}\mathcal{G}^{\circ}$) of <1 kcal/mol for charge-neutral solutes, whereas for ions the best methods approach the accuracy of the experimental data themselves,[302,303,312–315] which is 2–3 kcal/mol.[300,301,311] Recent versions of the SM*x* models remain the computational mainstays (with good reason),[302,303,312] but new methods including CMIRS and SCCS are now competitive,[313–315,468] despite using only a few empirical parameters per solvent. These new methods use a self-consistent, density-dependent definition of the solute/continuum interface, rather than relying on predetermined atomic radii. This eliminates much of the arbitrariness associated with continuum models and may be the key to obtaining a universal, transferable electrostatics model. That said, all of these models (including SM*x*) have been trained on relatively small solutes and it is unclear whether the same level of accuracy can be expected for significantly larger molecules. This is a relevant question, as new algorithms begin to facilitate application of PCM methodology to macromolecules.[23,190–193]

Regarding macromolecular solutes, it is clear that PCMs with linear-scaling solvers ought to be seriously considered as replacements for biomolecular electrostatics calculations based on finite-difference solution of the Poisson–Boltzmann equation. The ASC-PCM formalism provides an *exact* solution to the classical electrostatics problem,[23,24] up to controllable discretization errors, and can be formulated in such a way that potential energy surfaces are inherently continuous and smooth.[21,22] It is this author's opinion that theorists should not accept as their starting point any approach that does not provide intrinsically smooth potential energy surfaces, as the finite-difference Poisson–Boltzmann approach fails to do. The ability to explore the potential energy surface, and thus to have a well-defined "model chemistry,"[712] is too important to sacrifice.

ACKNOWLEDGMENTS

It is a pleasure to acknowledge current and former group members who have worked on these projects. In chronological order, they are: Dr. Adrian Lange, Benjamin Albrecht, Dr. Zhi-Qiang You, Dr. Marc Coons, Suranjan Paul, and Bushra Alam. Collaborations with Dr. Jan-Michael Mewes (from the group of Prof. Andreas Dreuw) and Dr. Christopher Stein (from the group of Prof. Martin Head-Gordon) are also happily acknowledged.

CONFLICT OF INTEREST

John M. Herbert serves on the Board of Directors of Q-Chem Inc.

DATA AVAILABILITY STATEMENT

Data sharing is not applicable to this article as no new data were created or analyzed in this study.

ORCID

John M. Herbert https://orcid.org/0000-0002-1663-2278

RELATED WIREs ARTICLES

Polarizable continuum model

Selected features of the polarizable continuum model for the representation of solvation

REFERENCES

1. Rinaldi D, Rivail J-L. Polarisabilités moléculaires et effet diélectrique de milieu à l'état liquide. Étude théorique de la molécule d'eau et de ses dimères. *Theor Chem Accounts*. 1973;*32*:57–70.
2. Rivail J-L, Rinaldi D. A quantum chemical approach to dielectric solvent effects in molecular liquids. *J Chem Phys*. 1976;*18*:233–42.
3. Miertuš S, Scrocco E, Tomasi J. Electrostatic interaction of a solute with a continuum. A direct utilization of ab initio molecular potentials for the prevision of solvent effects. *Chem Phys*. 1981;*55*:117–29.
4. Miertuš S, Tomasi J. Approximate evaluations of the electrostatic free energy and internal energy changes in solution processes. *Chem Phys*. 1982;*65*:239–45.
5. Bonaccorsi R, Cimiraglia R, Tomasi J. *Ab initio* evaluation of absorption and emission transitions for molecular solutes, including separate consideration of orientational and inductive solvent effects. *J Comput Chem*. 1983;*4*:567–77.
6. Tomasi J. Thirty years of continuum solvation chemistry: a review, and prospects for the near future. *Theor Chem Accounts*. 2004;*112*:184–203.
7. Grochowski P, Trylska J. Continuum molecular electrostatics, salt effects, and counterion binding—a review of the Poisson–Boltzmann theory and its modifications. *Biopolymers*. 2008;*89*:93–113.
8. Pliego JR Jr, Riveros JM. Hybrid discrete-continuum solvation methods. *WIREs Comput Mol Sci*. 2020;*10*:e1440.
9. Tomasi J, Persico M. Molecular interactions in solution: an overview of methods based on continuous distributions of the solvent. *Chem Rev*. 1994;*94*:2027–94.
10. Amovilli C, Barone V, Cammi R, Cancès E, Cossi M, Mennucci B, et al. Recent advances in the description of solvent effects with the polarizable continuum model. *Adv Quantum Chem*. 1999;*32*:227–61.
11. Tomasi J, Mennucci B, Cammi R, Cossi M. Quantum mechanical models for reactions in solution. In: Nâaray-Szabâo G, Warshel A, editors. *Computational approaches to biochemical reactivity*. Understanding chemical reactivity. Volume 19. New York: Springer; 2002; (chapter 1). p. 1–102.
12. Cammi R, Mennucci B, Tomasi J. Computational modelling of the solvent effects on molecular properties: an overview of the polarizable continuum model (PCM) approach. In: Leszczynski J, editor. *Computational chemistry: reviews of current trends*. Volume 8. Singapore: World Scientific; 2003; (chapter 1). p. 1–79.
13. Tomasi J, Mennucci B, Cammi R. Quantum mechanical continuum solvation models. *Chem Rev*. 2005;*105*:2999–3093.
14. Tomasi J. Selected features of the polarizable continuum model for the representation of solvation. *WIREs Comput Mol Sci*. 2011;*1*:855–67.
15. Mennucci B. Polarizable continuum model. *WIREs Comput Mol Sci*. 2012;*2*:386–404.
16. Lipparini F, Mennucci B. Perspective: polarizable continuum models for quantum-mechanical descriptions. *J Chem Phys*. 2016;*144*:160901.
17. Scrocco E, Tomasi J. The electrostatic molecular potential as a tool for the interpretation of molecular properties. *Top Curr Chem*. 1973;*42*:95–170.
18. Scrocco E, Tomasi J. Electronic molecular structure, reactivity and intermolecular forces: an heuristic interpretation by means of electrostatic molecular potentials. *Adv Quantum Chem*. 1978;*11*:115–93.
19. Tomasi J. On the use of the electrostatic molecular potential in theoretical investigations on chemical reactivity. In: Daudel R, Pullman A, Salem L, Veillard A, editors. *Quantum theory of chemical reactions*. Volume 1. Dordrecht: Reidel Publishing Company; 1980. p. 191–228.
20. Tomasi J. Use of the electrostatic potential as a guide to understanding molecular properties. In: Politzer P, Truhlar DG, editors. *Chemical applications of atomic and molecular electrostatic potentials*. New York: Plenum Press; 1981. p. 257–94.
21. Lange AW, Herbert JM. Polarizable continuum reaction-field solvation models affording smooth potential energy surfaces. *J Phys Chem Lett*. 2010;*1*:556–61.
22. Lange AW, Herbert JM. A smooth, nonsingular, and faithful discretization scheme for polarizable continuum models: the switching/Gaussian approach. *J Chem Phys*. 2010;*133*:244111.
23. Herbert JM, Lange AW. Polarizable continuum models for (bio)molecular electrostatics: basic theory and recent developments for macromolecules and simulations. In: Cui Q, Ren P, Meuwly M, editors. *Many-body effects and electrostatics in biomolecules*. Boca Raton: Pan Stanford; 2016; (chapter 11). p. 363–416.
24. Lange AW, Herbert JM. Symmetric versus asymmetric discretization of the integral equations in polarizable continuum solvation models. *Chem Phys Lett*. 2011;*509*:77–87.
25. Lange AW, Herbert JM, Albrecht BJ, You Z-Q. Intrinsically smooth discretization of Connolly's solvent-excluded molecular surface. *Mol Phys*. 2020;*118*:e1644384.
26. Cappelli C. Integrated QM/polarizable MM/continuum approaches to model chiroptical properties of strongly interacting solute–solvent systems. *Int J Quantum Chem*. 2016;*116*:1532–42.
27. Caricato M. Coupled cluster theory with the polarizable continuum model of solvation. *Int J Quantum Chem*. 2019;*119*:e25674.
28. Andreussi O, Fisicaro G. Continuum embeddings in condensed-matter simulations. *Int J Quantum Chem*. 2019;*119*:e25725.
29. Sadlej J, Pecul M. Computational modelling of the solvent–solute effect on NMR parameters by a polarizable continuum model. In: Mennucci B, Cammi R, editors. *Continuum solvation models in chemical physics*. Chichester, UK: Wiley; 2007. p. 125–44.
30. Barone V, Cimino P, Pavone M. EPR spectra of organic free radicals in solution from an integrated computational approach. In: Mennucci B, Cammi R, editors. *Continuum solvation models in chemical physics*. Chichester, UK: Wiley; 2007. p. 145–66.

31. Cappelli C. Continuum solvation approach to vibrational properties. In: Mennucci B, Cammi R, editors. *Continuum solvation models in chemical physics*. Chichester, UK: Wiley; 2007. p. 167–79.
32. Pecul M, Ruud K. Solvent effects on natural optical activity. In: Mennucci B, Cammi R, editors. *Continuum solvation models in chemical physics*. Chichester, UK: Wiley; 2007. p. 180–205.
33. Cammi R, Mennucci B. Macroscopic nonlinear optical properties from cavity models. In: Mennucci B, Cammi R, editors. *Continuum solvation models in chemical physics*. Chichester, UK: Wiley; 2007. p. 238–51.
34. Ågren H, Mikkelsen KV. Homogeneous and heterogeneous solvent models for nonlinear optical properties. In: Mennucci B, Cammi R, editors. *Continuum solvation models in chemical physics*. Chichester, UK: Wiley; 2007. p. 282–99.
35. Improta R. UV–visible absorption and emission energies in condensed phase by PCM/TD-DFT methods. In: Barone V, editor. *Computational strategies for spectroscopy: from small molecules to nano systems*. 1st ed. Hoboken, NJ: John Wiley & Sons; 2012; (chapter 1). p. 39–76.
36. Basilevsky MV, Parsons DF. An advanced continuum medium model for treating solvation effects: nonlocal electrostatics with a cavity. *J Chem Phys*. 1996;*105*:3734–46.
37. Jenkins OS, Hunt KLC. Nonlocal dielectric functions on the nanoscale: screened forces from unscreened potentials. *J Chem Phys*. 2003;*119*:8250–6.
38. Basilevsky MV, Chuev GN. Nonlocal solvation theories. In: Mennucci B, Cammi R, editors. *Continuum solvation models in chemical physics*. Chichester, UK: Wiley; 2007. p. 94–109.
39. Bardhan BRJ. Comparative assessment of nonlocal continuum solvent models exhibiting overscreening. *Mol Based Math Biol*. 2017;*5*:40–57.
40. Whiffen DH. Manual of symbols and terminology for physicochemical quantities and units. *Pure Appl Chem*. 1979;*51*:1–41.
41. Rizzo A. Birefringences in liquids. In: Mennucci B, Cammi R, editors. *Continuum solvation models in chemical physics*. Chichester, UK: Wiley; 2007. p. 252–64.
42. Ferrarini A. Anisotropic fluids. In: Mennucci B, Cammi R, editors. *Continuum solvation models in chemical physics*. Chichester, UK: Wiley; 2007. p. 265–81.
43. Wangsness RK. *Electromagnetic fields*. 2nd ed. John Wiley & Sons, Hoboken, NJ: Wiley; 1986.
44. Coons MP, Herbert JM. Quantum chemistry in arbitrary dielectric environments: theory and implementation of nonequilibrium Poisson boundary conditions and application to compute vertical ionization energies at the air/water interface. *J Chem Phys*. 2018;*148*:222834. Erratum: *J. Chem. Phys*., **151**, 189901 (2019).
45. Böttcher CJF. *Theory of electric polarization*. Vol 1. 2nd ed. Elsevier, Amsterdam: Elsevier; 1976.
46. Rashin AA, Honig B. Reevaluation of the Born model of ion hydration. *J Phys Chem*. 1985;*89*:5588–93.
47. Jacobson LD, Williams CF, Herbert JM. The static-exchange electron-water pseudopotential, in conjunction with a polarizable water model: a new Hamiltonian for hydrated-electron simulations. *J Chem Phys*. 2009;*130*:124115.
48. Cammi R. The quantum mechanical formulation of continuum models. In: Mennucci B, Cammi R, editors. *Continuum solvation models in chemical physics*. Chichester, UK: Wiley; 2007. p. 82–93.
49. Caricato M, Scalmani G, Frisch MJ. A Lagrangian formulation for continuum models. In: Mennucci B, Cammi R, editors. *Continuum solvation models in chemical physics*. Chichester, UK: Wiley; 2007. p. 64–81.
50. Nakamura H. Roles of electrostatic interaction in proteins. *Q Rev Biophys*. 1996;*29*:1–90.
51. Alexov E, Mehler EL, Baker N, Baptista AM, Huang Y, Milletti F, et al. Progress in the prediction of pK_a values in proteins. *Proteins*. 2011;*79*:3260–75.
52. Antosiewicz J, McCammon JA, Gilson MK. Prediction of pH-dependent properties of proteins. *J Mol Biol*. 1994;*238*:415–36.
53. Demchuk E, Wade RC. Improving the continuum dielectric approach to calculating pK_as of ionizable groups in proteins. *J Phys Chem*. 1996;*100*:17373–87.
54. Grycuk T. Revision of the model system concept for the prediction of pK_a's in proteins. *J Phys Chem B*. 2002;*106*:1434–45.
55. Truchon J-F, Nicholls A, Roux B, Iftimie RI, Bayly CI. Integrated continuum dielectric approaches to treat molecular polarizability and the condensed phase: refractive index and implicit solvation. *J Chem Theory Comput*. 2009;*5*:1785–802.
56. Warshel A, Russell ST. Calculations of electrostatic interactions in biological systems and in solutions. *Q Rev Biophys*. 1984;*17*:283–422.
57. Schutz CN, Warshel A. What are the dielectric "constants" of proteins and how to validate electrostatic models? *Proteins*. 2001;*44*:400–17.
58. Warshel A, Sharma PK, Kato M, Parson WW. Modeling electrostatic effects in proteins. *Biochim Biophys Acta*. 2006;*1764*:1647–76.
59. Li L, Li C, Zhang Z, Alexov E. On the dielectric "constant" of proteins: smooth dielectric function for macromolecular modeling and its implementation in DelPhi. *J Chem Theory Comput*. 2013;*9*:2126–36.
60. Bardhan JP, Knepley MG, Brune P. Nonlocal electrostatics in spherical geometries using eigenfunction expansions of boundary-integral operators. *Mol Based Math Biol*. 2015;*3*:1–22.
61. Sharp KA, Honig B. Electrostatic interactions in macromolecules. *Annu Rev Biophys Biophys Chem*. 1990;*19*:301–32.
62. Fogolari F, Brigo A, Molinari H. The Poisson–Boltzmann equation for biomolecular electrostatics: a tool for structural biology. *J Mol Recognit*. 2002;*15*:377–92.
63. Baker NA. Biomolecular applications of Poisson–Boltzmann methods. In: Lipkowitz K, Larter R, Cundari TR, editors. *Reviews in computational chemistry*. Volume 21. John Wiley & Sons, Hoboken, NJ: Wiley; 2005. p. 349–79.
64. Botello-Smith WM, Cai Q, Luo R. Biological applications of classical electrostatics methods. *J Theor Comput Chem*. 2014;*13*:1440008.

65. Schnieders MJ, Ponder JW. Polarizable atomic multipole solutes in a generalized Kirkwood continuum. *J Chem Theory Comput*. 2007;*3*:2083–97.
66. Schnieders MJ, Baker NA, Ren P, Ponder JW. Polarizable atomic multipole solutes in a Poisson–Boltzmann continuum. *J Chem Phys*. 2007;*126*:124114.
67. Sharp KA, Honig B. Calculating total electrostatic energies with the nonlinear Poisson–Boltzmann equation. *J Phys Chem*. 1990;*94*:7684–92.
68. Deserno M, Holm C. Cell model and Poisson–Boltzmann theory: a brief introduction. In: Holm C, Kékicheff P, Podgornik R, editors. *Electrostatic effects in soft matter and biophysics*. NATO science series. Volume 46. Dordrecht: Springer Science + Business Media; 2001. p. 27–52.
69. Lamm G. The Poisson–Boltzmann equation. In: Lipkowitz KB, Larter R, Cundari TR, Boyd DB, editors. *Reviews in computational chemistry*. Volume 19. New York: Wiley-VCH; 2003; (chapter 4). p. 147–366.
70. Baker NA. Poisson–Boltzmann methods for biomolecular electrostatics. *Methods Enzymol*. 2004;*383*:94–118.
71. Moreira AG, Netz RR. Field-theoretic approaches to classical charged systems. In: Holm C, Kékicheff P, Podgornik R, editors. *Electrostatic effects in soft matter and biophysics*. NATO science series. Volume 46. Dordrecht: Springer Science + Business Media; 2001. p. 367–408.
72. Bardhan JP. Biomolecular electrostatics—I want your solvation (model). *Comput Sci Discov*. 2012;*5*:013001.
73. Stein CJ, Herbert JM, Head-Gordon M. The Poisson–Boltzmann model for implicit solvation of electrolyte solutions: quantum chemical implementation and assessment via Sechenov coefficients. *J Chem Phys*. 2019;*151*:224111.
74. Zhou H-X. Macromolecular electrostatic energy within the nonlinear Poisson–Boltzmann equation. *J Chem Phys*. 1993;*100*:3152–62.
75. Fogolari F, Zuccato P, Esposito G, Viglino P. Biomolecular electrostatics with the linearized Poisson–Boltzmann equation. *Biophys J*. 1999;*76*:1–16.
76. Debye P, Hückel E. Zur Theorie der Elektrolyte. I. Gefrierpunktserniedrigung und verwandte Erscheinungen. *Physik Z*. 1923;*24*:185–206.
77. Debye P, Hückel E. On the theory of electrolytes. I. Freezing point depression and related phenomena. *Collected papers of Peter J. W. Debye*. Interscience, New York: Interscience Publishers, Inc.; 1954. p. 217–63.
78. Onsager L. Theories of concentrated electrolytes. *Chem Rev*. 1933;*13*:73–89.
79. Lange AW, Herbert JM. A simple polarizable continuum solvation model for electrolyte solutions. *J Chem Phys*. 2011;*134*:204110.
80. Wang C, Ren P, Luo R. Ionic solution: what goes right and wrong with continuum solvation modeling. *J Phys Chem B*. 2017;*121*:11159–79.
81. Vlachy V. Ionic effects beyond Poisson–Boltzmann theory. *Annu Rev Phys Chem*. 1999;*50*:145–65.
82. Dziedzic J, Bhandari A, Anton L, Peng C, Womack J, Famili M, et al. Practical approach to large-scale electronic structure calculations in electrolyte solutions via continuum-embedded linear-scaling density functional theory. *J Phys Chem C*. 2020;*124*:7860–72.
83. Born M. Volumen und Hydratationswärme der Ionen. *Z Phys*. 1920;*1*:45–8.
84. Onsager L. Electric moments of molecules in liquids. *J Am Chem Soc*. 1936;*58*:1486–93.
85. Bell RP. The electrostatic energy of dipole molecules in different media. *Trans Faraday Soc*. 1931;*27*:797–802.
86. Kirkwood JG. Theory of solutions of molecules containing widely separated charges with special application to zwitterions. *J Chem Phys*. 1934;*2*:351–61.
87. Böttcher CJF. The dielectric constant of dipole liquids. *Phys Ther*. 1938;*5*:635–9.
88. Kirkwood JG. The dielectric polarization of polar liquids. *J Chem Phys*. 1939;*7*:911–9.
89. Hasted JB. Liquid water: dielectric properties. In: Franks F, editor. *Water: a comprehensive treatise*. Volume 1. New York: Plenum Press; 1972. p. 255–309.
90. Omini M. A theory of electric polarisation in liquids: II. Polar liquids. *Physica A*. 1976;*84*:129–42.
91. Bokov OG, Naberukhin YI. Application of the Onsager model to the theory of the dielectric constant of nonpolar liquids. *J Chem Phys*. 1981;*75*:2357–65.
92. Høye JS, Stell G. Statistical mechanics of polar systems. II. *J Chem Phys*. 1976;*64*:1952–66.
93. Hannay JH. The Clausius–Mossotti equation: an alternative derivation. *Eur J Phys*. 1983;*4*:141–3.
94. Bonner WB. The electrostatic energy of molecules in solution. *Trans Faraday Soc*. 1951;*47*:1143–52.
95. Rinaldi D, Ruiz-Lopez MF, Rivail J-L. *Ab initio* SCF calculations on electrostatically solvated molecules using a deformable three axes ellipsoidal cavity. *J Chem Phys*. 1983;*78*:834–8.
96. Mikkelsen KV, Dalgaard E, Swanstrøm P. Electron-transfer reactions in solution. An ab initio approach. *J Phys Chem*. 1987;*91*:3081–92.
97. Mikkelsen KV, Ågren H, Jensen HJA, Helgaker T. A multiconfigurational self-consistent reaction-field method. *J Chem Phys*. 1988;*89*:3086–95.
98. Mikkelsen KV, Jørgensen P, Jensen HJA. A multiconfigurational self-consistent reaction field response method. *J Chem Phys*. 1994;*100*:6597–607.
99. Kong Y, Ponder JW. Calculation of the reaction field due to off-center point multipoles. *J Chem Phys*. 1997;*107*:481–92.
100. Medved' M, Budzák Š, Bartkowiak W, Reis H. Solvent effects on molecular electric properties. In: Leszczynski J, Kaczmarek-Kedziera A, Puzyn T, Papadopoulos MG, Reis H, Shukla MK, editors. *Handbook of computational chemistry*. 2nd ed. Switzerland: Springer International Publishing; 2017; (chapter 17). p. 741–94.

101. Westheimer FH, Kirkwood JG. The electrostatic influence of substituents on the dissociation constants of organic acids. II. *J Chem Phys*. 1938;*6*:513–7.
102. Kirkwood JG, Westheimer FH. The electrostatic influence of substituents on the dissociation constants of organic acids. I. *J Chem Phys*. 1938;*6*:506–12.
103. Gomez-Jeria JS, Morales-Lagos D. Free energy of a charge distribution in a spheroidal cavity surrounded by concentric dielectric continua. *J Phys Chem*. 1990;*94*:3790–5.
104. Morales-Lagos D, Gómez-Jeria JS. New developments in the continuum representation of solvent effects. *J Phys Chem*. 1991;*95*:5308–14.
105. Lotan I, Head-Gordon T. An analytical electrostatic model for salt screened interactions between multiple proteins. *J Chem Theory Comput*. 2006;*2*:541–55.
106. Alavi DS, Waldeck DH. Dielectric continuum models of solute/continuum interactions. In: Simon JD, editor. *Ultrafast dynamics of chemical systems*. Understanding chemical reactivity. Volume 7. Dordrecht: Springer Science + Business Media; 1994; (chapter 9). p. 249–65.
107. Zhan C-G, Bentley J, Chipman DM. Volume polarization in reaction field theory. *J Chem Phys*. 1998;*108*:177–92.
108. Chipman DM. Charge penetration in dielectric models of solvation. *J Chem Phys*. 1997;*106*:10194–206.
109. Chipman DM. Simulation of volume polarization in reaction field theory. *J Chem Phys*. 1999;*110*:8012–8.
110. Chipman DM. Reaction field treatment of charge penetration. *J Chem Phys*. 2000;*112*:5558–65.
111. Chipman DM. Comparison of solvent reaction field representations. *Theor Chem Accounts*. 2002;*107*:80–9.
112. Chipman DM. New formulation and implementation for volume polarization in dielectric continuum theory. *J Chem Phys*. 2006;*124*:224111.
113. Chipman DM. Energy correction to simulation of volume polarization in reaction field theory. *J Chem Phys*. 2002;*116*:10129–38.
114. Karelson MM, Katritzky AR, Zerner MC. Reaction field effects on the electron distribution and chemical reactivity of molecules. *Int J Quantum Chem Symp*. 1986;*20*:521–7.
115. Karelson M, Tamm T, Zerner MC. Multicavity reaction field method for the solvent effect description in flexible molecular systems. *J Phys Chem*. 1993;*97*:11901–7.
116. Luque FJ, Curutchet C, Muñoz-Muriedas J, Bidon-Chanal A, Soteras I, Morreale A, et al. Continuum solvation models: dissecting the free energy of solvation. *Phys Chem Chem Phys*. 2003;*5*:3827–36.
117. Beglov D, Roux B. Finite representation of an infinite bulk system: solvent boundary potential for computer simulations. *J Chem Phys*. 1994;*100*:9050–63.
118. Tironi IG, Sperb R, Smith PE, van Gunsteren WF. A generalized reaction field method for molecular dynamics simulations. *J Chem Phys*. 1995;*102*:5451–9.
119. Im W, Bernèche S, Roux B. Generalized solvent boundary potential for computer simulations. *J Chem Phys*. 2001;*114*:2924–37.
120. Schaefer P, Riccardi D, Cui Q. Reliable treatment of electrostatics in combined QM/MM simulation of macromolecules. *J Chem Phys*. 2005;*123*:014905.
121. Benighaus T, Thiel W. Efficiency and accuracy of the generalized solvent boundary potential for hybrid QM/MM simulations: implementation for semiempirical Hamiltonians. *J Chem Theory Comput*. 2008;*4*:1600–9.
122. Benighaus T, Thiel W. A general boundary potential for hybrid QM/MM simulations of solvated biomolecular systems. *J Chem Theory Comput*. 2009;*5*:3114–28.
123. Benighaus T, Thiel W. Long-range electrostatic effects in QM/MM studies of enzymatic reactions: application of the solvated macromolecule boundary potential. *J Chem Theory Comput*. 2011;*7*:238–49.
124. Aleksandrov A, Field M. Efficient solvent boundary potential for hybrid potential simulations. *Phys Chem Chem Phys*. 2011;*13*:10503–9.
125. Zienau J, Cui Q. Implementation of the solvent macromolecular boundary potential and application to model and realistic enzyme systems. *J Phys Chem B*. 2012;*116*:12522–34.
126. Lu X, Cui Q. Charging free energy calculations using the generalized solvent boundary potential (GSBP) and periodic boundary condition: a comparative analysis using ion solvation and oxidation free energy in proteins. *J Phys Chem B*. 2013;*117*:2005–18.
127. Rega N, Brancato G, Barone V. Non-periodic boundary conditions for ab initio molecular dynamics in condensed phase using localized basis functions. *Chem Phys Lett*. 2006;*422*:367–71.
128. Brancato G, Rega N, Barone V. Reliable molecular simulations of solute–solvent systems with a minimum number of solvent shells. *J Chem Phys*. 2006;*124*:214505.
129. Brancato G, Rega N, Barone V. A hybrid explicit/implicit solvation method for first-principle molecular dynamics simulations. *J Chem Phys*. 2008;*128*:144501.
130. Brancato G, Rega N, Barone V. Molecular dynamics simulations in a *NpT ensemble* using non-periodic boundary conditions. *Chem Phys Lett*. 2009;*483*:177–81.
131. Linder B, Hoernschemeyer D. Cavity concept in dielectric theory. *J Chem Phys*. 1967;*46*:784–90.
132. Luo Y, Ågren H, Mikkelsen KV. Unique determination of the cavity radius in Onsager reaction field theory. *Chem Phys Lett*. 1997;*275*:145–50.
133. Swanson JMJ, Adcock SA, McCammon JA. Optimized radii for Poisson–Boltzmann calculations with the AMBER force field. *J Chem Theory Comput*. 2005;*1*:484–93.

134. Manjeera M, Chamberlin AC, Valero R, Cramer CJ, Truhlar DG. Consistent van der Waals radii for the whole main group. *J Phys Chem A*. 2009;*113*:5806–12.
135. Bondi A. Van der Waals volumes and radii. *J Phys Chem*. 1964;*68*:441–51.
136. Rowland RS, Taylor R. Intermolecular nonbonded contact distances in organic crystal structures: comparison with distances expected from van der Waals radii. *J Phys Chem*. 1996;*100*:7384–91.
137. Bonaccorsi R, Palla P, Tomasi J. Conformational energy of glycine in aqueous solutions and relative stability of the zwitterionic and neutral forms. An ab initio study. *J Am Chem Soc*. 1984;*106*:1945–50.
138. Brookes DH, Head-Gordon T. Family of oxygen–oxygen radial distribution functions for water. *J Phys Chem Lett*. 2015;*6*:2938–43.
139. Onufriev AV, Aguilar B. Accuracy of continuum electrostatic calculations based on three common dielectric boundary definitions. *J Theor Comput Chem*. 2014;*13*:1440006.
140. Connolly ML. Solvent-accessible surfaces of proteins and nucleic acids. *Science*. 1983;*221*:709–13.
141. Richards FM. Areas, volumes, packing, and protein structure. *Annu Rev Biophys Bioeng*. 1977;*6*:151–76.
142. Kim D-S, Won C-I, Bhak J. A proposal for the revision of molecular boundary typology. *J Biomol Struct Dyn*. 2010;*28*:277–87.
143. Lee B, Richards FM. The interpretation of protein structures: estimation of static accessibility. *J Mol Biol*. 1971;*55*:379–400.
144. Pomelli CS. Cavity surfaces and their discretization. In: Mennucci B, Cammi R, editors. *Continuum solvation models in chemical physics*. Chichester, UK: Wiley; 2007. p. 49–63.
145. Connolly ML. The molecular surface package. *J Mol Graph*. 1993;*11*:139–41.
146. Gasteiger J, Engel T, editors. *Chemoinformatics: a textbook*. Weinheim: Wiley-VCH; 2003.
147. Xu D, Zhang Y. Generating triangulated macromolecular surfaces by Euclidean distance transform. *PLoS One*. 2009;*4*:e8140.
148. Decherchi S, Rocchia W. A general and robust ray-casting-based algorithm for triangulating surfaces at the nanoscale. *PLoS One*. 2013;*8*:e59744.
149. Zhan C-G, Chipman DM. Cavity size in reaction field theory. *J Chem Phys*. 1998;*109*:10543–58.
150. Barone V, Cossi M, Tomasi J. A new definition of cavities for the computation of solvation free energies by the polarizable continuum model. *J Chem Phys*. 1997;*107*:3210–21.
151. Ginovska B, Camaioni DM, Dupuis M, Schwerdtfeger CA, Gil Q. Charge-dependent cavity radii for an accurate dielectric continuum model of solvation with emphasis on ions: aqueous solutes with oxo, hydroxo, amino, methyl, chloro, bromo, and fluoro functionalities. *J Phys Chem A*. 2008;*112*:10604–13.
152. Lange AW, Herbert JM. Improving generalized Born models by exploiting connections to polarizable continuum models. I. An improved effective Coulomb operator. *J Chem Theory Comput*. 2012;*8*:1999–2011.
153. Lange AW, Herbert JM. Improving generalized Born models by exploiting connections to polarizable continuum models. II. Corrections for salt effects. *J Chem Theory Comput*. 2012;*8*:4381–92.
154. Foresman JB, Keith TA, Wiberg KB, Snoonian J, Frisch MJ. Solvent effects. 5. Influence of cavity shape, truncation of electrostatics, and electron correlation on ab initio reaction field calculations. *J Phys Chem*. 1996;*100*:16098–104.
155. Chipman DM, Dupuis M. Implementation of solvent reaction fields for electronic structure. *Theor Chem Accounts*. 2002;*107*:90–102.
156. Chen F, Chipman DM. Boundary element methods for dielectric cavity construction and integration. *J Chem Phys*. 2003;*119*:10289–97.
157. Holst M, Saied F. Multigrid solution of the Poisson–Boltzmann equation. *J Comput Chem*. 1993;*14*:105–13.
158. Holst MJ, Saied F. Numerical solution of the nonlinear Poisson–Boltzmann equation: developing more robust and efficient methods. *J Comput Chem*. 1995;*16*:337–64.
159. Holst M, Baker N, Wang F. Adaptive multilevel finite element solution of the Poisson–Boltzmann equation I. Algorithms and examples. *J Comput Chem*. 2000;*21*:1319–42. Erratum: *J. Comput. Chem.*, **22**, 45 (2001).
160. Lu BZ, Zhou YC, Holst MJ, McCammon JA. Recent progress in numerical methods for the Poisson–Boltzmann equation in biophysical applications. *Commun Comput Phys*. 2008;*3*:973–1009.
161. Wang J, Luo R. Assessment of linear finite-difference Poisson–Boltzmann solvers. *J Comput Chem*. 2010;*31*:1689–98.
162. Yap E-H, Head-Gordon T. New and efficient Poisson–Boltzmann solver for interaction of multiple proteins. *J Chem Theory Comput*. 2010;*6*:2214–24.
163. Boschitsch AH, Fenley MO. A fast and robust Poisson–Boltzmann solver based on adaptive Cartesian grids. *J Chem Theory Comput*. 2011;*7*:1524–40.
164. Holst M, McCammon JA, Yu Z, Zhou YC. Adaptive finite element modeling techniques for the Poisson–Boltzmann equation. *Commun Comput Phys*. 2012;*11*:179–214.
165. Li C, Li L, Petukh M, Alexov E. Progress in developing Poisson–Boltzmann equation solvers. *Mol Based Math Biol*. 2013;*1*:42–62.
166. Geng W, Krasny R. A treecode-accelerated boundary integral Poisson–Boltzmann solver for electrostatics of solvated biomolecules. *J Comput Phys*. 2013;*247*:62–78.
167. Sakalli I, Schöberl J, Knapp EW. mFES: a robust molecular finite element solver for electrostatic energy computations. *J Chem Theory Comput*. 2014;*10*:5095–112.
168. Fisicaro G, Genovese L, Andreussi O, Marzari N, Goedecker S. A generalized Poisson and Poisson–Boltzmann solver for electrostatic environments. *J Chem Phys*. 2016;*144*:014103.
169. Ringe S, Oberhofer H, Hille C, Matera S, Reuter K. Function-space-based solution scheme for the size-modified Poisson–Boltzmann equation in full-potential DFT. *J Chem Theory Comput*. 2016;*12*:4052–66.

170. Womack JC, Anton L, Dziedzic J, Hasnip PJ, Probert MIJ, Skylaris C-K. DL_MG: a parallel multigrid Poisson and Poisson–Boltzmann solver for electronic structure calculations in vacuum and solution. *J Chem Theory Comput*. 2018;*14*:1412–32.
171. Luzhkov V, Warshel A. Microscopic models for quantum mechanical calculations of chemical processes in solutions: LD/AMPAC and SCAAS/AMPAC calculations of solvation energies. *J Comput Chem*. 1992;*13*:199–213.
172. Florián J, Warshel A. Langevin dipoles model for ab initio calculations of chemical processes in solution: parameterization and application to hydration free energies of neutral and ionic solutes and conformational analysis in aqueous solution. *J Phys Chem B*. 1997;*101*: 5583–95.
173. Papazyan A, Warshel A. Continuum and dipole-lattice models of solvation. *J Phys Chem B*. 1997;*101*:11254–64.
174. Langlet J, Claverie P, Caillet J, Pullman A. Improvements of the continuum model. 1. Application to the calculation of the vaporization of thermodynamic quantities of nonassociated liquids. *J Phys Chem*. 1988;*92*:1617–31.
175. Constanciel R. Theoretical basis of the empirical reaction field approximations through continuum model. *Theor Chem Accounts*. 1986; *69*:505–23.
176. Bardhan JP. Numerical solution of boundary-integral equations for molecular electrostatics. *J Chem Phys*. 2009;*130*:094102.
177. Cancès E. Integral equation approaches for continuum models. In: Mennucci B, Cammi R, editors. *Continuum solvation models in chemical physics*. Chichester, UK: Wiley; 2007. p. 29–48.
178. Cossi M, Scalmani G, Rega N, Barone V. New developments in the polarizable continuum model for quantum mechanical and classical calculations on molecules in solution. *J Chem Phys*. 2002;*117*:43–54.
179. Tomasi J, Mennucci B, Cancès E. The IEF version of the PCM solvation method: an overview of a new method addressed to study molecular solutes at the QM ab initio level. *J Mol Struct (THEOCHEM)*. 1999;*464*:211–26.
180. Cancés E, Mennucci B, Tomasi J. A new integral equation formalism for the polarizable continuum model: theoretical background and applications to isotropic and anisotropic dielectrics. *J Chem Phys*. 1997;*107*:3032–41.
181. Mennucci B, Cancès E, Tomasi J. Evaluation of solvent effects in isotropic and anisotropic dielectrics and in ionic solutions with a unified integral equation method: theoretical bases, computational implementation, and numerical applications. *J Phys Chem B*. 1997;*101*: 10506–17.
182. Cancès E, Mennucci B. New applications of integral equations methods for solvation continuum models: ionic solutions and liquid crystals. *J Math Chem*. 1998;*23*:309–26.
183. Cancès E, Mennucci B. Comment on 'reaction field treatment of charge penetration'. *J Chem Phys*. 2001;*114*:4744–5.
184. Davis ME, McCammon JA. Solving the finite difference linearized Poisson–Boltzmann equation: a comparison of relaxation and conjugate gradient methods. *J Comput Chem*. 1989;*10*:386–91.
185. Luty BA, Davis ME, McCammon JA. Solving the finite-difference non-linear Poisson–Boltzmann equation. *J Comput Chem*. 1992;*13*: 1114–8.
186. Wang J, Cai Q, Xiang Y, Luo R. Reducing grid dependence in finite-difference Poisson–Boltzmann calculations. *J Chem Theory Comput*. 2012;*8*:2741–51.
187. Xiao L, Cai Q, Ye X, Wang J, Luo R. Electrostatic forces in the Poisson–Boltzmann systems. *J Chem Phys*. 2013;*139*:094106.
188. Xiao L, Wang C, Luo R. Recent progress in adapting Poisson–Boltzmann methods to molecular simulations. *J Theor Comput Chem*. 2014;*13*:1430001.
189. Chipman DM. Solution of the linearized Poisson–Boltzmann equation. *J Chem Phys*. 2004;*120*:5566–75.
190. Lipparini F, Stamm B, Cancès E, Maday Y, Mennucci B. Fast domain decomposition algorithm for continuum solvation models: energy and first derivatives. *J Chem Theory Comput*. 2013;*9*:3637–48.
191. Lipparini F, Lagardère L, Scalmani G, Stamm B, Cancès E, Maday Y, et al. Quantum calculations in solution for large to very large molecules: a new linear scaling QM/continuum approach. *J Phys Chem Lett*. 2014;*5*:953–8.
192. Lipparini F, Scalmani G, Lagardère L, Stamm B, Cancès E, Maday Y, et al. Quantum, classical, and hybrid QM/MM calculations in solution: general implementation of the ddCOSMO linear scaling strategy. *J Chem Phys*. 2014;*141*:184108.
193. Caprasecca S, Jurinovich S, Lagardère L, Stamm B, Lipparini F. Achieving linear scaling in computational cost for a fully polarizable MM/continuum embedding. *J Chem Theory Comput*. 2015;*11*:694–704.
194. Klamt A, Schüürmann G. COSMO: a new approach to dielectric screening in solvents with explicit expressions for the screening energy and its gradient. *J Chem Soc Perkin Trans*. 1993;*2*:799–805.
195. Andzelm J, Kölmel C, Klamt A. Incorporation of solvent effects into density functional calculations of molecular energies and geometries. *J Chem Phys*. 1995;*103*:9312–20.
196. Klamt A, Jonas V. Treatment of the outlying charge in continuum solvation models. *J Chem Phys*. 1996;*105*:9972–81.
197. Klamt A. The COSMO and COSMO-RS solvation models. *WIREs Comput Mol Sci*. 2018;*8*:e1338.
198. Barone V, Cossi M. Quantum calculation of molecular energies and energy gradients in solution by a conductor solvent model. *J Phys Chem A*. 1998;*102*:1995–2001.
199. Cossi M, Rega N, Scalmani G, Barone V. Energies, structures, and electronic properties of molecules in solution with the C-PCM solvation model. *J Comput Chem*. 2003;*24*:669–81.
200. Stefanovich EV, Truong TN. Optimized atomic radii for quantum dielectric continuum solvation models. *Chem Phys Lett*. 1995;*244*: 65–74.
201. Truong TN, Stefanovich EV. A new method for incorporating solvent effects into the classical, ab initio molecular orbital and density functional theory frameworks for arbitrary cavity shape. *Chem Phys Lett*. 1995;*240*:253–60.

202. Truong TN, Stefanovich EV. Analytical first and second energy derivatives of the generalized conductorlike screening model for free energy of solvation. *J Chem Phys*. 1995;*103*:3709–17.
203. Truong TN, Nguyen UN, Stefanovich EV. Generalized conductor-like screening model (GCOSMO) for solvation: an assessment of its accuracy and applicability. *Int J Quantum Chem Symp*. 1996;*60*:1615–22.
204. Schäfer A, Klamt A, Sattel D, Lohrenz JCW, Eckert F. COSMO implementation in TURBOMOLE: extension of an efficient quantum chemical code towards liquid systems. *Phys Chem Chem Phys*. 2000;*2*:2187–93.
205. Andrade do Monte S, Müller T, Dallos M, Lischka H, Diedenhofen M, Klamt A. Solvent effects in electronically excited states using the continuum solvation model COSMO in combination with multireference configuration interaction with singles and doubles (MR-CISD). *J Mol Struct (THEOCHEM)*. 2004;*111*:78–89.
206. Klamt A, Diedenhofen M. A refined cavity construction algorithm for the conductor-like screening model. *J Comput Chem*. 2018;*39*:1648–55.
207. Pye CC, Ziegler T. An implementation of the conductor-like screening model of solvation within the Amsterdam density functional package. *Theor Chem Accounts*. 1999;*101*:396–408.
208. Diedenhofen M. Conductor-like screening model COSMO. In: Grotendorst J, editor. *High performance computing in chemistry*. NIC series. Volume 25. Jülich: John von Neumann Institute for Computing; 2005; (chapter 6). p. 133–49.
209. Křž K, Řezáč J. Reparameterization of the COSMO solvent model for semiempirical methods PM6 and PM7. *J Chem Inf Model*. 2019;*59*:229–35.
210. Klamt A, Moya C, Palomar J. A comprehensive comparison of the IEFPCM and SS(V)PE continuum solvation methods with the COSMO approach. *J Chem Theory Comput*. 2015;*11*:4220–5.
211. Cancès E, Mennucci B. The escaped charge problem in solvation continuum models. *J Chem Phys*. 2001;*115*:6130–5.
212. Cammi R, Tomasi J. Analytical derivatives for molecular solutes. I. Hartree–Fock energy first derivatives with respect to external parameters in the polarizable continuum model. *J Chem Phys*. 1994;*100*:7495–502.
213. Cammi R, Tomasi J. Remarks on the use of apparent surface charges (ASC) methods in solvation problems: iterative versus matrix-inversion procedures and the renormalization of the apparent surface charges. *J Comput Chem*. 1995;*16*:1449–58.
214. Baldridge K, Klamt A. First principles implementation of solvent effects without outlying charge error. *J Chem Phys*. 1997;*106*:6622–33.
215. Mennucci B, Tomasi J. Continuum solvation models: a new approach to the problem of solute's charge distribution and cavity boundaries. *J Chem Phys*. 1997;*106*:5151–8.
216. Cammi R, Cossi M, Tomasi J. Analytical derivatives for molecular solutes. III. Hartree–Fock static polarizabilities in the polarizable continuum model. *J Chem Phys*. 1996;*104*:4611–20.
217. Gauss J. Molecular properties. In: Grotendorst J, editor. *Modern methods and algorithms of quantum chemistry*. NIC series. Volume 3 of. 2nd ed. Jülich: John von Neumann Institute for Computing; 2000. p. 541–92.
218. Rizzo A, Coriani S, Ruud K. Response function theory computational approaches to linear and nonlinear optical spectroscopy. In: Barone V, editor. *Computational strategies for spectroscopy: from small molecules to nano systems*. 1st ed. Hoboken, NJ: John Wiley & Sons; 2012; (chapter 2). p. 77–136.
219. Helgaker T, Coriani S, Jørgensen P, Kristensen K, Olsen J, Ruud K. Recent advances in wave function-based methods of molecular-property calculations. *Chem Rev*. 2012;*112*:543–631.
220. Jurrus E, Engel D, Star K, Monson K, Brandi J, Felberg LE, et al. Improvements to the APBS biomolecular solvation software suite. *Protein Sci*. 2018;*27*:112–28.
221. You Z-Q, Mewes J-M, Dreuw A, Herbert JM. Comparison of the Marcus and Pekar partitions in the context of non-equilibrium, polarizable-continuum reaction-field solvation models. *J Chem Phys*. 2015;*143*:204107.
222. Silla E, Villar F, Nilsson O, Pascual-Ahuir JL, Tapia O. Molecular volumes and surfaces of biomacromolecules via GEPOL: a fast and efficient algorithm. *J Mol Graph*. 1990;*8*:168–72.
223. Pascual-Ahuir JL, Silla E. GEPOL: an improved description of molecular surfaces. I. Building the spherical surface set. *J Comput Chem*. 1990;*11*:1047–60.
224. Silla E, Tuñon I, Pascual-Ahuir JL. GEPOL: an improved description of molecular surfaces. II. Computing the molecular area and volume. *J Comput Chem*. 1991;*12*:1077–88.
225. Pascual-Ahuir JL, Silla E, Tuñon I. GEPOL: an improved description of molecular surfaces. III. A new algorithm for the computation of a solvent-excluding surface. *J Comput Chem*. 1994;*15*:1127–38.
226. Scalmani G, Rega N, Cossi M, Barone V. Finite elements molecular surfaces in continuum solvent models for large chemical systems. *J Comput Methods Sci Eng*. 2002;*2*:469–74.
227. Liotard DA, Hawkins GD, Lynch GC, Cramer CJ, Truhlar DG. Improved methods for semiempirical solvation models. *J Comput Chem*. 1995;*16*:422–40.
228. Cossi M, Mennucci B, Cammi R. Analytical first derivatives of molecular surfaces with respect to nuclear coordinates. *J Comput Chem*. 1996;*17*:57–73.
229. York DM, Karplus M. Smooth solvation potential based on the conductor-like screening model. *J Phys Chem A*. 1999;*103*:11060–79.
230. Gregersen BA, York DM. High-order discretization schemes for biochemical applications of boundary element solvation and variational electrostatic projection methods. *J Chem Phys*. 2005;*122*:194110.
231. Khandogin J, Gregersen BA, Thiel W, York DM. Smooth solvation method for d-orbital semiempirical calculations of biological reactions. 1. Implementation. *J Phys Chem B*. 2005;*109*:9799–809.

232. Murray CW, Handy NC, Laming GJ. Quadrature schemes for integrals of density functional theory. *Mol Phys*. 1993;*78*:997–1014.
233. Gill PMW, Johnson BG, Pople JA. A standard grid for density-functional calculations. *Chem Phys Lett*. 1993;*209*:506–12.
234. Chien S-H, Gill PMW. SG-0: a small standard grid for DFT quadrature on large systems. *J Comput Chem*. 2006;*27*:730–9.
235. Dasgupta S, Herbert JM. Standard grids for high-precision integration of modern density functionals: SG-2 and SG-3. *J Comput Chem*. 2017;*38*:869–82.
236. Liu J, Liang W. Analytical second derivatives of excited-state energy within the time-dependent density functional theory coupled with a conductor-like polarizable continuum model. *J Chem Phys*. 2013;*138*:024101.
237. Wawak RJ, Gibson KD, Scheraga HA. Gradient discontinuities in calculations involving molecular surface area. *J Math Chem*. 1994;*15*: 207–32.
238. Li H, Jensen JH. Improving the efficiency and convergence of geometry optimization with the polarizable continuum model: new energy gradients and molecular surface tessellation. *J Comput Chem*. 2004;*25*:1449–62.
239. Su P, Li H. Continuous and smooth potential energy surface for conductor-like screening solvation model using fixed points with variable areas. *J Chem Phys*. 2009;*130*:074109.
240. Delley B. The conductor-like screening model for polymers and surfaces. *Mol Phys*. 2006;*32*:117–23.
241. Krylov AI, Gill PMW. Q-Chem: an engine for innovation. *WIREs Comput Mol Sci*. 2013;*3*:317–26.
242. Scalmani G, Frisch MJ. Continuous surface charge polarizable continuum models of solvation. I. General formalism. *J Chem Phys*. 2010;*132*:114110.
243. Garcia-Ratès M, Neese F. Effect of the solute cavity on the solvation energy and its derivatives within the framework of the Gaussian charge scheme. *J Comput Chem*. 2020;*41*:922–39.
244. Harbrecht H, Randrianarivony M. Wavelet BEM on molecular surfaces: parameterization and implementation. *Computing*. 2009; *86*:1–22.
245. Weijo V, Randrianarivony M, Harbrecht H, Frediani L. Wavelet formulation of the polarizable continuum model. *J Comput Chem*. 2010;*31*:1469–77.
246. Bugeanu M, Di Remigio R, Mozgawa K, Reine SS, Harbrecht H, Frediani L. Wavelet formulation of the polarizable continuum model. II. Use of piecewise bilinear boundary elements. *Phys Chem Chem Phys*. 2015;*17*:31566–81.
247. Bugeanu M, Harbrecht H. Parametric representation of molecular surfaces. *Int J Quantum Chem*. 2019;*119*:e25695.
248. Beck TL. The influence of water interfacial potentials on ion hydration in bulk water and near interfaces. *Chem Phys Lett*. 2013; *561–562*:1–13.
249. Marenich AV, Cramer CJ, Truhlar DG. Perspective on foundations of solvation modeling: the electrostatic contribution to the free energy of solvation. *J Chem Theory Comput*. 2008;*4*:877–87.
250. Zhan C-G, Chipman DM. Reaction field effects on nitrogen shielding. *J Chem Phys*. 1999;*110*:1611–22.
251. Tjong H, Zhou H-X. On the dielectric boundary in Poisson–Boltzmann calculations. *J Chem Theory Comput*. 2008;*4*:507–14.
252. Acevedo O, Jorgensen WL. Solvent effects and mechanism for a nucleophilic aromatic substitution from QM/MM simulations. *Org Lett*. 2004;*6*:2881–4.
253. Miguel ELM, Santos CIL, Silva CM, Pliego JR Jr. How accurate is the SMD model for predicting free energy barriers for nucleophilic substitution reactions in polar protic and dipolar aprotic solvents? *J Braz Chem Soc*. 2016;*27*:2055–61.
254. Lorensen WE, Cline HE. Marching cubes: a high resolution 3D surface construction algorithm. *Comput Graph*. 1987;*21*:163–9.
255. Rajon DA, Bolch WE. Marching cubes algorithm: review and trilinear interpolation adaptation for image-based dosimetric models. *Comput Med Imaging Graph*. 2003;*27*:411–35.
256. Yu Z, Jacobson MP, Friesner R. What role do surfaces play in GB models? A new-generation of surface-generalized Born model based on a novel Gaussian surface for biomolecules. *J Comput Chem*. 2005;*27*:72–89.
257. Zhou B, Agarwal M, Wong CF. Variable atomic radii for continuum-solvent electrostatics calculation. *J Chem Phys*. 2008;*129*:014509.
258. Fattebert J-L, Gygi F. Density functional theory for efficient *ab initio* molecular dynamics simulations in solution. *J Comput Chem*. 2002;*23*:662–6.
259. Fattebert J-L, Gygi F. First-principles molecular dynamics simulations in a continuum solvent. *Int J Quantum Chem*. 2003;*93*:139–47.
260. Scherlis DA, Fattebert J-L, Gygi F, Cococcioni M, Marzari N. A unified electrostatic and cavitation model for first-principles molecular dynamics in solution. *J Chem Phys*. 2006;*124*:074103.
261. Dziedzic J, Helal HH, Skylaris C-K, Mostofi AA, Payne MC. Minimal parameter implicit solvent model for ab initio electronic-structure calculations. *Europhys Lett*. 2011;*95*:43001.
262. Andreussi O, Dabo I, Marzari N. Revised self-consistent continuum solvation in electronic-structure calculations. *J Chem Phys*. 2012; *136*:064102.
263. Mathew K, Sundararaman R, Letchworth-Weaver K, Arias TA, Hennig RG. Implicit solvation model for density-functional study of nanocrystal surfaces and reaction pathways. *J Chem Phys*. 2014;*140*:084106.
264. Sánchez VM, Sued M, Scherlis DA. First-principles molecular dynamics simulations at solid–liquid interfaces with a continuum solvent. *J Chem Phys*. 2009;*131*:174108.
265. Im W, Beglov D, Roux B. Continuum solvation model: computation of electrostatic forces from numerical solutions to the Poisson–Boltzmann equation. *Comput Phys Commun*. 1998;*111*:59–75.
266. Grant JA, Pickup BT, Nicholls A. A smooth permittivity function for Poisson–Boltzmann solvation methods. *J Comput Chem*. 2001;*22*: 608–40.

267. Basilevsky MV, Grigoriev FV, Nikitina EA, Leszczynski J. Implicit electrostatic solvent model with continuous dielectric permittivity function. *J Phys Chem B*. 2010;*114*:2457–66.
268. Nattino F, Truscott M, Marzari N, Andreussi O. Continuum models of the electrochemical diffuse layer in electronic-structure calculations. *J Chem Phys*. 2019;*150*:041722.
269. Andreussi O, Hörmann NG, Nattino F, Fisicaro G, Goedecker S, Marzari N. Solvent-aware interfaces in continuum solvation. *J Chem Theory Comput*. 2019;*15*:1996–2009.
270. Sundararaman R, Schwarz K. Evaluating continuum solvation models for the electrode-electrolyte interface: challenges and strategies for improvement. *J Chem Phys*. 2017;*146*:084111.
271. Sundararaman R, Letchworth-Weaver K, Schwarz KA. Improving accuracy of electrochemical capacitance and solvation energetics in first-principles calculations. *J Chem Phys*. 2018;*148*:144105.
272. Schwarz K, Sundararaman R. The electrochemical interface in first-principles calculations. *Surf Sci Rep*. 2020;*75*:100492.
273. Bramley G, Nguyen M-T, Glezakou V-A, Rousseau R, Sylaris C-K. Reconciling work functions and adsorption enthalpies for implicit solvent models: a Pt(111)/water interface case study. *J Chem Theory Comput*. 2020;*16*:2703–15.
274. Bhandari A, Anton L, Dziedzic J, Peng C, Kramer D, Skylaris C-K. Electronic structure calculations in electrolyte solutions: methods for neutralization of extended charged interfaces. *J Chem Phys*. 2020;*153*:124101.
275. Booth F. The dielectric constant of water and the saturation effect. *J Chem Phys*. 1951;*19*:391–4.
276. Daniels L, Scott M, Mišković ZL. The role of Stern layer in the interplay of dielectric saturation and ion steric effects for the capacitance of graphene in aqueous electrolytes. *J Chem Phys*. 2017;*146*:094101.
277. Davis ME, McCammon JA. Dielectric boundary smoothing in finite difference solutions of the Poisson equation: an approach to improve accuracy and convergence. *J Comput Chem*. 1991;*12*:909–12.
278. Gilson MK, Davis ME, Luty BA, McCammon JA. Computation of electrostatic forces on solvated molecules using the Poisson–Boltzmann equation. *J Phys Chem*. 1993;*97*:3591–600.
279. Lu B, Zhang D, McCammon JA. Computation of electrostatic forces between solvated molecules determined by the Poisson–Boltzmann equation using a boundary element method. *J Chem Phys*. 2005;*122*:214102.
280. Wang J, Tan C, Chanco E, Luo R. Quantitative analysis of Poisson–Boltzmann implicit solvent in molecular dynamics. *Phys Chem Chem Phys*. 2010;*12*:1194–202.
281. Cai Q, Ye X, Wang J, Luo R. Dielectric boundary force in numerical Poisson–Boltzmann methods: theory and numerical strategies. *Chem Phys Lett*. 2011;*514*:368–73.
282. Rega N, Cossi M, Barone V. Towards linear scaling in continuum solvent models. A new iterative procedure for energies and geometry optimizations. *Chem Phys Lett*. 1998;*293*:221–9.
283. Scalmani G, Barone V, Kudin KN, Pomelli CS, Scuseria GE, Frisch MJ. Achieving linear-scaling computational cost for the polarizable continuum model of solvation. *Theor Chem Accounts*. 2004;*111*:90–100.
284. Lindgren EB, Stace AJ, Polack E, Maday Y, Stamm B, Besley E. An integral equation approach to calculate electrostatic interactions in many-body dielectric systems. *J Comput Phys*. 2018;*371*:712–31.
285. Cancès E, Maday Y, Stamm B. Domain decomposition for implicit solvation models. *J Chem Phys*. 2013;*139*:054111.
286. Gatto P, Lipparini F, Stamm B. Computation of forces arising from the polarizable continuum model within the domain-decomposition paradigm. *J Chem Phys*. 2017;*147*:224108.
287. Stamm B, Lagardère L, Scalmani G, Gatto P, Cancès E, Piquemal J-P, et al. How to make continuum solvation incredibly fast in a few simple steps: a practical guide to the domain decomposition paradigm for the conductor-like screening model. *Int J Quantum Chem*. 2019;*119*:e25669.
288. Nottoli M, Stamm B, Scalmani G, Lipparini F. Quantum calculations in solution of energies, structures, and properties with a domain decomposition polarizable continuum model. *J Chem Theory Comput*. 2019;*15*:6061–73.
289. Lagardère L, Jolly L-H, Lipparini F, Aviat F, Stamm B, Jing ZF, et al. Tinker-HP: a massively parallel molecular dynamics package for multiscale simulations of large complex systems with advanced point dipole polarizable force fields. *Chem Sci*. 2018;*9*:956–72.
290. Lipparini F, Lagardère L, Raynaud C, Stamm B, Cancès E, Mennucci B, et al. Polarizable molecular dynamics in a polarizable continuum solvent. *J Chem Theory Comput*. 2014;*11*:623–34.
291. Casasnovas R, Fernández D, Ortega-Castro J, Frau J, Donoso J, Muñoz F. Avoiding gas-phase calculations in theoretical pK_a predictions. *Theor Chem Accounts*. 2011;*130*:1–13.
292. Sastre S, Casasnovas R, Muñoz F, Frau J. Isodesmic reaction for pK_a calculations of common organic molecules. *Theor Chem Accounts*. 2013;*132*:1310.
293. Casasnovas R, Ortega-Castro J, Frau J, Donoso J, Muñoz F. Theoretical pK_a calculations with continuum model solvents, alternative protocols to thermodynamic cycles. *Int J Quantum Chem*. 2014;*114*:1350–63.
294. Ho J, Coote ML. First-principles prediction of acidities in the gas and solution phase. *WIREs Comput Mol Sci*. 2011;*1*:649–60.
295. Ho J. Are thermodynamic cycles necessary for continuum solvent calculation of pK_as and reduction potentials? *Phys Chem Chem Phys*. 2015;*17*:2859–68.
296. Ho J, Ertem MZ. Calculating free energy changes in continuum solvation models. *J Phys Chem B*. 2016;*120*:1319–29.
297. Ho J, Klamt A, Coote ML. Comment on the correct use of continuum solvent models. *J Phys Chem A*. 2010;*114*:13442–4.
298. Ribeiro RF, Marenich AV, Cramer CJ, Truhlar DG. Use of solution-phase vibrational frequencies in continuum models for the free energy of solvation. *J Phys Chem B*. 2011;*115*:14556–62.

299. Jensen JH. Predicting accurate absolute binding energies in aqueous solution: thermodynamic considerations for electronic structure methods. *Phys Chem Chem Phys*. 2015;*17*:12441–51.
300. Thompson JD, Cramer CJ, Truhlar DG. New universal solvation model and comparison of the accuracy of the SM5.42R, SM5.43R, C-PCM, D-PCM, and IEF-PCM continuum solvation models for aqueous and organic solvation free energies and for vapor pressures. *J Phys Chem A*. 2004;*108*:6532–42.
301. Kelly CP, Cramer CJ, Truhlar DG. SM6: a density functional theory continuum solvation model for calculating aqueous solvation free energies of neutrals, ions, and solute–water clusters. *J Chem Theory Comput*. 2005;*1*:1133–52.
302. Marenich AV, Cramer CJ, Truhlar DG. Universal solvation model based on solute electron density and on a continuum model of the solvent defined by the bulk dielectric constant and atomic surface tensions. *J Phys Chem B*. 2009;*113*:6378–96.
303. Marenich AV, Cramer CJ, Truhlar DG. Generalized Born solvation model SM12. *J Chem Theory Comput*. 2013;*9*:609–20.
304. Marenich AV, Olson RM, Kelly CP, Cramer CJ, Truhlar DG. Self-consistent reaction field model for aqueous and nonaqueous solutions based on accurate polarized partial charges. *J Chem Theory Comput*. 2007;*3*:2011–33.
305. Cramer CJ, Truhlar DG. A universal approach to solvation modeling. *Acc Chem Res*. 2008;*41*:760–8.
306. Cramer CJ, Truhlar DG. Reply to comment on 'a universal approach to solvation modeling'. *Acc Chem Res*. 2009;*42*:493–7.
307. Amado AM, Fiuza SM, Batista de Carvalho LAE, Ribeiro-Ciaro PJA. On the effects of changing Gaussian program version and SCRF defining parameters: isopropylamine as a case study. *Bull Chem Soc Jpn*. 2012;*85*:962–75.
308. Wen M, Jiang J, Wang Z-X, Wu C. How accurate are the popular PCM/GB continuum solvation models for calculating the solvation energies of amino acid side-chain analogs? *Theor Chem Accounts*. 2014;*133*:1471.
309. Shields GC, Seybold PG. *Computational approaches for the prediction of* pK_a *values*. Boca Raton, FL: CRC Press; 2014.
310. Giles J. Software company bans competitive users. *Nature*. 2004;*429*:231.
311. Pliego JR Jr, Riveros JM. Gibbs energy of solvation of organic ions in aqueous and dimethyl sulfoxide solutions. *Phys Chem Chem Phys*. 2002;*4*:1622–7.
312. Liu J, Kelly CP, Goren AC, Marenich AV, Cramer CJ, Truhlar DG, et al. Free energies of solvation with surface, volume, and local electrostatic effects and atomic surface tensions to represent the first solvation shell. *J Chem Theory Comput*. 2010;*6*:1109–17.
313. You Z-Q, Herbert JM. Reparameterization of an accurate, few-parameter implicit solvation model for quantum chemistry: composite method for implicit representation of solvent, CMIRS v. 1.1. *J Chem Theory Comput*. 2016;*12*:4338–46.
314. Dupont C, Andreussi O, Marzari N. Self-consistent continuum solvation (SCCS): the case of charged systems. *J Chem Phys*. 2013;*139*:214110.
315. Fisicaro G, Genovese L, Andreussi O, Mandai S, Nair NN, Marzari N, et al. Soft-sphere continuum solvation in electronic-structure calculations. *J Chem Theory Comput*. 2017;*13*:3829–45.
316. Tissandier MD, Cowen KA, Feng WY, Gundlach E, Cohen MH, Earhart AD, et al. The proton's absolute aqueous enthalpy and Gibbs free energy of solvation from cluster-ion solvation data. *J Phys Chem A*. 1998;*102*:7787–94.
317. Tuttle TR Jr, Malaxos S, Coe JV. A new cluster pair method of determining absolute single ion solvation energies demonstrated in water and applied to ammonia. *J Phys Chem A*. 2002;*106*:925–32.
318. Vlcek L, Chialvo AA, Simonson JM. Correspondence between cluster-ion and bulk solution thermodynamic properties: on the validity of the cluster-pair-based approximation. *J Phys Chem A*. 2013;*117*:11328–38.
319. Malloum A, Fifen JJ, Conradie J. Determination of the absolute solvation free energy and enthalpy of the proton in solutions. *J Mol Liq*. 2021;*322*:114919.
320. Ashbaugh HS, Asthagiri D. Single ion hydration free energies: a consistent comparison between experiment and classical molecular simulation. *J Chem Phys*. 2008;*129*:204501.
321. Hünenberger P, Reif M. *Single-ion solvation: experimental and theoretical approaches to elusive thermodynamic quantities*. Cambridge: Royal Society of Chemistry; 2011.
322. Vlcek L, Chialvo AA. Single-ion hydration thermodynamics from clusters to bulk solutions: recent insights from molecular modeling. *Fluid Phase Equilib*. 2016;*407*:58–75.
323. Hofer TS, Hünenberger PH. Absolute proton hydration free energy, surface potential of water, and redox potential of the hydrogen electrode from first principles: QM/MM MD free-energy simulations of sodium and potassium hydration. *J Chem Phys*. 2018;*148*:222814.
324. Zhan C-G, Dixon DA. Absolute hydration free energy of the proton from first-principles electronic structure calculations. *J Phys Chem A*. 2001;*105*:11534–40.
325. Grabowski P, Riccardi D, Gomez MA, Asthagiri D, Pratt LR. Quasi-chemical theory and the standard free energy of H^+(aq). *J Phys Chem A*. 2002;*106*:9145–8.
326. Kelly CP, Cramer CJ, Truhlar DG. Aqueous solvation free energies of ions and ion–water clusters based on an accurate value for the absolute aqueous solvation free energy of the proton. *J Phys Chem B*. 2006;*110*:16066–81.
327. Kelly CP, Cramer CJ, Truhlar DG. Single-ion solvation free energies and the normal hydrogen electrode potential in methanol, acetonitrile, and dimethyl sulfoxide. *J Phys Chem B*. 2007;*111*:408–22.
328. Pollard TP, Beck TL. The thermodynamics of proton hydration and the electrochemical surface potential of water. *J Chem Phys*. 2014;*141*:18C512.
329. Palascak MW, Shields GC. Accurate experimental values for the free energies of hydration of H^+, OH^-, and H_3O^+. *J Phys Chem A*. 2004;*108*:3692–4.

330. Bazhin NM. Standard values of the thermodynamic functions of the formation of ions in an aqueous solution and their change during solvation. *J Phys Chem A*. 2020;*124*:11051–60.
331. Tomaník L, Muchová E, Slavíček P. Solvation energies of ions with ensemble cluster-continuum approach. *Phys Chem Chem Phys*. 2020;*22*:22357–68.
332. Fawcett WR. The ionic work function and its role in estimating absolute electrode potentials. *Langmuir*. 2008;*24*:9868–75.
333. Carvalho NF, Pliego JR Jr. Cluster-continuum quasichemical theory calculation of the lithium ion solvation in water, acetonitrile and dimethyl sulfoxide: an absolute single-ion free energy scale. *Phys Chem Chem Phys*. 2015;*17*:26745–54.
334. Rossini E, Knapp E-W. Proton solvation in protic and aprotic solvents. *J Comput Chem*. 2016;*37*:1082–91. Erratum: *J. Comput. Chem.*, **37**, 2163–2164 (2016).
335. Pliego JR Jr, Miguel ELM. Absolute single-ion solvation free energy scale in methanol determined by the lithium cluster-continuum approach. *J Phys Chem B*. 2013;*117*:5129–35.
336. Lin Y-L, Aleksandrov A, Simonson T, Roux B. An overview of electrostatic free energy computations for solutions and proteins. *J Chem Theory Comput*. 2014;*10*:2690–709.
337. Pollard T, Beck TL. Quasichemical analysis of the cluster-pair approximation for the thermodynamics of proton hydration. *J Chem Phys*. 2014;*140*:224507.
338. Duignan TT, Baer MD, Schenter GK, Mundy CJ. Real single ion solvation free energies with quantum mechanical simulation. *Chem Sci*. 2017;*8*:6131–40.
339. Zhang H, Jiang Y, Yan H, Yin C, Tan T, van der Spoel D. Free-energy calculations of ionic hydration consistent with the experimental hydration free energy of the proton. *J Phys Chem Lett*. 2017;*8*:2705–12.
340. Shi Y, Beck TL. Absolute ion hydration free energy scale and the surface potential of water via quantum simulation. *Proc Natl Acad Sci U S A*. 2020;*117*:30151–8.
341. Pliego JR, Riveros JM. The cluster-continuum model for the calculation of the solvation free energy of ionic species. *J Phys Chem A*. 2001;*105*:7241–7.
342. Bryantsev VS, Diallo MS, Goddard WA III. Calculation of solvation free energies of charged solutes using mixed cluster/continuum models. *J Phys Chem B*. 2008;*112*:9709–19.
343. Pliego JR Jr, Riveros JM. Theoretical calculation of pK_a using the cluster-continuum model. *J Phys Chem A*. 2002;*106*:7434–9.
344. Eckert F, Diedenhofen M, Klamt A. Towards a first principles prediction of pK_a: COSMO-RS and the cluster-continuum approach. *Mol Phys*. 2010;*108*:229–41.
345. Marenich AV, Ding W, Cramer CJ, Truhlar DG. Resolution of a challenge for solvation modeling: calculation of dicarboxylic acid dissociation constants using mixed discrete-continuum solvation models. *J Phys Chem Lett*. 2012;*3*:1437–42.
346. Abramson R, Baldridge KK. Defined-sector explicit solvent in the continuum model approach for computational prediction of pK_a. *Mol Phys*. 2012;*110*:2401–12.
347. Abramson R, Baldridge KK. Defined-sector explicit solvent in continuum cluster model for computational prediction of pK_a: consideration of secondary functionality and higher degree of solvation. *J Chem Theory Comput*. 2013;*9*:1027–35.
348. Ho J. Predicting pK_a in implicit solvents: current status and future directions. *Aust J Chem*. 2014;*67*:1441–60.
349. Thapa B, Schlegel HB. Calculations of pK_a's and redox potentials of nucleobases with explicit waters and polarizable continuum solvation. *J Phys Chem A*. 2015;*119*:5134–44.
350. Thapa B, Schlegel HB. Density functional theory calculation of pK_a's of thiols in aqueous solution using explicit water molecules and the polarizable continuum model. *J Phys Chem A*. 2016;*120*:5726–35.
351. Alongi KS, Shields GC. Theoretical calculations of acid dissociation constants: a review article. *Annu Rep Comput Chem*. 2010;*6*: 113–38.
352. Riccardi D, Guo H-B, Parks JM, Gu B, Liang L, Smith JC. Cluster-continuum calculations of hydration free energies of anions and group 12 divalent cations. *J Chem Theory Comput*. 2013;*9*:555–69.
353. Dhillon S, East AL. Challenges in predicting $\Delta_{rxn}G$ in solution: hydronium, hydroxide, and water autoionization. *Int J Quantum Chem*. 2018;*118*:e25703.
354. Patel DH, East ALL. Semicontinuum (cluster-continuum) modeling of acid-catalyzed aqueous reactions: alkene hydration. *J Phys Chem A*. 2020;*124*:9088–104.
355. Pratt LR, LaViolette RA. Quasi-chemical theories of associated liquids. *Mol Phys*. 1998;*94*:909–15.
356. Pratt LR, Rempe SD. Quasi-chemical theory and implicit solvent models for simulations. In: Pratt LR, Hummer G, editors. *Simulation and theory of electostatic interactions in solution*. AIP conference proceedings. Volume 492. American Institute of Physics, Woodbury, NY: American Institute of Physics; 1999. p. 172–201.
357. Asthagiri D, Pratt LR, Ashbaugh HS. Absolute hydration free energies of ions, ion–water clusters, and quasichemical theory. *J Chem Phys*. 2003;*119*:2702–8.
358. Asthagiri D, Pratt LR, Paulaitis ME, Rempe SB. Hydration structure and free energy of biomolecularly specific aqueous dications, including Zn^{2+} and first transition row metals. *J Am Chem Soc*. 2004;*126*:1285–9.
359. Rempe SB, Asthagiri D, Pratt LR. Inner-shell definition and absolute hydration free energy of K^+(aq) on the basis of quasi-chemical theory and *ab initio* molecular dynamics. *Phys Chem Chem Phys*. 2004;*6*:1966–9.
360. Beck TL, Paulaitis ME, Pratt LR. Quasi-chemical theory. *The potential distribution theorem and models of molecular solutions*. Cambridge: Cambridge University Press; 2006; (chapter 7). p. 142–71.

361. Rogers DM, Jiao D, Pratt LR, Rempe SB. Structural models and molecular thermodynamics of hydration of ions and small molecules. *Annu Rep Comput Chem*. 2012;*8*:71–127.
362. Muralidharan A, Pratt LR, Chaudhari MI, Rempe SB. Quasi-chemical theory with cluster sampling from ab initio molecular dynamics: fluoride (F^-) anion hydration. *J Phys Chem A*. 2018;*122*:9806–12.
363. Maldonado AM, Basdogan Y, Berryman JT, Rempe SB, Keith JA. First-principles modeling of chemistry in mixed solvents: where to go from here? *J Chem Phys*. 2020;*152*:130902.
364. Bachs M, Luque FJ, Orozco M. Optimization of solute cavities and van der Waals parameters in *ab initio* MST-SCRF calculations of neutral molecules. *J Comput Chem*. 1994;*15*:446–54.
365. Luque FJ, Bachs M, Alemán C. Extension of MST/SCRF method to organic solvents: *ab initio* and semiempirical parametrization for neutral solutes in CCl_4. *J Comput Chem*. 1996;*17*:806–20.
366. Luque FJ, Bidon-Chanall A, Muñoz-Muriedas J, Soteras I, Curutchet C, Morreale A, et al. Solute–solvent interactions from QM SCRF methods: analysis of group contributions to solvation. In: Brändas EJ, Kryachko ES, editors. *Fundamental world of quantum chemistry*. Volume III. Kluwer, Dordrecht: Kluwer Academic Publishers; 2004. p. 475–95.
367. Soteras I, Morreale A, López JM, Orozco M, Luque FJ. Group contributions to the solvation free energy from MST continuum calculations. *Braz J Phys*. 2004;*34*:48–57.
368. Soteras I, Curutchet C, Bidon-Chanal A, Orozco M, Luque FJ. Extension of the MST model to the IEF formalism: HF and B3LYP parameterizations. *J Mol Struct (THEOCHEM)*. 2005;*727*:29–40.
369. Curutchet C, Orozco M, Luque FJ, Mennucci B, Tomasi J. Dispersion and repulsion contributions to the solvation free energy: comparison of quantum mechanical and classical approaches in the polarizable continuum model. *J Comput Chem*. 2006;*27*:1769–80.
370. Klamt A, Mennucci B, Tomasi J, Barone V, Curutchet C, Orozco M, et al. On the performance of continuum solvation methods. A comment on 'universal approaches to solvation modeling'. *Acc Chem Res*. 2009;*42*:489–92.
371. Pomogaeva A, Thompson DW, Chipman DM. Modeling short-range contributions to hydration energies with minimal parameterization. *Chem Phys Lett*. 2011;*511*:161–5.
372. Pomogaeva A, Chipman DM. Field-extremum model for short-range contributions to hydration free energy. *J Chem Theory Comput*. 2011;*7*:3952–60.
373. Pomogaeva A, Chipman DM. New implicit solvation models for dispersion and exchange energies. *J Phys Chem A*. 2013;*117*:5812–20.
374. Pomogaeva A, Chipman DM. Hydration energy from a composite method for implicit representation of the solvent. *J Chem Theory Comput*. 2014;*10*:211–9.
375. Pomogaeva A, Chipman DM. Composite method for implicit representation of solvent in dimethyl sulfoxide and acetonitrile. *J Phys Chem A*. 2015;*119*:5173–80.
376. Klamt A. Conductor-like screening model for real solvents: a new approach to the quantitative calculation of solvation phenomena. *J Phys Chem*. 1995;*99*:2224–35.
377. Klamt A, Jonas V, Bürger T, Lohrenz JCW. Refinement and parameterization of COSMO-RS. *J Phys Chem A*. 1998;*102*:5074–85.
378. Eckert F, Klamt A. Fast solvent screening via quantum chemistry: COSMO-RS approach. *AIChE J*. 2002;*48*:369–85.
379. Klamt A. *COSMO-RS: from quantum chemistry to fluid phase thermodynamics and drug design*. Elsevier, Amsterdam: Elsevier; 2005.
380. Klamt A, Eckert F, Arlt W. COSMO-RS: an alternative to simulation for calculating thermodynamic properties of mixtures. *Annu Rev Chem Biomol Eng*. 2010;*1*:101–22.
381. Sandler SI, Sum AK, Lin S-T. Some chemical engineering applications of quantum chemical calculations. *Adv Chem Eng*. 2001;*28*:315–51.
382. Lei Z, Chen B, Li C, Liu H. Predictive molecular thermodynamic models for liquid solvents, solid salts, polymers, and ionic liquids. *Chem Rev*. 2008;*108*:1419–55.
383. Gmehling J. Present status and potential of group contribution methods for process development. *J Chem Thermodyn*. 2009;*41*:731–47.
384. Gmehling J, Constantinescu D, Schmid B. Group contribution methods for phase equilibrium calculations. *Annu Rev Chem Biomol Eng*. 2015;*6*:267–92.
385. Lin S-T, Sandler SI. A priori phase equilibrium predictions from a segment contribution solvation model. *Ind Eng Chem Res*. 2002;*41*:899–913. Erratum: *Ind. Eng. Chem. Res*., **43**, 1322 (2004).
386. Klamt A. Comments on 'a priori phase equilibrium prediction from a segment contribution solvation model'. *Ind Eng Chem Res*. 2002;*41*:2330–1.
387. Lin S-T, Sandler SI. Reply to comments on 'a priori phase equilibrium prediction from a segment contribution solvation model'. *Ind Eng Chem Res*. 2002;*41*:2332–4.
388. Neiman M, Cheng H, Parekh V, Peterson B, Klier K. A critical assessment on two predictive models of binary vapor–liquid equilibrium. *Phys Chem Chem Phys*. 2004;*6*:3474–83.
389. Klamt A. Comment on 'a critical assessment on two predictive models of binary vapor–liquid equilibrium'. *Phys Chem Chem Phys*. 2004;*6*:5081.
390. Cheng H, Parekh V, Peterson BK. Response to 'comment on 'a critical assessment on two predictive models of binary vapor–liquid equilibrium'. *Phys Chem Chem Phys*. 2004;*6*:5082.
391. Grensemann H, Gmehling J. Performance of a conductor-like screening model for real solvents model in comparison to classical group contribution methods. *Ind Eng Chem Res*. 2005;*44*:1610–24.

392. Klamt A. Comments on 'performance of a conductor-like screening model for real solvents model in comparison to classical group contribution methods'. *Ind Eng Chem Res*. 2005;*44*:7042.
393. Grensemann H, Gmehling J. Rebuttal to the comments of Andreas Klamt on 'performance of a COSMO-RS model in comparison to classical group contribution methods'. *Ind Eng Chem Res*. 2005;*44*:7043–4.
394. Wang S, Lin S-T, Chang J, Goddard WA, Sandler SI. Application of the COSMO-SAC-BP solvation model to predictions of normal boiling temperatures for environmentally significant substances. *Ind Eng Chem Res*. 2006;*45*:5426–34.
395. Klamt A, Eckert F. Comment on 'application of the COSMO-SAC-BP solvation model to predictions of normal boiling temperatures for environmentally significant substances'. *Ind Eng Chem Res*. 2006;*45*:3766.
396. Wang S, Lin S-T, Chang J, Goddard WA, Sandler SI. Reply to the comment on 'application of the COSMO-SAC-BP solvation model to predictions of normal boiling temperatures for environmentally significant substances'. *Ind Eng Chem Res*. 2006;*45*:3767.
397. Mu T, Rarey J, Gmehling J. Performance of COSMO-RS with sigma profiles from different model chemistries. *Ind Eng Chem Res*. 2007;*46*:6612–29.
398. Klamt A. Comments on 'performance of COSMO-RS with sigma profiles from different model chemistries'. *Ind Eng Chem Res*. 2008;*47*:987–8.
399. Mu T, Rarey J, Gmehling J. Reply to "comments on 'performance of COSMO-RS with sigma profiles from different model chemistries'". *Ind Eng Chem Res*. 2008;*47*:989.
400. Sakuratani Y, Kasai K, Noguchi Y, Yamada J. Comparison of predictivities of log *P* calculation models based on experimental data for 134 simple organic compounds. *QSAR Comb Sci*. 2007;*26*:109–16.
401. Wittekindt C, Klamt A. Comment on 'comparison of predictivities of log *P* calculation models based on experimental data for 134 simple organic compounds'. *QSAR Comb Sci*. 2008;*27*:232–3.
402. Sakuratani Y. Reply to the 'comment on comparison of predictivities of log *P* calculation models based on experimental data for 134 simple organic compounds'. *QSAR Comb Sci*. 2008;*27*:231.
403. Wang S, Sandler SI, Chen C-C. Refinement of COSMO-SAC and the applications. *Ind Eng Chem Res*. 2007;*46*:7275–88.
404. Klamt A, Eckert F. Comment on 'refinement of COSMO-SAC and the applications'. *Ind Eng Chem Res*. 2008;*47*:1351–2.
405. Sandler SI, Wang S, Lin ST, Goddard WA. Reply to "comments on 'refinement of COSMO-SAC and the applications'". *Ind Eng Chem Res*. 2008;*47*:1353–4.
406. Lin S-T, Hsieh M-K, Hsieh C-M, Hsu C-C. Towards the development of theoretically correct liquid activity coefficient models. *J Chem Thermodyn*. 2009;*41*:1145–53.
407. Klamt A, Krooshof GJP, Taylor R. Comment on 'towards the development of theoretically correct liquid activity coefficients models'. *J Chem Thermodyn*. 2009;*41*:1312–3.
408. Lin S-T, Hsieh M-K, Hsieh C-M, Hsu C-C. Reply to "comment on 'towards the development of theoretically correct liquid activity coefficient models'". *J Chem Thermodyn*. 2009;*41*:1314–6.
409. Xue Z, Mu T, Gmehling J. Comparison of the a priori COSMO-RS models and group contribution methods: original UNIFAC, modified UNIFAC(Do), and modified UNIFAC(Do) consortium. *Ind Eng Chem Res*. 2012;*51*:11809–17. Erratum: *Ind. Eng. Chem. Res.*, **51**, 16163 (2012).
410. Klamt A. Comment on 'comparison of the a priori COSMO-RS models and group contribution methods: original UNIFAC, modified UNIFAC(Do), and modified UNIFAC(Do) consortium'. *Ind Eng Chem Res*. 2012;*51*:13538–40.
411. Gmehling J, Xue Z, Mu T. Reply to "comments on 'comparison of the a priori COSMO-RS models and group contribution methods: original UNIFAC, modified UNIFAC(Do), and modified UNIFAC(Do) consortium'". *Ind Eng Chem Res*. 2012;*51*:13541–3.
412. Xiong R, Sandler SI, Burnett RI. An improvement to COSMO-SAC for predicting thermodynamic properties. *Ind Eng Chem Res*. 2014;*53*:8265–78.
413. Klamt A. Comment on 'an improvement to COSMO-SAC for predicting thermodynamic properties'. *Ind Eng Chem Res*. 2014;*53*:8935.
414. Xiong R, Sandler SI, Burnett RI. Reply to "comment on 'an improvement to COSMO-SAC for predicting thermodynamic properties'". *Ind Eng Chem Res*. 2014;*53*:8936.
415. Pye CC, Ziegler T, van Lenthe E, Louwen JN. An implementation of the conductor-like screening model of solvation within Amsterdam density functional package—part II. COSMO for real solvents. *Can J Chem*. 2009;*87*:790–7.
416. Chamberlin AC, Cramer CJ, Truhlar DG. Performance of SM8 on a test to predict small-molecule solvation free energies. *J Phys Chem B*. 2008;*112*:8651–5.
417. Marenich AV, Cramer CJ, Truhlar DG. Performance of SM6, SM8, and SMD on the SAMPL1 test set for the prediction of small-molecule solvation free energies. *J Phys Chem B*. 2009;*113*:4538–43.
418. Bashford D, Case DA. Generalized Born models of macromolecular solvation effects. *Annu Rev Phys Chem*. 2000;*51*:129–52.
419. Onufriev AV, Case DA. Generalized Born implicit solvent models for biomolecules. *Annu Rev Biophys*. 2019;*48*:275–96.
420. Cramer CJ, Truhlar DG. Generalized parameterized SCF model for free energies of solvation in aqueous solution. *J Am Chem Soc*. 1991;*113*:8305–11.
421. Still WC, Tempczyk A, Hawley RC, Hendrickson T. Semianalytical treatment of solvation for molecular mechanics and dynamics. *J Am Chem Soc*. 1990;*112*:6127–9.
422. Onufriev A, Bashford D, Case DA. Modification of the generalized Born models suitable for macromolecules. *J Phys Chem B*. 2000;*104*:3712–20.

423. Onufriev A, Case DA, Bashford D. Effective Born radii in the generalized Born model approximation: the importance of being perfect. *J Comput Chem*. 2002;*23*:1297–304.
424. Mongan J, Svrcek-Seiler WA, Onufriev A. Analysis of integral expressions for effective Born radii. *J Chem Phys*. 2007;*127*:185101.
425. Lee MS, Salsbury FR Jr, Brooks CL III. Novel generalized Born methods. *J Chem Phys*. 2002;*116*:10606–14.
426. Salsbury FR Jr. Analysis of errors in Still's equation for macromolecular electrostatic solvation energies. *Mol Phys*. 2006;*104*:1299–309.
427. Scarsi M, Apostolakis J, Caflisch A. Continuum electrostatics energies of macromolecules in aqueous solutions. *J Phys Chem A*. 1997;*101*:8098–106.
428. Pierotti RA. A scaled particle theory of aqueous and nonaqueous solutions. *Chem Rev*. 1976;*76*:717–26.
429. Floris FM, Selmi M, Tani A, Tomasi J. Free energy and entropy for inserting cavities in water: comparison of Monte Carlo simulation and scaled particle theory results. *J Chem Phys*. 1997;*107*:6353–65.
430. Cossi M, Rega N. First and second derivatives of the free energy in solution. In: Mennucci B, Cammi R, editors. *Continuum solvation models in chemical physics*. Chichester, UK: Wiley; 2007. p. 313–22.
431. Floris FM, Tomasi J, Ahuir JLP. Dispersion and repulsion contributions to the solvation energy: refinements to a simple computational model in the continuum approximation. *J Comput Chem*. 1991;*12*:784–91.
432. Gallicchio E, Levy RM. AGBNP: an analytic implicit solvent model suitable for molecular dynamics simulations and high-resolution modeling. *J Comput Chem*. 2004;*25*:479–99.
433. Hou T, Wang J, Li Y, Wang W. Assessing the performance of the MM/PBSA and MM/GBSA methods. 1. The accuracy of binding free energy calculations based on molecular dynamics simulations. *J Chem Inf Model*. 2011;*51*:69–82.
434. Hou T, Wang J, Li Y, Wang W. Assessing the performance of the molecular mechanics/Poisson Boltzmann surface area and molecular mechanics generalized/Born surface area methods. II. The accuracy of ranking poses generated from docking. *J Comput Chem*. 2011;*32*:866–77.
435. Xu L, Sun H, Li Y, Wang J, Hou T. Assessing the performance of MM/PBSA and MM/GBSA methods. 3. The impact of force fields and ligand charge models. *J Phys Chem B*. 2013;*117*:8408–21.
436. Sun H, Li Y, Shen M, Tian S, Xu L, Pan P, et al. Assessing the performance of MM/PBSA and MM/GBSA methods. 5. Improved docking performance using high solute dielectric constant MM/GBSA and MM/PBSA rescoring. *Phys Chem Chem Phys*. 2014;*16*:22035–45.
437. Sun H, Li Y, Tian S, Xu L, Hou T. Assessing the performance of MM/PBSA and MM/GBSA methods. 4. Accuracies of MM/PBSA and MM/GBSA methodologies evaluated by various simulation protocols using PDBbind data set. *Phys Chem Chem Phys*. 2014;*16*:15719–6729.
438. Chen F, Liu H, Sun H, Pan P, Li Y, Li D, et al. Assessing the performance of the MM/PBSA and MM/GBSA methods. 6. Capability to predict protein–protein binding free energies and re-rank binding poses generated by protein–protein docking. *Phys Chem Chem Phys*. 2016;*18*:22129–39.
439. Sun H, Duan L, Chen F, Liu H, Wang Z, Pan P, et al. Assessing the performance of MM/PBSA and MM/GBSA methods. 7. Entropy effects on the performance of end-point binding free energy calculation approaches. *Phys Chem Chem Phys*. 2018;*20*:14450–60.
440. Weng G, Wang E, Chen F, Sun H, Wang Z, Hou T. Assessing the performance of MM/PBSA and MM/GBSA methods. 9. Prediction of reliability of binding affinities and binding poses for protein–peptide complexes. *Phys Chem Chem Phys*. 2019;*21*:10135–45.
441. Wang E, Weng G, Sun H, Du H, Zhu F, Chen F, et al. Assessing the performance of the MM/PBSA and MM/GBSA methods. 10. Impacts of enhanced sampling and variable dielectric model on protein–protein interactions. *Phys Chem Chem Phys*. 2019;*21*:18958–69.
442. Wang C, Greene D, Xiao L, Qi R, Luo R. Recent developments and applications of the MMPBSA method. *Front Mol Biosci*. 2018;*4*:87.
443. Genheden S, Ryde U. The MM/PBSA and MM/GBSA methods to estimate ligand-binding affinities. *Expert Opin Drug Discovery*. 2015;*10*:449–61.
444. Wang E, Sun H, Wang J, Wang Z, Liu H, Zhang JZH, et al. End-point binding free energy calculation with MM/PBSA and MM/GBSA: strategies and applications in drug design. *Chem Rev*. 2019;*119*:9478–508.
445. Poli G, Granchi C, Rizzolio F, Tuccinardi T. Applications of MM-PBSA methods in virtual screening. *Molecules*. 2020;*25*:1971.
446. Li J, Zhu T, Cramer CJ, Truhlar DG. New class IV charge model for extracting accurate partial charges from wave functions. *J Phys Chem A*. 1998;*102*:1820–31.
447. Winget P, Thompson JD, Xidos JD, Cramer CJ, Truhlar DG. Charge model 3: a class IV charge model based on hybrid density functional theory with variable exchange. *J Phys Chem A*. 2002;*106*:10707–17.
448. Olson RM, Marenich AV, Cramer CJ, Truhlar DG. Charge model 4 and intramolecular charge polarization. *J Chem Theory Comput*. 2007;*3*:2046–54.
449. Marenich AV, Jerome SV, Cramer CJ, Truhlar DG. Charge model 5: an extension of Hirshfeld population analysis for the accurate description of molecular interactions in gaseous and condensed phases. *J Chem Theory Comput*. 2012;*8*:527–41.
450. Davidson ER, Chakravorty S. A test of the Hirshfeld definition of atomic charges and moments. *Theor Chem Accounts*. 1992;*83*:319–30.
451. Chamberlin AC, Cramer CJ, Truhlar DG. Predicting aqueous free energies of solvation as functions of temperature. *J Phys Chem B*. 2006;*110*:5665–75.
452. Chamberlin AC, Cramer CJ, Truhlar DG. Extension of a temperature-dependent aqueous solvation model to compounds containing nitrogen, fluorine, chlorine, bromine, and sulfur. *J Phys Chem B*. 2008;*112*:3024–39.
453. Abraham MH. Scales of solute hydrogen-bonding: their construction and application to physicochemical and biochemical processes. *Chem Soc Rev*. 1993;*22*:73–83.

454. Vassetti D, Labat F. Evaluation of the performances of different atomic charge and nonelectrostatic models in the finite-difference Poisson–Boltzmann approach. *Int J Quantum Chem*. 2020;*121*:e26560.
455. Zhang H, Jiang Y, Yan H, Cui Z, Yin C. Comparative assessment of computational methods for free energy calculations of ionic hydration. *J Chem Inf Model*. 2017;*57*:2763–75.
456. Dearden JC. Partitioning and lipophilicity in quantitative structure–activity relationships. *Environ Health Perspect*. 1985;*61*:203–28.
457. Amézqueta S, Subirats X, Fuguet E, Rosés M, Ràfols C. Octanol–water partition constant. In: Poole CF, editor. *Liquid-phase extraction*. Amsterdam: Elsevier; 2020; (chapter 6). p. 183–208.
458. Ginex T, Vazquez J, Gilbert E, Herrero E, Luque FJ. Lipophilicity in drug design: an overview of lipophilicity descriptors in 3D-QSAR studies. *Future Med Chem*. 2019;*11*:1177–93.
459. Sahoo S, Adhikari C, Kuanar M, Mishra BK. A short review of the generation of molecular descriptors and their applications in quantitative structure property/activity relationships. *Curr Comput Aided Drug Des*. 2016;*12*:181–205.
460. Tsopelas F, Giaginis C, Tsantili-Kakoulidou A. Lipophilicity and biomimetic properties to support drug discovery. *Expert Opin Drug Discovery*. 2017;*12*:885–96.
461. Hermens JLM, de Bruijn JHM, Brooke DN. The octanol–water partition coefficient: strengths and limitations. *Environ Toxicol Chem*. 2013;*32*:732–3.
462. Işik M, Bergazin TD, Fox T, Rizzi A, Chodera JD, Mobley DL. Assessing the accuracy of octanol–water partition coefficient predictions in the SAMPL6 part II log *P* challenge. *J Comput Aided Mol Des*. 2020;*34*:335–70.
463. Ouimet JA, Paluch AS. Predicting octanol/water partition coefficients for the SAMPL6 challenge using the SM12, SM8, and SMD solvation models. *J Comput Aided Mol Des*. 2020;*34*:575–88.
464. Chipman DM. Anion electric field is related to hydration energy. *J Chem Phys*. 2003;*118*:9937–42.
465. Chipman DM, Chen F. Cation electric field is related to hydration energy. *J Chem Phys*. 2006;*124*:144507.
466. Voityuk AA, Vyboishchikov SF. A simple COSMO-based method for calculation of hydration energies of neutral molecules. *Phys Chem Chem Phys*. 2019;*21*:18706–13.
467. Voityuk AA, Vyboishchikov SF. Fast and accurate calculation of hydration energies of molecules and ions. *Phys Chem Chem Phys*. 2020;*22*:14591–8.
468. Hille C, Ringe S, Deimel M, Kunkel C, Acree WE, Reuter K, et al. Generalized molecular solvation in non-aqueous solutions by a single parameter implicit solvation scheme. *J Chem Phys*. 2019;*150*:041710.
469. Amovilli C. Calculation of the dispersion energy contribution to the solvation free energy. *Chem Phys Lett*. 1994;*229*:244–9.
470. Amovilli C, Mennucci B. Self-consistent-field calculation of Pauli repulsion and dispersion contributions to the solvation free energy in the polarizable continuum model. *J Phys Chem B*. 1997;*101*:1051–7.
471. Weijo V, Mennucci B, Frediani L. Toward a general formulation of dispersion effects for solvation continuum models. *J Chem Theory Comput*. 2010;*6*:3358–64.
472. Cupellini L, Amovilli C, Mennucci B. Electronic excitations in nonpolar solvents: can the polarizable continuum model accurately reproduce solvent effects? *J Phys Chem B*. 2015;*119*:8984–91.
473. Duignan TT, Parsons DF, Ninham BW. A continuum solvent model of the multipolar dispersion solvation energy. *J Phys Chem B*. 2013;*117*:9412–20.
474. Duignan TT, Parsons DF, Ninham BW. A continuum model of solvation energies including electrostatic, dispersion, and cavity contributions. *J Phys Chem B*. 2013;*117*:9421–9.
475. Huron M-J, Claverie P. Calculation of the interaction energy of one molecule with its whole surrounding. I. Method and application to pure nonpolar compounds. *J Phys Chem*. 1972;*76*:2123–33.
476. Floris F, Tomasi J. Evaluation of the dispersion contribution to the solvation energy. A simple computational model in the continuum approximation. *J Comput Chem*. 1989;*10*:616–27.
477. Floris FM, Tani A, Tomasi J. Evaluation of dispersion–repulsion contributions to the solvation energy. Calibration of the uniform approximation with the aid of RISM calculations. *Chem Phys*. 1993;*169*:11–20.
478. Truong TN. Quantum modelling of reactions in solution: an overview of the dielectric continuum methodology. *Int Rev Phys Chem*. 1998;*17*:525–46.
479. McLachlan AD. Retarded dispersion forces between molecules. *Proc R Soc Lond A*. 1963;*271*:387–401.
480. McWeeny R. Weak interactions between molecules. *Croat Chem Acta*. 1984;*57*:865–78.
481. Jaszunski M, McWeeny R. Time-dependent Hartree–Fock calculations of dispersion energy. *Mol Phys*. 1985;*55*:1275–86.
482. McWeeny R. Electron density and response theory. *J Mol Struct (THEOCHEM)*. 1985;*123*:231–42.
483. Amovilli C, McWeeny M. A matrix partitioning approach to the calculation of intermolecular potentials. General theory and some examples. *Chem Phys*. 1990;*140*:343–61.
484. McWeeny R. *Methods of molecular quantum mechanics*. 2nd ed. New York: Academic Press; 1992.
485. Tang KT. Dynamic polarizabilities and van der Waals coefficients. *Phys Rev*. 1969;*177*:108–14.
486. Langhoff PW, Karplus M. Application of Padé approximants to dispersion force and optical polarizability computations. In: Baker GA Jr, Gammel JL, editors. *The Padé approximant in theoretical physics*. Mathematics in science and engineering. Volume 71. New York: Academic Press; 1970; (chapter 2). p. 41–97.
487. Szabo A, Ostlund NS. The correlation energy in the random phase approximation: intermolecular forces between closed-shell systems. *J Chem Phys*. 1977;*67*:4351–60.

488. Kaplan IG, Rodimova OB. Intermolecular interactions. *Sov Phys Usp*. 1978;*21*:918–43.
489. Buhmann SY, Welsch D-G. Dispersion forces in macroscopic quantum electrodynamics. *Prog Quantum Electron*. 2007;*31*:51–130.
490. London F. Zur Theorie und Systematik der Molekularkräfte. *Z Phys*. 1930;*63*:245–79.
491. Longuet-Higgins HC. Intermolecular forces. *Discuss Faraday Soc*. 1965;*40*:7–18.
492. Norman P, Ruud K. Microscopic theory of nonlinear optics. In: Papadopoulos MG, Sadlej AJ, Leszczynski J, editors. *Non-linear optical properties of matter*. Challenges and advances in computational chemistry and physics. Volume 1 of. Dordrecht: Springer; 2006; (chapter 1). p. 1–49.
493. Rösch N, Zerner MC. Calculation of dispersion energy shifts in molecular electronic spectra. *J Phys Chem*. 1994;*98*:5817–23.
494. Dyzaloshinskii IE, Lifshitz EM, Pitaevskii LP. The general theory of van der Waals forces. *Adv Phys*. 1961;*10*:165–209.
495. Zaremba E, Kohn W. Van der Waals interaction between an atom and a solid surface. *Phys Rev B*. 1976;*13*:2270–85.
496. Parsegian VA. *Van der Waals forces: a handbook for biologists, chemists, engineers, and physicists*. New York: Cambridge University Press; 2006.
497. Vydrov OA, Van Voorhis T. Improving the accuracy of the nonlocal van der Waals density functional with minimal empiricism. *J Chem Phys*. 2009;*130*:104105.
498. Vydrov OA, Van Voorhis T. Nonlocal van der Waals density functional theory made simple. *Phys Rev Lett*. 2009;*103*:063004.
499. Vydrov OA, Van Voorhis T. Nonlocal van der Waals density functional: the simpler the better. *J Chem Phys*. 2010;*133*:244103.
500. Vydrov OA, Van Voorhis T. Nonlocal van der Waals density functionals based on local response models. In: Marques MAL, Maitra NT, Nogueira FMS, Gross EKU, Rubio A, editors. *Fundamentals of time-dependent density functional theory*. Lecture notes in physics. Volume 837 of. Berlin: Springer-Verlag; 2012; (chapter 23). p. 443–56.
501. Calbo J, Ortí E, Sancho-García JC, Aragó J. The nonlocal correlation density function VV10: a successful attempt to accurately capture noncovalent interactions. *Annu Rep Comput Chem*. 2015;*11*:37–102.
502. Langreth DC, Dion M, Rydberg H, Schröder E, Hyldgaard P, Lundqvist BI. Van der Waals density functional theory with applications. *Int J Quantum Chem*. 2005;*101*:599–610.
503. Dion M, Rydberg H, Schröder E, Langreth DC, Lundqvist BI. Van der Waals density functional for general geometries. *Phys Rev Lett*. 2004;*92*:246401.
504. Langreth DC, Lundqvist BI, Chakarova-Käck SD, Cooper VR, Dion M, Hyldgaard P, et al. A density functional for sparse matter. *J Phys Condens Matter*. 2009;*21*:084203.
505. Lee K, Murray ÉD, Kong L, Lundqvist BI, Langreth DC. Higher-accuracy van der Waals density functional. *Phys Rev B*. 2010;*82*:081101.
506. Herring C, Flicker M. Asymptotic exchange coupling of two hydrogen atoms. *Phys Rev*. 1964;*134*:A362–6.
507. Cammi R, Verdolino V, Mennucci B, Tomasi J. Towards the elaboration of a QM method to describe molecular solutes under the effect of a very high pressure. *Chem Phys*. 2008;*344*:135–41.
508. Cammi R, Cappelli C, Mennucci B, Tomasi J. Calculation and analysis of the harmonic vibrational frequencies in molecules at extreme pressure: methodology and diborane as a test case. *J Chem Phys*. 2012;*137*:154112.
509. Chen B, Hoffmann R, Cammi R. The effect of pressure on organic reactions in fluids—a new theoretical perspective. *Angew Chem Int Ed Engl*. 2017;*56*:11126–42.
510. Cammi R. Quantum chemistry at the high pressures: the eXtreme pressure polarizable continuum model (XP-PCM). In: Wójcik MJ, Nakatsuji H, Kirtman B, Ozaki Y, editors. *Frontiers of quantum chemistry*. Singapore: Springer Nature; 2018; (chapter 12). p. 273–88.
511. Fecko CJ, Eaves JD, Loparo JJ, Tokmakoff A, Geissler PL. Ultrafast hydrogen-bond dynamics in the infrared spectroscopy of water. *Science*. 2003;*301*:1698–702.
512. Corcelli SA, Lawrence CP, Skinner JL. Combined electronic structure/molecular dynamics approach for ultrafast infrared spectroscopy of dilute HOD in liquid H_2O and D_2O. *J Chem Phys*. 2004;*120*:8107–17.
513. Smith JD, Cappa CD, Wilson KR, Cohen RC, Geissler PL, Saykally RJ. Unified description of temperature-dependent hydrogen-bond rearrangements in liquid water. *Proc Natl Acad Sci U S A*. 2005;*102*:14171–4.
514. Klamt A, Reinisch J, Eckert F, Hellweg A, Diedenhofen M. Polarization charge densities provide a predictive quantification of hydrogen bond energies. *Phys Chem Chem Phys*. 2012;*14*:955–63.
515. Klamt A, Reinisch J, Eckert F, Graton J, Le Questel J-Y. Interpretation of experimental hydrogen-bond enthalpies and entropies from COSMO polarisation charge densities. *Phys Chem Chem Phys*. 2013;*15*:7147–54.
516. Silva NM, Deglmann P, Pliego JR Jr. CMIRS solvation model for methanol: parameterization, testing, and comparison with SMD, SM8, and COSMO-RS. *J Phys Chem B*. 2016;*120*:12660–8.
517. Pratt LR, Chaudhari MI, Rempe SB. Statistical analyses of hydrophobic interactions: a mini-review. *J Phys Chem B*. 2016;*120*:6455–60.
518. He S, Biedermann F, Vankova N, Zhechkov L, Heine T, Hoffman RE, et al. Cavitation energies can outperform dispersion interactions. *Nat Chem*. 2018;*10*:1252–7.
519. Ansari N, Laio A, Hassanali A. Spontaneously forming dendritic voids in liquid water can host small polymers. *J Phys Chem Lett*. 2019;*10*:5585–91.
520. Böttcher CJF, Bordewijk P. *Theory of electric polarization*. Vol 2. Amsterdam: Elsevier; 1978.
521. Vaughan WE. Dielectric relaxation. *Annu Rev Phys Chem*. 1979;*30*:103–24.
522. Feldman Y, Puzenko A, Ryabov Y. Dielectric relaxation phenomena in complex materials. *Adv Chem Phys*. 2006;*133*:1–125.
523. Feldman Y, Ishai PB, Puzenko A, Raicu V. Elementary theory of the interaction of electromagnetic fields with dielectric materials. In: Raicu V, Feldman Y, editors. *Dielectric relaxation in biological systems*. 1st ed. Oxford: Oxford University Press; 2015. p. 33–59.

524. Kaatze U. Complex permittivity of water as a function of frequency and temperature. *J Chem Eng Data*. 1989;*34*:371–4.
525. Kaatze U. Dielectric spectroscopy of aqueous solutions. Hydration phenomena and hydrogen-bonded networks. *J Mol Liq*. 1993;*56*: 95–115.
526. Kaatze U. Dielectric relaxation of water. In: Raicu V, Feldman Y, editors. *Dielectric relaxation in biological systems*. 1st ed. Oxford: Oxford University Press; 2015. p. 189–227.
527. Hsu C-P, Song X, Marcus RA. Time-dependent Stokes shift and its calculation from solvent dielectric dispersion data. *J Phys Chem B*. 1997;*101*:2546–51.
528. Ingrosso F, Mennucci B, Tomasi J. Quantum mechanical calculations coupled with a dynamical continuum model for the description of dielectric relaxation: time dependent Stokes shift of coumarin C153 in polar solvents. *J Mol Liq*. 2003;*108*:21–46.
529. Caricato M, Mennucci B, Tomasi J, Ingrosso F, Cammi R, Corni S, et al. Formation and relaxation of excited states in solution: a new time dependent polarizable continuum model based on time dependent density functional theory. *J Chem Phys*. 2006;*124*:124520.
530. Ding F, Lingerfelt DB, Mennucci B, Li X. Time-dependent non-equilibrium dielectric response in QM/continuum approaches. *J Chem Phys*. 2015;*142*:034120.
531. Wildman A, Donati G, Lipparini F, Mennucci B, Li X. Nonequilibrium environment dynamics in a frequency-dependent polarizable embedding model. *J Chem Theory Comput*. 2019;*15*:43–51.
532. Debye PJW. *Polar molecules*. New York: The Chemical Catalog Company; 1929.
533. Gil G, Pipolo S, Delgado A, Rozzi CA, Corni S. Nonequilibrium solvent polarization effects in real-time electronic dynamics of solute molecules subject to time-dependent electric fields: a new feature of the polarizable continuum model. *J Chem Theory Comput*. 2019; *15*:2306–19.
534. Goings JJ, Lestrange PJ, Li X. Real-time time-dependent electronic structure theory. *WIREs Comput Mol Sci*. 2018;*8*:e1341.
535. Li X, Govind N, Isborn C, DePrince AE III, Lopata K. Real-time time-dependent electronic structure theory. *Chem Rev*. 2020;*120*: 9951–93.
536. Mistrik J, Kasap S, Ruda HE, Koughia C, Singh J. Optical properties of electronic materials: fundamentals and characterization. In: Kasap S, Capper P, editors. *Springer handbook of electronic and photonic materials*. Springer International, Cham, Switzerland: Springer International Publishing; 2017; (chapter 3). p. 47–83.
537. Wohlfarth C, Wohlfarth B. *Refractive indices of organic liquids*. Landolt-Börnstein, Group III Condensed Matter. Vol 38B. Springer-Verlag, Berlin: Springer; 1996.
538. Hale GM, Querry MR. Optical constants of water in the 200-nm to 200-μm wavelength region. *Appl Opt*. 1973;*12*:555–63.
539. Cossi M, Barone V. Separation between fast and slow polarizations in continuum solvation models. *J Phys Chem A*. 2000;*104*:10614–22.
540. Dinpajooh M, Newton MD, Matyushov DV. Free energy functionals for polarization fluctuations: Pekar factor revisited. *J Chem Phys*. 2017;*146*:064504.
541. Collie CH, Hasted JB, Ritson DM. The dielectric properties of water and heavy water. *Proc Phys Soc*. 1948;*60*:145–60.
542. Rønne C, Thrane L, Åstrand P-O, Wallqvist A, Mikkelsen KV, Keiding SR. Investigation of the temperature dependence of dielectric relaxation in liquid water by THz reflection spectroscopy and molecular dynamics simulation. *J Chem Phys*. 1997;*107*:5319–31.
543. Rønne C, Keiding SR. Low frequency spectroscopy of liquid water using THz-time domain spectroscopy. *J Mol Liq*. 2002;*101*:199–218.
544. Nagai M, Yada H, Arikawa T, Tanaka K. Terahertz time-domain attenuated total reflection spectroscopy in water and biological solution. *Int J Infrared Milli*. 2006;*27*:505–15.
545. Zhou J, Rao X, Liu X, Li T, Zhou L, Zheng Y, et al. Temperature dependent optical and dielectric properties of liquid water studied by terahertz time-domain spectroscopy. *AIP Adv*. 2019;*9*:035346.
546. Popov I, Ishai PB, Khamzin A, Feldman Y. The mechanism of the dielectric relaxation of water. *Phys Chem Chem Phys*. 2016;*18*: 13941–53.
547. Elton DC. The origin of the Debye relaxation in liquid water and fitting the high frequency excess response. *Phys Chem Chem Phys*. 2017;*19*:18739–49.
548. Kaatze U, Uhlendorf V. The dielectric properties of water at microwave frequencies. *Z Phys Chem Neue Folge*. 1981;*126*:151–65.
549. Wohlfarth C. *Static dielectric constants of pure liquids and binary liquid mixtures*. Landolt-Börnstein, New Series IV. Vol 6. Springer-Verlag, Berlin: Springer Science + Business Media; 1991.
550. Tilton LW, Taylor JK. Refractive index and dispersion of distilled water for visible radiation, at temperatures 0 to 60°C. *J Res Natl Bur Stand*. 1938;*20*:419–77.
551. Kittel C. *Introduction to solid state physics*. 8th ed. Hoboken: John Wiley & Sons; 2005.
552. Wemple SH, Didomenico M Jr, Camlibel I. Dielectric and optical properties of melt-grown $BaTiO_3$. *J Phys Chem Solids*. 1968;*29*: 1797–803.
553. Mataga N, Kaifu Y, Koizumi M. Solvent effects upon fluorescence spectra and the dipole moments of excited molecules. *Bull Chem Soc Jpn*. 1956;*29*:465–70.
554. Lippert E. Spektroskopische Bestimmung des Dipolmomentes aromatischer Verbindungen im ersten angeregten Singulettzustand. *Z Electrochem*. 1957;*61*:962–75.
555. Mataga N, Chosrowjan H, Taniguchi S. Ultrafast charge transfer in excited electronic states and investigations into fundamental problems of exciplex chemistry: our early studies and recent developments. *J Photochem Photobiol C*. 2005;*6*:37–79.
556. Bayliss NS. The effect of the electrostatic polarization of the solvent on electronic absorption spectra in solution. *J Chem Phys*. 1950;*18*: 292–6.

557. Ooshika Y. Absorption spectra of dyes in solution. *J Phys Soc Jpn*. 1954;*9*:594–602.
558. McRae EG. Theory of solvent effects on molecular electronic spectra. Frequency shifts. *J Phys Chem*. 1957;*61*:562–72.
559. Bilot L, Kawski A. Zue Theorie des Einflusses von Lösungsmitteln auf die Electronenspektren der Moleküle. *Z Naturforsch A*. 1962;*17*: 621–7.
560. Bakshiev NG. Universal intermolecular interactions and their effect on the position of the electronic spectra of molecules in two component solutions. *Opt Spectrosc*. 1964;*16*:821–32.
561. Liptay W. Dipole moments of molecules in excited states and the effect of external electric fields on the optical absorption of molecules in solution. In: Sinanoğlu O, editor. *Modern quantum chemistry: Istanbul lectures. Part III. Action of light and organic crystals*. New York: Academic Press; 1965. p. 45–66.
562. Abe T. Theory of solvent effects on molecular electronic spectra. Frequency shifts. *Bull Chem Soc Jpn*. 1965;*38*:1314–8.
563. Chamma A, Viallet P. Determination du moment dipolaire d'une molecule dans un etat excite singulet. *Sci Paris Ser C*. 1970;*270*: 1901–4.
564. Brady JE, Carr PW. An analysis of dielectric models of solvatochromism. *J Phys Chem*. 1985;*89*:5759–66.
565. Józefowicz M, Milart P, Heldt JR. Determination of ground and excited state dipole moments of 4,5′-diamino[1,1′:3′,1″-terphenyl]-4′,6′-dicarbonitrile using solvatochromic method and quantum-chemical calculations. *Spectrochim Acta A*. 2009;*74*:959–63.
566. Siddlingeshwar R, Hanagodimath SM. Estimation of the ground and the first excited singlet-state dipole moments of 1,4-disubstituted anthraquinone dyes by the solvatochromic method. *Spectrochim Acta A*. 2010;*75*:1203–10.
567. Manohara SR, Kumar VU, Shivakumaraiah, Gerward G. Estimation of ground and excited-state dipole moments of 1,2-diazines by solvatochromic method and quantum-chemical calculation. *J Mol Liq*. 2013;*181*:97–104.
568. Demissie EG, Mengesha ET, Woyessa GW. Modified solvatochromic equations for better determination of ground and excited state dipole moments of *p*-aminobenzoicacid (PABA): accounting for real shape over hypothetical spherical solvent shell. *J Photochem Photobiol A*. 2017;*337*:184–91.
569. Kumari R, Varghese A, George L, Sudhaker YN. Effect of solvent polarity on the photophysical properties of chalcone derivatives. *RSC Adv*. 2017;*7*:24204–14.
570. Renuka CG, Nadaf YF, Sriprakash G, Prasad SR. Solvent dependence on structure and electronic properties of 7-(diethylamino)-2H-1-benzopyran-2-one (C-466) laser dye. *J Fluoresc*. 2018;*28*:839–54.
571. Divac VM, Šakić D, Weitner T, Gabričević M. Solvent effects on the absorption and fluorescence spectra of Zaleplon: determination of ground and excited state dipole moments. *Spectrochim Acta A*. 2019;*212*:356–62.
572. Marcus RA. On the theory of oxidation-reduction reactions involving electron transfer. I. *J Chem Phys*. 1956;*24*:966–78.
573. Marcus RA. Chemical and electrochemical electron-transfer theory. *Annu Rev Phys Chem*. 1964;*15*:155–96.
574. Marcus RA, Sutin N. Electron transfers in chemistry and biology. *Biochim Biophys Acta*. 1985;*811*:265–322.
575. Newton MD. The role of solvation in electron transfer: theoretical and computational aspects. In: Mennucci B, Cammi R, editors. *Continuum solvation models in chemical physics*. Chichester, UK: Wiley; 2007. p. 389–413.
576. Li X-Y. An overview of continuum models for nonequilibrium solvation: popular theories and new challenge. *Int J Quantum Chem*. 2015;*115*:700–21.
577. Hsu C-P. Reorganization energies and spectral densities for electron transfer problems in charge transporting materials. *Phys Chem Chem Phys*. 2020;*22*:21630–41.
578. Cramer CJ, Truhlar DG. Implicit solvation models: equilibria, structure, spectra, and dynamics. *Chem Rev*. 1999;*99*:2161–200.
579. Kim HJ, Hynes JT. Equilibrium and nonequilibrium solvation and solute electronic structure. I. Formulation. *J Chem Phys*. 1990;*93*: 5194–210.
580. Aguilar MA, Olivares del Valle FJ, Tomasi J. Nonequilibrium solvation: an *ab initio* quantum-mechanical method in the continuum cavity model approximation. *J Chem Phys*. 1993;*98*:7375–84.
581. Mennucci B. Continuum models for excited states. In: Mennucci B, Cammi R, editors. *Continuum solvation models in chemical physics*. Chichester, UK: Wiley; 2007. p. 110–23.
582. Guido CA, Caprasecca S. On the description of the environment polarization response to electronic transitions. *Int J Quantum Chem*. 2019;*119*:e25711.
583. Mennucci B, Cammi R, Tomasi J. Excited states and solvatochromatic shifts within a nonequilibrium solvation approach: a new formulation of the integral equation formalism method at the self-consistent field, configuration interaction, and multiconfiguration self-consistent field level. *J Chem Phys*. 1998;*109*:2798–807.
584. Cossi M, Barone V. Solvent effect on vertical electronic transitions by the polarizable continuum model. *J Chem Phys*. 2000;*112*: 2427–35.
585. Chipman DM. Vertical electronic excitation with a dielectric continuum model of solvation including volume polarization. I. Theory. *J Chem Phys*. 2009;*131*:014103.
586. Mewes J-M, You Z-Q, Wormit M, Kriesche T, Herbert JM, Dreuw A. Experimental benchmark data and systematic evaluation of two *a posteriori*, polarizable-continuum corrections for vertical excitation energies in solution. *J Phys Chem A*. 2015;*119*:5446–64.
587. Mewes J-M, Herbert JM, Dreuw A. On the accuracy of the state-specific polarizable continuum model for the description of correlated ground and excited states in solution. *Phys Chem Chem Phys*. 2017;*19*:1644–54.
588. Coons MP, You Z-Q, Herbert JM. The hydrated electron at the surface of neat liquid water appears to be indistinguishable from the bulk species. *J Am Chem Soc*. 2016;*138*:10879–86.

589. Cammi R, Tomasi J. Nonequilibrium solvation theory for the polarizable continuum model: a new formulation at the SCF level with application to the case of the frequency-dependent linear electric response function. *Int J Quantum Chem Symp*. 1995;*29*:465–74.
590. Aguilar MA. Separation of the electric polarization into fast and slow components: a comparison of two partition schemes. *J Phys Chem A*. 2001;*105*:10393–6.
591. Pekar SI. *Untersuchungen über die Elektronentheorie der Kristalle*. Berlin: Akademie-Verlag; 1954.
592. Pekar SI. Research in electron theory of crystals. Technical Report AEC-tr-5575, U.S. Atomic Energy Commission, Division of Technical Information. 1963.
593. Bayliss NS, McRae EG. Solvent effects in organic spectra: dipole forces and the Franck–Condon principle. *J Phys Chem*. 1954;*58*:1002–6.
594. Basilevsky MV, Chudinov GE. Dynamics of charge transfer chemical reactions in a polar medium within the scope of the Born–Kirkwood–Onsager model. *Chem Phys*. 1991;*157*:327–44.
595. Houjou H, Sakurai M, Inoue Y. Theoretical evaluation of medium effects on absorption maxima of molecular solutes. I. Formulation of a new method based on the self-consistent reaction field theory. *J Chem Phys*. 1997;*107*:5652–60.
596. Cammi R, Frediani L, Mennucci B, Tomasi J, Ruud K, Mikkelsen KV. A second-order, quadratically convergent multiconfigurational self-consistent field polarizable continuum model for equilibrium and nonequilibrium solvation. *J Chem Phys*. 2002;*117*:13–26.
597. Marenich AV, Cramer CJ, Truhlar DG, Guido CA, Mennucci B, Scalmani G, et al. Practical computation of electronic excitation in solution: vertical excitation model. *Chem Sci*. 2011;*2*:2143–61.
598. Jacobson LD, Herbert JM. A simple algorithm for determining orthogonal, self-consistent excited-state wave functions for a state-specific Hamiltonian: application to the optical spectrum of the aqueous electron. *J Chem Theory Comput*. 2011;*7*:2085–93.
599. Lunkenheimer B, Köhn A. Solvent effects on electronically excited states using the conductor-like screening model and the second-order correlated method ADC(2). *J Chem Theory Comput*. 2013;*9*:977–94.
600. Winter B, Faubel M. Photoemission from liquid aqueous solutions. *Chem Rev*. 2006;*106*:1176–211.
601. Seidel R, Thürmer S, Winter B. Photoelectron spectroscopy meets aqueous solution: studies from a vacuum liquid microjet. *J Phys Chem Lett*. 2011;*2*:633–41.
602. Seidel R, Winter B, Bradforth SE. Valence electronic structure of aqueous solutions: insights from photoelectron spectroscopy. *Annu Rev Phys Chem*. 2016;*67*:283–305.
603. Winter B, Weber R, Hertel IV, Faubel M, Jungwirth P, Brown EC, et al. Electron binding energies of aqueous alkali and halide ions: EUV photoelectron spectroscopy of liquid solutions and combined ab initio and molecular dynamics calculations. *J Am Chem Soc*. 2005;*127*:7203–14.
604. Jacobson LD, Herbert JM. A one-electron model for the aqueous electron that includes many-body electron-water polarization: bulk equilibrium structure, vertical electron binding energy, and optical absorption spectrum. *J Chem Phys*. 2010;*133*:154506.
605. Ghosh D, Isayev O, Slipchenko LV, Krylov AI. Effect of solvation on the vertical ionization energy of thymine: from microhydration to bulk. *J Phys Chem A*. 2011;*115*:6028–38.
606. Ghosh D, Roy A, Seidel R, Winter B, Bradforth S, Krylov AI. First-principle protocol for calculating ionization energies and redox potentials of solvated molecules and ions: theory and application to aqueous phenol and phenolate. *J Phys Chem B*. 2012;*116*:7269–80.
607. Tazhigulov RN, Gurunathan PK, Kim Y, Slipchenko LV, Bravaya KB. Polarizable embedding for simulating redox potentials of biomolecules. *Phys Chem Chem Phys*. 2019;*21*:11642–50.
608. Tóth Z, Kubečka J, Muchová E, Slaviček P. Ionization energies in solution with QM:QM approach. *Phys Chem Chem Phys*. 2020;*22*:10550–60.
609. Provorse MR, Peev T, Xiong C, Isborn CM. Convergence of excitation energies in mixed quantum and classical solvent: comparison of continuum and point charge models. *J Phys Chem B*. 2016;*120*:12148–59. Erratum: *J. Phys. Chem. B*, **121**, 2372 (2017).
610. Paul SK, Coons MP, Herbert JM. Erratum: 'quantum chemistry in arbitrary dielectric environments: theory and implementation of nonequilibrium Poisson boundary conditions and application to compute vertical ionization energies at the air/water interface'. *J Chem Phys*. 2019;*151*:189901.
611. Perry CF, Zhang P, Nunes FB, Jordan I, von Conta A, Wörner HJ. Ionization energy of liquid water revisited. *J Phys Chem Lett*. 2020;*11*:1789–94.
612. Luckhaus D, Yamamoto Y, Suzuki T, Signorell R. Genuine binding energy of the hydrated electron. *Sci Adv*. 2017;*3*:e1603224.
613. Herbert JM. Structure of the aqueous electron. *Phys Chem Chem Phys*. 2019;*21*:20538–65.
614. Muñoz-Losa A, Markovitsi D, Improta R. A state-specific PCM-DFT method to include dynamic solvent effects in the calculation of ionization energies: application to DNA bases. *Chem Phys Lett*. 2015;*634*:20–4.
615. Khani SK, Khah AM, Hättig C. Comparison of reaction field schemes for coupling continuum solvation models with wave function methods for excitation energies. *J Chem Theory Comput*. 2020;*16*:4554–64.
616. Thompson MA, Schenter GK. Excited states of the bacteriochlorophyll *b* dimer of *Rhodopseudomonas viridis*: a QM/MM study of the photosynthetic reaction center that includes MM polarization. *J Phys Chem*. 1995;*99*:6374–86.
617. Arora P, Slipchenko LV, Webb SP, DeFusco A, Gordon MS. Solvent-induced frequency shifts: configuration interaction singles combined with the effective fragment potential method. *J Phys Chem A*. 2010;*114*:6742–50.
618. Cammi R, Corni S, Mennucci B, Tomasi J. Electronic excitation energies of molecules in solution: state specific and linear response methods for nonequilibrium continuum solvation models. *J Chem Phys*. 2005;*122*:104513.

619. Improta R, Barone V, Scalmani G, Frisch MJ. A state-specific polarizable continuum model time dependent density functional method for excited state calculations in solution. *J Chem Phys*. 2006;*125*:054103.
620. Improta R, Scalmani G, Frisch MJ, Barone V. Toward effective and reliable fluorescence energies in solution by a new state specific polarizable continuum model time dependent density functional theory approach. *J Chem Phys*. 2007;*127*:074504.
621. Furche F, Ahlrichs R. Adiabatic time-dependent density functional methods for excited state properties. *J Chem Phys*. 2002;*117*: 7433–47. Erratum: *J. Chem. Phys*., **121**, 12772–12773 (2004).
622. Ronca E, Angeli C, Belpassi L, De Angelis F, Tarantelli F, Pastore M. Density relaxation in time-dependent density functional theory: combining relaxed density natural orbitals and multireference perturbation theories for an improved description of excited states. *J Chem Theory Comput*. 2014;*10*:4014–24.
623. Maschietto F, Campetella M, Frisch MJ, Scalmani G, Adamo C, Ciofini I. How are the charge transfer descriptors affected by the quality of the underpinning electronic density? *J Comput Chem*. 2018;*39*:735–42.
624. Mennucci B, Cappelli C, Guido CA, Cammi R, Tomasi J. Structures and properties of electronically excited chromophores in solution from the polarizable continuum model coupled to the time-dependent density functional theory. *J Phys Chem A*. 2009;*113*:3009–20.
625. Amos AT, Burrows BL. Solvent-shift effects on electronic spectra and excited-state dipole moments and polarizabilities. *Adv Quantum Chem*. 1973;*7*:289–313.
626. Suppan P. Solvent effects on the energy of electronic transitions: experimental observations and applications to structural problems of excited molecules. *J Chem Soc A*. 1968;3125–33.
627. Suppan P. Polarizability of excited molecules from spectroscopic studies. *Spectrochim Acta A*. 1968;*24*:1161–5.
628. Amos AT, Burrows BL. Dispersion interactions and solvent-shift effects. *Theor Chem Accounts*. 1973;*29*:139–50.
629. Marenich AV, Cramer CJ, Truhlar DG. Uniform treatment of solute–solvent dispersion in the ground and excited electronic states of the solute based on a solvation model with state-specific polarizability. *J Chem Theory Comput*. 2013;*9*:3649–59.
630. Marenich AV, Cramer CJ, Truhlar DG. Electronic absorption spectra and solvatochromic shifts by the vertical excitation model: solvated clusters and molecular dynamics sampling. *J Phys Chem B*. 2015;*119*:958–67.
631. Jacquemin D, Planchat A, Adamo C, Mennucci B. TD-DFT assessment of functionals for optical 0–0 transitions in solvated dyes. *J Chem Theory Comput*. 2012;*8*:2359–72.
632. Olivares del Valle FJ, Tomasi J. Electron correlation and solvation effects. I. Basic formulation and preliminary attempt to include the electron correlation in the quantum mechanical polarizable continuum model so as to study solvation phenomena. *Chem Phys*. 1991; *150*:139–50.
633. Aguilar MA, Olivares del Valle FJ, Tomasi J. Electron correlation and solvation effects. II. The description of the vibrational properties of a water molecule in a dielectric given by the application of the polarizable continuum model with inclusion of correlation effects. *Chem Phys*. 1991;*150*:151–61.
634. Ángyán J. Choosing between alternative MP2 algorithms in the self-consistent reaction field theory of solvent effects. *Chem Phys Lett*. 1995;*241*:51–6.
635. Lipparini F, Scalmani G, Mennucci B. Non covalent interactions in RNA and DNA base pairs: a quantum-mechanical study of the coupling between solvent and electronic density. *Phys Chem Chem Phys*. 2009;*11*:11617–23.
636. Cammi R. Quantum cluster theory for the polarizable continuum model. I. The CCSD level with analytical first and second derivatives. *J Chem Phys*. 2009;*131*:164104.
637. Cammi R, Tomasi J. Quantum cluster theory for the polarizable continuum model (PCM). In: Leszczynski J, Kaczmarek-Kedziera A, Puzyn T, Papadopoulos MG, Reis H, Shukla MK, editors. *Handbook of computational chemistry*. 2nd ed. Switzerland: Springer International Publishing; 2017; (chapter 34). p. 1517–56.
638. Caricato M, Mennucci B, Scalmani G, Trucks GW, Frisch MJ. Electronic excitation energies in solution at equation of motion CCSD level within a state specific polarizable continuum model approach. *J Chem Phys*. 2010;*132*:084102.
639. Caricato M. CCSD-PCM: improving upon the reference reaction field approximation at no cost. *J Chem Phys*. 2011;*135*:074113.
640. Caricato M. Coupled cluster theory in the condensed phase within the singles-T density scheme for the environment response. *WIREs Comput Mol Sci*. 2020;*10*:e1463.
641. Khani SK, Khah AM, Hättig C. COSMO-RI-ADC(2) excitation energies and excited state gradients. *Phys Chem Chem Phys*. 2018;*20*: 16354–63.
642. Dreuw A, Wormit M. The algebraic diagrammatic construction scheme for the polarization propagator for the calculation of excited states. *WIREs Comput Mol Sci*. 2015;*5*:82–95.
643. De Vetta M, Menger MFSJ, Nogueira JJ, González L. Solvent effects on electronically excited states: QM/continuum versus QM/explicit models. *J Phys Chem B*. 2018;*122*:2975–84.
644. Cossi M, Barone V. Time-dependent density functional theory for molecules in liquid solutions. *J Chem Phys*. 2001;*115*:4708–17.
645. Cammi R, Mennucci B. Linear response theory for the polarizable continuum model. *J Chem Phys*. 1999;*110*:9877–86.
646. Cammi R, Mennucci B, Tomasi J. Fast evaluation of geometries and properties of excited molecules in solution: a Tamm–Dancoff model with application to 4-dimethylaminobenzonitrile. *J Phys Chem A*. 2000;*104*:5631–7.
647. Corni S, Tomasi J. Excitation energies of a molecule close to a metal surface. *J Chem Phys*. 2002;*117*:7266–78.
648. Iozzi MF, Mennucci B, Tomasi J, Cammi R. Excitation energy transfer (EET) between molecules in condensed matter: a novel application of the polarizable continuum model (PCM). *J Chem Phys*. 2004;*120*:7029–40.

649. Cammi R, Cossi M, Mennucci B, Tomasi J. Analytical Hartree–Fock calculation of the dynamical polarizabilities α, β, and γ of molecules in solution. *J Chem Phys*. 1996;*105*:10556–64.
650. Duchemin I, Guido CA, Jacquemin D, Blase X. The Bethe–Salpeter formalism with polarisable continuum embedding: reconciling linear-response and state-specific features. *Chem Sci*. 2018;*9*:4430–43.
651. Cammi R. Coupled-cluster theories for the polarizable continuum model. II. Analytical gradients for excited states of molecular solutes by the equation of motion coupled-cluster method. *Int J Quantum Chem*. 2010;*110*:3040–52.
652. Cammi R. Coupled-cluster theory for the polarizable continuum model. III. A response theory for molecules in solution. *Int J Quantum Chem*. 2012;*112*:2547–60.
653. Caricato M. A comparison between state-specific and linear-response formalisms for the calculation of vertical electronic transition energy in solution with the CCSD-PCM method. *J Chem Phys*. 2013;*139*:044116.
654. Caricato M. Linear response coupled cluster theory with the polarizable continuum model within the singles approximation for the solvent response. *J Chem Phys*. 2018;*148*:134113.
655. Caricato M. CCSD-PCM excited state energy gradients with the linear response singles approximation to study the photochemistry of molecules in solution. *ChemPhotoChem*. 2019;*3*:747–54.
656. Helgaker T, Jørgensen P, Olsen J. *Molecular electronic-structure theory*. New York: Wiley; 2000.
657. Corni S, Cammi R, Mennucci B, Tomasi J. Electronic excitation energies of molecules in solution within continuum solvation models: investigating the discrepancy between state-specific and linear-response methods. *J Chem Phys*. 2005;*123*:134512.
658. Pedone A. Role of solvent on charge transfer in 7-aminocoumarin dyes: new hints from TD-CAM-B3LYP and state specific PCM calculations. *J Chem Theory Comput*. 2013;*9*:4087–96.
659. Minezawa N. State-specific solvation effect on the intramolecular charge transfer reaction in solution: a linear-response free energy TDDFT method. *Chem Phys Lett*. 2014;*608*:140–4.
660. Bernini C, Zani L, Calamante M, Reginato G, Mordini A, Taddei M, et al. Excited state geometries and vertical emission energies of solvated dyes for DSSC: a PCM/TD-DFT benchmark study. *J Chem Theory Comput*. 2014;*10*:3925–33.
661. Budzák Š, Mach P, Medveď M, Kysel' O. Critical analysis of spectral solvent shifts calculated by the contemporary PCM approaches of a representative series of charge-transfer methylated benzenes. *Phys Chem Chem Phys*. 2015;*17*:17618–27.
662. Guido CA, Jacquemin D, Adamo C, Mennucci B. Electronic excitations in solution: the interplay between state specific approaches and a time-dependent density functional theory description. *J Chem Theory Comput*. 2015;*11*:5782–90.
663. Guido CA, Mennucci B, Scalmani G, Jacquemin D. Excited state dipole moments in solution: comparison between state-specific and linear-response TD-DFT values. *J Chem Theory Comput*. 2018;*14*:1544–53.
664. Klaumünzer B, Kröner D, Saalfrank P. (TD-)DFT calculation of vibrational and vibronic spectra of riboflavin in solution. *J Phys Chem B*. 2010;*114*:10826–34.
665. Bloino J, Baiardi A, Biczysko M. Aiming at an accurate prediction of vibrational and electronic spectra for medium-to-large molecules: an overview. *Int J Quantum Chem*. 2016;*116*:1543–74.
666. García-Iriepa C, Zemmouche M, Ponce-Vargas M, Navizet I. The role of solvation models on the computed absorption and emission spectra: the case of fireflies oxyluciferin. *Phys Chem Chem Phys*. 2019;*21*:4613–23.
667. Chibani S, Budzák Š, Medveď M, Mennucci B, Jacquemin D. Full cLR-PCM calculations of the solvatochromic effects on emission energies. *Phys Chem Chem Phys*. 2014;*16*:26024–9.
668. Schwabe T. General theory for environmental effects on (vertical) electron excitation energies. *J Chem Phys*. 2016;*145*:154105.
669. Mennucci B, Cossi M, Tomasi J. A theoretical model of solvation in continuum anisotropic dielectrics. *J Chem Phys*. 1995;*102*:6837–45.
670. Mennucci B, Cammi R. Ab initio model to predict NMR shielding tensors for solutes in liquid crystals. *Int J Quantum Chem*. 2003;*93*:121–30.
671. Hoshi H, Sakurai M, Inoue Y, Chûjô R. Medium effects on the molecular electronic structure. I. The formulation of a theory for the estimation of a molecular electronic structure surrounded by an anisotropic medium. *J Chem Phys*. 1987;*87*:1107–15.
672. Ghosh S, Horvath S, Soudackov AV, Hammes-Schiffer S. Electrochemical solvent reorganization energies in the framework of the polarizable continuum model. *J Chem Theory Comput*. 2014;*10*:2091–102.
673. Ghosh S, Hammes-Schiffer S. Calculation of electrochemical reorganization energies for redox molecules at self-assembled monolayer modified electrodes. *J Phys Chem Lett*. 2015;*6*:1–5.
674. Ghosh S, Soudackov AV, Hammes-Schiffer S. Electrochemical electron transfer and proton-coupled electron transfer: effects of double layer and ionic environment on solvent reorganization energies. *J Chem Theory Comput*. 2016;*12*:2917–25.
675. Frediani L, Mennucci B, Cammi R. Quantum-mechanical continuum solvation study of the polarizability of halides at the water/air interface. *J Phys Chem B*. 2004;*108*:13796–806.
676. Frediani L, Cammi R, Corni S, Tomasi J. A polarizable continuum model for molecules at diffuse interfaces. *J Chem Phys*. 2004;*120*:3893–907.
677. Bondesson L, Frediani L, Ågren H, Mennucci B. Solvation of N_3^- at the water surface: the polarizable continuum model approach. *J Phys Chem B*. 2006;*110*:11361–8.
678. Iozzi MF, Cossi M, Improta R, Rega N, Barone V. A polarizable continuum approach for the study of heterogeneous dielectric environments. *J Chem Phys*. 2006;*124*:184103.
679. Si D, Li H. Heterogeneous conductorlike solvation model. *J Chem Phys*. 2009;*131*:044123.
680. Wang J-B, Ma J-Y, Li X-Y. Polarizable continuum model associated with the self-consistent-reaction field for molecular adsorbates at the interface. *Phys Chem Chem Phys*. 2010;*12*:207–14.

681. Mozgawa K, Mennucci B, Frediani L. Solvation at surfaces and interfaces: a quantum-mechanical/continuum approach including non-electrostatic contributions. *J Phys Chem C*. 2014;*118*:4715–25.
682. Mozgawa K, Frediani L. Electronic structure of small surfactants: a continuum solvation study. *J Phys Chem C*. 2016;*120*:17501–13.
683. Jungwirth P, Tobias DJ. Ions at the air/water interface. *J Phys Chem B*. 2002;*106*:6361–73.
684. Jungwirth P, Tobias DJ. Specific ion effects at the air/water interface. *Chem Rev*. 2006;*106*:1259–81.
685. Chaplin M. Theory vs experiment: what is the surface charge of water? *Water*. 2009;*1*:1–28.
686. Duignan TT, Parsons DF, Ninham BW. Ion interactions with the air–water interface using a continuum solvent model. *J Phys Chem B*. 2014;*118*:8700–10.
687. Duignan TT, Parsons DF, Ninham BW. Hydronium and hydroxide at the air–water interface with a continuum solvent model. *Chem Phys Lett*. 2015;*635*:1–12.
688. Aksu H, Paul SK, Herbert JM, Dunietz BD. How well does a solvated octa-acid capsule shield the embedded chromophore? A computational analysis based on an anisotropic dielectric continuum model. *J Phys Chem B*. 2020;*124*:6998–7004.
689. Herbert JM, Coons MP. The hydrated electron. *Annu Rev Phys Chem*. 2017;*68*:447–72.
690. Swanson JMJ, Mongan J, McCammon JA. Limitations of atom-centered dielectric functions in implicit solvent models. *J Phys Chem B*. 2005;*109*:14769–72.
691. Zhou H-X, Qin S, Tjong H. Modeling protein–protein and protein–nucleic acid interactions: structure, thermodynamics, and kinetics. *Annu Rep Comput Chem*. 2008;*4*:67–87.
692. Pang X, Zhou H-X. Poisson–Boltzmann calculations: van der Waals or molecular surface? *Commun Comput Phys*. 2013;*13*:1–12.
693. Decherchi S, Colmenares J, Catalano CE, Spagnuolo M, Alexov E, Rocchia W. Between algorithm and model: different molecular surface definitions for the Poisson–Boltzmann based electrostatic characterization of biomolecules in solution. *Commun Comput Phys*. 2013;*13*:61–89.
694. Rajamani S, Ghosh T, Garde S. Size dependent ion hydration, its asymmetry, and convergence to macroscopic hydration. *J Chem Phys*. 2004;*120*:4457–66.
695. Bardhan JP, Jungwirth P, Makowski L. Affine-response model of molecular solvation of ions: accurate predictions of asymmetric charging free energies. *J Chem Phys*. 2012;*137*:124101.
696. Mukhopadhyay A, Fenley AT, Tolokh IS, Onufriev AV. Charge hydration asymmetry: the basic principle and how to use it to test and improve water models. *J Phys Chem B*. 2012;*116*:9776–83.
697. Mukhopadhyay A, Tolokh IS, Onufriev AV. Accurate evaluation of charge asymmetry in aqueous solvation. *J Phys Chem B*. 2015;*119*:6092–100.
698. Reif MM, Hünenberger PH. Origin of asymmetric solvation effects for ions in water and organic solvents investigated using molecular dynamics simulations: the Swain acity-basity scale revisited. *J Phys Chem B*. 2016;*120*:8485–517.
699. Duignan TT, Baer MD, Schenter GK, Mundy CJ. Electrostatic solvation free energies of charged hard spheres using molecular dynamics with density functional theory interactions. *J Chem Phys*. 2017;*147*:161716.
700. Mobley DL, Barber AE, Fennell CJ, Dill KA. Charge asymmetries in hydration of polar solutes. *J Phys Chem B*. 2008;*112*:2405–14. Erratum: *J. Phys. Chem. B*, **115**, 15145 (2011).
701. Tabrizi AM, Goossens S, Rahimi AM, Cooper CD, Knepley MG, Bardhan JP. Extending the solvation-layer interface condition continuum electrostatic model to a linearized Poisson–Boltzmann solvent. *J Chem Theory Comput*. 2017;*13*:2897–914.
702. Duignan TT, Zhao XS. The Born model can accurately describe electrostatic ion solvation. *Phys Chem Chem Phys*. 2020;*22*:25126–35.
703. Latimer WM, Pitzer KS, Slansky CM. The free energy of hydration of gaseous ions, and the absolute potential of the normal calomel electrode. *J Chem Phys*. 1939;*7*:108–11.
704. Purisima EO, Sulea T. Restoring charge asymmetry in continuum electrostatics calculations of hydration free energies. *J Phys Chem B*. 2009;*113*:8206–9.
705. Mukhopadhyay A, Aguilar BH, Tolokh IS, Onufriev AV. Introducing charge hydration asymmetry into the generalized Born model. *J Chem Theory Comput*. 2014;*10*:1788–94.
706. Bardhan JP, Knepley MG. Communication: modeling charge-sign asymmetric solvation free energies with nonlinear boundary conditions. *J Chem Phys*. 2014;*141*:131103.
707. Tabrizi AM, Knepley MG, Bardhan JP. Generalising the mean spherical approximation as a multiscale, nonlinear boundary condition at the solute–solvent interface. *Mol Phys*. 2016;*114*:2558–67.
708. Tabrizi AM, Goossens S, Rahimi AM, Knepley M, Bardhan JP. Predicting solvation free energies and thermodynamics in polar solvents and mixtures using a solvation-layer interface condition. *J Chem Phys*. 2017;*146*:094103.
709. Rahimi AM, Tabrizi AM, Goossens S, Knepley MG, Bardhan JP. Solvation thermodynamics of neutral and charged solutes using the solvation-layer interface condition continuum dielectric model. *Int J Quantum Chem*. 2018;*119*:e25771.
710. Schaaf C, Gekle S. Dielectric response of the water hydration layer around spherical solutes. *Phys Rev E*. 2015;*92*:032718.
711. Truscott M, Andreussi O. Field-aware interfaces in continuum solvation. *J Phys Chem B*. 2019;*123*:3513–24.
712. Hehre WJ, Radom L, Schleyer P v R, Pople JA. *Ab initio molecular orbital theory*. New York: Wiley-Interscience; 1986.

How to cite this article: Herbert JM. Dielectric continuum methods for quantum chemistry. *WIREs Comput Mol Sci*. 2021;11:e1519. https://doi.org/10.1002/wcms.1519